UNIVERSITY OF OKLAHOMA

GRADUATE COLLEGE

AN EXPERIMENTAL, MODELING AND MACHINE LEARNING BASED INVESTIGATION OF STICK-SLIP VIBRATIONS

A DISSERTATION

SUBMITTED TO THE GRADUATE FACULTY

in partial fulfillment of the requirements for the

Degree of

DOCTOR OF PHILOSOPHY

By

SAKET SRIVASTAVA
Norman, Oklahoma
2022

AN EXPERIMENTAL, MODELING AND MACHINE LEARNING BASED
INVESTIGATION OF STICK-SLIP VIBRATIONS

A DISSERTATION APPROVED FOR THE

MEWBOURNE SCHOOL OF PETROLEUM AND GEOLOGICAL ENGINEERING

BY THE COMMITTEE CONSISTING OF

Dr. Catalin Teodoriu, Chair

Dr. Zahed Siddique

Dr. Saeed Salehi

Dr. Deepak Devegowda

Dr. Hamidreza Karami Mirazizi

Acknowledgement

The journey of completing and earning this doctoral degree was long, arduous, and not done singlehandedly. Firstly, I would like to thank my parents, Meena and Sanjeev Srivastava, and my sister, Tanya Srivastava for their constant love and encouragement throughout my academic journey in India and the US. I would like to thank my partner, Simran, who has whole heartedly supported me every single day of my doctoral pursuit and motivated me to aim higher. She has always believed in me and been an emotional rock throughout. I am forever grateful for her companionship during this journey that the both of us will cherish forever.

I would like to thank my committee members for their valuable insight and feedback on my dissertation project. This research study would not have been possible without the constant guidance, support and belief of my advisor and mentor Dr. Catalin Teodoriu. His passion towards engineering and being a lifelong learner has motivated me tremendously. Moreover, Dr. Teodoriu and his wife Lavinia have welcomed me with open arms into their family during my time at the University of Oklahoma and have been strong pillars of support throughout this journey. I am forever grateful!

I would like to thank Helmerich & Payne, the sponsors of my PhD project, who constantly guided and supported our work. To Dr. Sridhar Radhakrishnan for his words of wisdom both as an advisor for ISA and when I started to explore the field of data science and analytics. His advice has been invaluable for my professional growth. I would like to express gratitude to Gurbinder Bali for believing in me, always being there to give advice and honest feedback and for giving me immense professional development opportunities. I am extremely thankful for the administration and staff within MPGE—Katie Shapiro, Annette Moran and Sonya Grant, thank you for your dedication, handwork and compassion towards your students.

I have spent seven years at the University of Oklahoma and earned three graduate degrees. The University and its community have helped fuel my academic curiosity, provided me a sense of belonging and pushed me to be a better version of myself. Even though I have spent majority of my time at the Sarkeys Energy Center, I feel at home throughout this campus. I cherish all my friendships, be it those from the research lab or various student organizations across campus. The memories I made at this university will last a lifetime.

Table of Contents

Acknowledgement iv

Table of Contents v

List of Figures ix

List of Tables xiv

Abstract xv

Chapter 1: Introduction 1

1.1 Background 1

1.2 Problem Definition 5

1.2.1 Stick-slip vibrations 5

1.2.2 Stick-slip severity 6

1.3 Research Methodology 7

1.3.1 Experimental analysis 7

1.3.2 Modeling of drillstring vibration 8

1.3.3 Data driven analysis 8

1.4 Research Objectives 9

1.5 Research Hypotheses 9

1.6 Dissertation Outline 10

Chapter 2: Literature Review 11

2.1 Experimental Studies on Drillstring Vibrations 11

2.1.1 Structural framework of test rig 12

2.1.2 Top drive assembly 13

2.1.3 Rig configuration 13

2.1.4 Drill String 14

2.1.5 Bottom hole assembly (BHA) 17

2.1.6 Sensors and data acquisition system 18

2.1.7 Stick-slip Vibration Experiments 19

2.2 Modeling of Drillstring Vibrations 24
Distributed Parameter Modeling 25
2.2.1 Lumped parameter models 26
2.2.2 High-fidelity discrete model 28
2.2.3 Analytical solution 29
2.2.4 Numerical modeling vs. experimental testing 31

2.3 Drillstring Vibration Mitigation 33
2.3.1 Vibration analysis during design stage 33
2.3.2 Passive control techniques 34
2.3.3 Active control techniques 36
2.3.4 Real-time vibration optimization 37

2.4 Data Acquisition and Sampling 38
2.4.1 Data Acquisition System 41
2.4.2 Sampling Theory 42
2.4.3 Nyquist-Shannon sampling theorem 43
2.4.4 Over-sampling and Under-sampling 43

2.5 Summary of literature review 44

Chapter 3: Design of an Experimental Test Rig for Torsional Vibrations 46

3.1 Components of an Experimental Setup 47
3.1.1 Top Drive Assembly 47
3.1.2 Drill String 47
3.1.3 Rock-bit interaction 56
3.1.4 Vertical to horizontal configuration 56
3.1.5 Electrical Sensors 57
3.1.6 Data acquisition and HMI (Human machine interface) 59

3.2 Experimental design 60
3.2.1 Test matrix 61
3.2.2 Severity estimation 62

3.3 Summary of experimental design 63

Chapter 4: Experimental Results ... 64
4.1 Effect of sampling rate for mild stick-slip vibrations ... 64
4.1.1 High frequency bit sticking / Mild stick-slip vibration results ... 64
4.1.2 Low frequency bit sticking / Severe stick-slip vibration results ... 66
4.2 Effect of drillstring stiffness for mild vs severe stick-slip vibrations ... 68
4.2.1 Mild stick-slip at 100 RPM ... 68
4.2.2 Severe stick-slip at 100 RPM ... 70
4.2.3 Mild stick-slip at 200 RPM ... 71
4.2.4 Severe stick-slip at 200RPM ... 72
4.3 Effect of RPM and WOB on mild vs severe stick-slip vibrations ... 73
4.3.1 Mild vs severe SS at WOB-0.5 Kg and RPM-100 ... 73
4.3.2 Mild vs severe SS at WOB-0.5 Kg and RPM-200 ... 74
4.3.3 Mild vs severe SS at WOB-1 Kg and RPM-100 ... 75
4.3.4 Mild vs severe SS at WOB-1 Kg and RPM-200 ... 76
4.4 Self-Induced Bit sticking ... 77
4.4.1 Horizontal well configuration ... 77
4.4.2 Vertical well configuration ... 79
4.5 Effect of well configuration on mild vs severe stick-slip vibrations ... 80
4.5.1 Vertical Configuration ... 81
4.5.2 Horizontal configuration ... 82
4.6 Effect of sticking time-period on vibration response ... 83
4.7 Summary of experimental results ... 84
Chapter 5: Mathematical modeling of torsional vibrations ... 85
5.1 Modeling using 2 DOF (Degree of freedom) model ... 85
5.1.1 Experimental comparison ... 90
5.2 Torsional model development in WellScan ... 91
5.2.1 Well design ... 92
5.2.2 Experimental design ... 93
5.2.3 Experimental results ... 94

5.2.4 Comparison with experimental data 95
5.3 Summary of modeling results 96
Chapter 6: Machine Learning for Drilling Vibrations 97
6.1 Review of ML studies on drilling vibrations 97
6.2 Data quality challenges 100
6.2.1 Sampling rate 100
6.2.2 Outliers 102
6.2.3 Noise 102
6.2.4 Data labeling 103
6.2.5 Feature extraction and scaling 105
6.2.6 Class imbalance 108
6.3 Dataset and experiments 109
6.4 Results 111
6.4.1 Sampling Frequency 111
6.4.2 Data Labeling 112
6.4.3 Feature Extraction 114
6.4.4 Class Imbalance 116
6.5 Summary of machine learning experiments 118
Chapter 7: Discussions 119
Chapter 8: Conclusion and Future work 126
Nomenclature 128
References 129

List of Figures

Figure 1-1-1 The different vibration modes in the drill string (Dong and Chen, 2016) 2
Figure 1-2 Severity level of vibrations based on accelerometer readings (Dushaishi et al., 2015) 4
Figure 1-3 Successive stick-slip cycle events during off-bottom conditions (Cayeux et al.,2021) 6
Figure 1-4 Modeling torsional vibrations (Patil and Teodoriu, 2013)... 8
Figure 2-1 (a) Test rig for torsional vibrations (Patil and Teodoriu, 2013) (b) Torsional vibration study by drilling rock sample (Kovalyshen, 2014) and (c) Automated drilling dysfunction mitigation test rig (Bilgesu et al., 2017) 12
Figure 2-2 (a) 25 m horizontal test rig (Lin et al., 2018), (b) Automated test rig (Cayeux et al., 2017), (c) Torsional analysis in horizontal setup (Cayres, 2015) and (d) Lateral vibration study in 79^{O} deviated well (Wen et al., 2018)... 14
Figure 2-3 Comparison of downscaling factor of laboratory test rigs across the world (Srivastava and Teodoriu, 2019).. 15
Figure 2-4 Using a flexible shaft (a) and shaft dampening for torsional vibrations (b) (Left) (Kapitaniak et al., 2015) and comparison of stick-slip index for steel, aluminum, and PVC (Patil and Teodoriu, 2013).. 17
Figure 2-5 Examples of data acquisition and control systems for drilling vibration study (Sharma et al., 2020; Raymond et al., 2008)... 18
Figure 2-6 Decaying torsional oscillations (a) and angular position x(t) in radians (b)............... 19
Figure 2-7 (a) Magnetic brake (Khulief and Sulaiman, 2009) (b) Torsional friction brake (Patil and Teodoriu, 2013) and (c) Lubricated disc brake (Mihajlovic et al., 2006)............................. 20
Figure 2-8 Soft string and stiff string model.. 24
Figure 2-9 Tension on short section of flexible bar (Marquez et al., 2015) 26
Figure 2-10 Two rotational degree of freedom in torsional spring model (Patil and Teodoriu 2013) and (b) Simplified axial and torsional (2 DOF) model (Marquez et al., 2015) 27
Figure 2-11 Discrete model with representation of dynamic forces and torque (Liu et al., 2012)28
Figure 2-12 Drill string with step change in diameter (Bailey and Finnie, 1960)........................ 31
Figure 2-13 (a) Bit RPM vs time for experimental test of stick-slip vibrations and (b) numerical model result for downhole RPM for stick-slip conditions.. 32
Figure 2-14 Stability map for PDC bits (Dong and Chen, 2016) 34

Figure 2-15 (a) Anti stick tool working mechanism (Dong and Chen, 2016) and (b) Stroke travel length for a popular AST tool (Vromen et al., 2019).. 35
Figure 2-16 (a) Open loop vs closed loop system (Gurjao et al., 2018) and (b) PID controller in action (Ogata, 2010).. 36
Figure 2-17 (a) STRS working principle (Dong and Chen 2016) and (b) Optimum drilling zone as a relation between WOB and TOB (Wu et al., 2010).. 37
Figure 2-18 Major vibration modes and associated characteristic frequencies (Marquez et al., 2015, Patil and Ochua, 2020)... 38
Figure 2-19 A review of sampling frequency for surface and downhole measurements with associated limits for detecting drill string vibrations 39
Figure 2-20 A standard DAQ system.. 41
Figure 2-21 (a) A continuous time domain sine wave, (b) discrete sample representation (Ploennigs, 2010) 42
Figure 2-22 (a) Adequately sampled sine wave, (b) Under-sampled sine wave.......................... 44
Figure 3-1 Schematic of the vertical experimental setup (Sharma et al., 2020) 46
Figure 3-2 Top drive assembly of experimental setup... 47
Figure 3-3 Comparison of downscaling factor of laboratory test rigs across the world (Srivastava and Teodoriu, 2019).. 49
Figure 3-4 Stick-slip period calculation vs. RPM for different strings....................................... 50
Figure 3-5 Torsional stiffness laboratory experiment 51
Figure 3-6 Experimental results for torsional stiffness tests... 52
Figure 3-7 Bit sticking of 1 second observed in drilling data sampled at 1Hz 53
Figure 3-8 Experimental test reproducing 1 second sticking at 1 Hz with string 1 (polyethylene 1) 53
Figure 3-9 Experimental test reproducing 1 second sticking at 1 Hz with string 2 (steel wire)... 53
Figure 3-10 Experimental test reproducing 1 second sticking at 1 Hz with string 3 (nylon) 54
Figure 3-11 Experimental test reproducing 1 second sticking at 1 Hz with string 4 (polyethylene 2) 54
Figure 3-12 Experimental test reproducing 1 second sticking at 1 Hz with string 5 (polyethylene 3) 55
Figure 3-13 Experimental test reproducing 1 second sticking at 1 Hz with string 6 (aluminum) 55

Figure 3-14 Electromagnetic brake (a) and its performance curve (b) 56
Figure 3-15 Schematic diagram of the horizontal well configuration 57
Figure 3-16 Experimental calibration of torque sensor 58
Figure 3-17 Experimental calibration of displacement sensor 58
Figure 3-18 Experimental calibration of load cell sensor 59
Figure 3-19 A snippet of the HMI (Human machine interface) for the experimental setup 60
Figure 3-20 Experimental design of torsional stick-slip test (Vertical configuration) 61
Figure 3-21 Experimental design of torsional stick-slip test (Horizontal configuration) 62
Figure 4-1 Mild stick-slip test, measured at 1 Hz sampling 65
Figure 4-2 Mild stick-slip test, measured at 10 Hz sampling 65
Figure 4-3 Mild stick-slip measurements, sampled at 100 Hz 66
Figure 4-4 Severe stick-slip measurements, sampled at 100 Hz 67
Figure 4-5 Severe stick-slip measurements, sampled at 10 Hz 67
Figure 4-6 Severe stick-slip measurements, sampled at 100 Hz 68
Figure 4-7 RPM response for mild stick-slip vibrations at 100RPM 69
Figure 4-8 Surface torque response for mild stick-slip vibrations at 100RPM 69
Figure 4-9 RPM response for severe stick-slip vibrations at 100RPM 70
Figure 4-10 Surface torque response for severe stick-slip vibrations at 100RPM 70
Figure 4-11 RPM response for mild stick-slip vibrations at 200RPM 71
Figure 4-12 Surface torque response for mild stick-slip vibrations at 200RPM 71
Figure 4-13 RPM response for severe stick-slip vibrations at 200RPM 72
Figure 4-14 Surface torque response for severe stick-slip vibrations at 200RPM 72
Figure 4-15 Mild stick slip at 0.5 kg WOB and 100 RPM 73
Figure 4-16 Severe stick slip at 0.5 kg WOB and 100 RPM 73
Figure 4-17 Mild stick slip at 0.5 kg WOB and 200 RPM 74
Figure 4-18 Severe stick slip at 0.5 kg WOB and 200 RPM 74
Figure 4-19 Mild stick slip at 1 kg WOB and 100 RPM 75
Figure 4-20 Severe stick slip at 1 kg WOB and 100 RPM 75
Figure 4-21 Mild stick slip at 1 kg WOB and 200 RPM 76
Figure 4-22 Severe stick slip at 1 kg WOB and 200 RPM 76
Figure 4-23 Self-induced vibrations for horizontal setup from 25-100RPM 77

Figure 4-24 Self-induced vibrations for horizontal setup from 125-200RPM 78
Figure 4-25 Self-induced vibrations for vertical setup from 25-100RPM.................................. 79
Figure 4-26 Self-induced vibrations for vertical setup from 125-200RPM................................ 80
Figure 4-27 Mild stick slip for vertical setup at 200 RPM 81
Figure 4-28 Severe stick slip for vertical setup at 200 RPM 81
Figure 4-29 Mild stick slip for horizontal setup at 200 RPM 82
Figure 4-30 Severe stick slip for horizontal setup at 200 RPM 82
Figure 4-31 Possible combinations of bit stick and slip phase 83
Figure 4-32 A stick slip cycle is shown for 0.1s slip and 0.5 s stick 83
Figure 5-1 Representation of drill string as a torsional pendulum (left) and block diagram 86
Figure 5-2 Schematic explanation of using experimental parameters as input for mathematical modeling 87
Figure 5-3 Programming mild and severe stick-slip vibrations using torque on bit sequence 88
Figure 5-4 Mild stick-slip at 100RPM 89
Figure 5-5 Mild stick-slip at 200RPM 89
Figure 5-6 Severe stick-slip at 100RPM 90
Figure 5-7 Severe stick-slip at 200RPM 90
Figure 5-8 Experimental vs. modeling result for severe bit sticking at 100RPM........................ 91
Figure 5-9 WellScan interface for stick-slip analysis 92
Figure 5-10 Conversion of laboratory parameters to single casing open well design 92
Figure 5-11 Vertical well profile based on vertical experimental setup 93
Figure 5-12 Horizontal well profile based on horizontal experimental setup 93
Figure 5-13 Process parameters used in WellScan computation 93
Figure 5-14 Comparison of three strings at 100 RPM 94
Figure 5-15 Comparison of three strings at 200RPM 94
Figure 5-16 Comparison of experimental results with PVC, Al and steel strings at 100RPM..... 96
Figure 6-1 Summary of machine learning applications of drillstring vibrations 98
Figure 6-2 Data quality issues and solutions during machine learning workflow on drilling data 100
Figure 6-3 Comparison of bit RPM at 1, 10 and 100 Hz sampling frequency measurement 101
Figure 6-4 Time window sampling visualization as a data labeling procedure 104

Figure 6-5 Frequency domain analysis of surface torque (left) and downhole accelerometer response (right) (Millan et al., 2019; Ignova et al., 2019) 108
Figure 6-6 Example of torsional oscillations (a), mild stick-slip (b) and severe stick-slip (c) vibrations, sampled at 100Hz 110
Figure 6-7 Comparison of test accuracies of different classifiers trained on data collected at different sampling frequencies 112
Figure 6-8 Comparison of label distributions obtained using the two labeling techniques 113
Figure 6-9 Comparison of test accuracies of different classifiers trained on data labeled using two different techniques 114
Figure 6-10 Comparison of test accuracies of different classifiers trained on data obtained from different feature extraction techniques 115
Figure 6-11 Pairwise scatterplots for different statistical features using statistical features makes the data classes linearly separable 116
Figure 6-12 Test accuracy and F1 scores for different classifiers trained on data containing imbalance 118
Figure 7-1 Plot of SSI and STS for mild vs severe sticking at 1, 10 and 100 Hz sampling 119
Figure 7-2 Comparison of stick slip index (SSI) and surface torque index (STS) for mild vs severe vibrations at 200RPM 120
Figure 7-3 SSI comparison for effect of RPM (a) and WOB (b) on mild vs severe stick-slip vibrations 121
Figure 7-4 Comparison of bit sticking period (a), SSI (b) and STS(c) for vertical vs horizontal well profile 122
Figure 7-5 Comparison of stick-slip index (SSI) and Surface Torque Severity (STS) for Vertical vs Horizontal configuration 123
Figure 7-6 Comparison of SSI for stick and slip combinations at 200RPM 124

List of Tables

Table 1 Summary of experimental test rigs for investigating drillstring vibrations 22

Table 2 (Continued) Summary of experimental test rigs for investigating drillstring vibrations . 23

Table 3 Summary of vibration detection tools 40

Table 4 Downscaled design parameters for PVC drill pipe (Srivastava and Teodoriu, 2019) 48

Table 5 Summary of drill string materials and their properties 50

Table 6 Parameter input values for modeling derived from experimental analysis...................... 87

Table 7 SSI comparison of vertical and horizontal configuration for PVC, Al and Steel for 100 and 200 RPM 95

Table 8 Summary of machine learning applications for drillstring vibrations 99

Table 9 Number of samples collected from each of the three experiments at different sampling frequencies 109

Abstract

Drilling technologies have improved considerably since the first well drilled by Colonel E.L Drake in 1859 (Giddens, 1945). Drilling technologies enable us to safely drill complex well profiles with advanced downhole tools and sensors to reach target zones faster. However, some of the basic inefficiencies in the drilling system have been consistent with time. Drilling vibrations is just one such example. The process of drilling rock involves transfer of energy from the top drive motor to the bit. Naturally, vibrations are inevitable during drilling and cause a reduction in the rate of penetration. While the understanding and mitigation of drilling vibrations has improved, the complexity of drilling conditions has considerably increased as well. The study identifies the different modes of drilling vibrations and presents a comprehensive review of the different methodologies to study and investigate them. The broad topics included in the study are:

a. Types of drilling vibrations and their effects on drillstring
b. Mechanisms of failures induced by drilling vibrations and ways to mitigate them
c. Detailed literature review, specifically gap analysis in cause, detecting and measuring
    a. drilling vibrations with respect to experimental investigation
d. Overview of drillstring mechanics concept related to drilling vibrations
e. Review of techniques to mitigate drilling vibrations
f. Compare and evaluate different data acquisition (sampling rates) concepts for vibration
    a. evaluation with experimental results
g. Definition and quantification of the stick slip vibrations
h. Parametric analysis of stick-slip vibrations using experimental test setup
i. Comparison of experimental and modeling results for examining stick-slip vibrations
j. Data driven technique to classify vibration severity of stick slip vibrations

With the above-mentioned different approaches taken to examine drilling vibrations, especially stick-slip vibrations, a deeper understanding of this severe form of torsional vibrations is achieved. With experimental results, it was observed that both drillstring properties (stiffness, inertia) and drilling properties (RPM, WOB, TOB etc.) influenced the severity of stick-slip vibrations downhole. PVC was observed to have the highest stick-slip severity out of different drillstring materials chosen due to its lower torsional stiffness. Additionally, the sampling rate of the measurements significantly impacted diagnostics of stick-slip vibrations. 10 Hz of sampling is the

minimum operational sampling rate advised for reliable downhole vibration diagnostics. Moreover, 100 Hz is the ideal sampling rate for complete diagnostics of stick-slip vibrations. The modeling results were in tune with experimental results and provided a fast method to analyze sensitivity of properties such as drillstring stiffness, friction, well angle, bit aggressivity etc. After successfully characterizing stick-slip vibrations using modeling and experimental approach, classifiers were built using machine learning algorithms that were hugely successful in isolating severe downhole vibrations from mild ones. These models were trained on the high-resolution experimental datasets and the issues related to data quality for machine learning applications are also highlighted. It is observed that high resolution dataset improves accuracy of vibration severity classifiers used. Additionally, adding spectral features contribute to an average 5% increase in performance whereas statistical features account for greater than 15% model improvement.

Overall, a comprehensive understanding of severe torsional vibrations has been gained in this study which can be used in the field for better diagnostics, characterization, and mitigation of stick-slip vibrations.

Chapter 1: Introduction

The process of drilling involves transfer of rotational energy from the surface to the bit along the drillstring. With advancements in drilling technologies, the industry is moving towards deeper formations that have low drillability and high rock strength (Zhu et al., 2014). To maintain the target rate of penetration and drill safely with lower incurred cost, process parameters such as RPM, weight on bit (WOB) and torque are monitored and optimized. However, due to the nature of the drilling process, drilling vibrations are unavoidable. Drilling vibrations can be axial, lateral, or torsional in nature and often coupled in most cases. Stick-slip vibrations, a severe form of torsional vibrations is one of the most harmful forms of drilling vibration. It increases drilling cost and is reduces rate of penetration (ROP) and downhole tool life (Navarro-Lopez and Suarez, 2004) This study aims to investigate stick-slip vibrations for a deeper understanding of its influencing factors and to develop its effective measurement and monitoring strategy. This chapter introduces the study by looking into the background of vibrations and discusses the methodologies used in the study. Furthermore, the research objectives are defined, and the dissertation outline is presented.

1.1 Background

Vibrations are to-and-fro motion of an object around an equilibrium position. The drillstring has mass and elasticity due to its length in the well. Disturbances to the drillstring are caused due to non-linear friction along the length of the string as well as due to the process of cutting rock, which is destructive in nature (Patil and Teodoriu, 2013). These disturbances are excitations that cause unavoidable vibrations in the drillstring. For classification, drill string vibrations can be grouped into three modes/directions. Namely lateral, axial, and torsional vibrations. These vibration modes are often coupled in the drillstring (Dong and Chen, 2016). Figure 1-1 shows the three modes of vibrations in the drillstring along the three different axes. In the following section, the modes of vibrations are discussed in further detail:

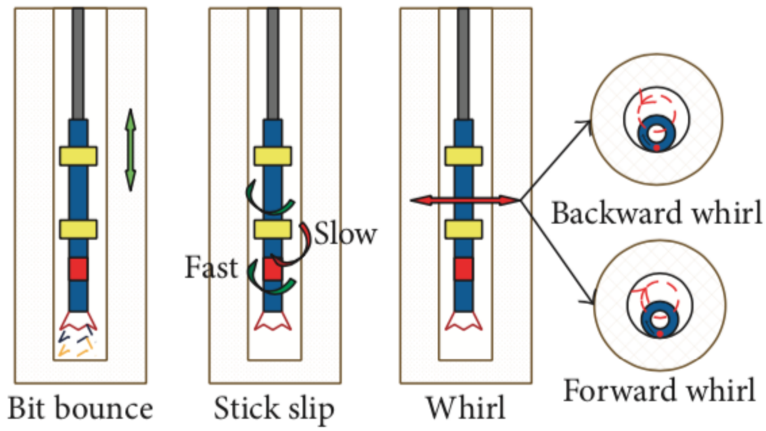

Figure 1-1-1 The different vibration modes in the drill string (Dong and Chen, 2016)

1.1.1 Lateral vibrations

Lateral vibrations are one of the most severe forms of drilling vibrations. The drillstring is subjected to sideways motion that causes bending stresses along the drillstring. Furthermore, the dynamic forces acting on the drillstring destabilize it and cause the bit and the BHA to rotate off center from the well axis. This phenomenon is also called whirling. Whirling can also occur due to imbalance in BHA design causing a slight shift of the center of gravity from the axis of the drillstring. Whirling was identified in 1989 through high-frequency downhole data and bit behavior (Brett et al., 1989). Whirling, occurring in the range of 20-60 Hz, is high frequency vibration and can be seen in figure 1. It can be classified as:

i. Forward whirl: In this whirling motion, the drillstring and the off-center drill bit rotation is in the same direction (clockwise) with different rotational speeds
ii. Backward whirl: In this whirling motion, the drillstring rotates clockwise whereas the off-center rotation of the drill bit is in anticlockwise direction
iii. Chaotic whirl: No defined direction of off-center rotation exists in this unstable whirling motion (Jansen, 1992)

Lateral vibrations are difficult to identify at the surface but with the inclusion of sophisticated downhole tools, forward and backward whirl conditions can be identified with a greater accuracy (Patil and Teodoriu, 2013).

1.1.2 Axial Vibrations

Axial vibrations involve the irregular movement of the drillstring in its longitudinal axis. Often recognized as bit bouncing, this vibration mode can reduce the overall efficiency of the drilling process by reducing contact between the bit and the formation. The use of tri-cone bit has often been related to the occurrence of axial vibrations due to the erratic interaction of the bit and formation with tri-cone bits (Kessai et al., 2020; Patil and Teodoriu, 2013). The resultant axial wave propagation can travel to the surface through steel pipes with speeds up to 16,850 ft/sec (Shyu, 1989). The typical frequency for axial vibrations is between 1 and 10Hz (Srivastava and Teodoriu, 2019). Axial vibrations are easy to identify for shallower depth, but it often gets coupled with other vibration modes downhole. For example, research has shown that axial vibrations excite lateral vibrations of the string (Kessai et al., 2020). In certain cases, axial vibrations are also introduced artificially through tools like drilling jars and agitators to help in stuck pipe situations and dampen severe torsional vibrations. The wide use of PDC bits in the industry today has given it the distinction of secondary drilling vibrations (Pastusek et al., 2007).

1.1.3 Torsional Vibrations

Torsional vibrations are the most severe form of drillstring vibrations (Lines, 2013). As the rotational energy is imparted to the string at its surface, due to non-linear friction between the drillstring and wellbore and/or the bit and formation, the energy is not entirely transferred to the bit. This causes bit RPM fluctuations. Torsional vibrations of this mechanism range between 10-100Hz where fluctuations are mild in nature (Pastusek et al., 2007). Hence, stick-slip rotations are often identified by large fluctuations in downhole parameters. A severe form of torsional vibrations called stick-slip vibrations is a low-frequency torsional vibration (<2 Hz). Stick-slip vibrations are also associated to weight transfer issues during drilling long laterals and deep wells. There is also reduction in rate of penetration and hole quality during this process.

1.1.4 Mechanism of drillstring failure

After understanding the different modes of drilling vibrations in the drillstring, it is crucial to further understand the extent of downhole issues caused due to these vibrations. While inefficiencies like rate of penetration reduction and hole quality issues can be dealt with during drilling, failure of drillstring and the associated downhole components can be expensive and hard to deal with. Even though drilling vibrations are inevitable, highly severe drilling vibrations have a detrimental effect on the drillstring. Since drilling vibrations are not always recognized at the surface, downhole measurements are necessary to quantify its severity. Figure 1-2 shows the classification of normal, moderate, and severe vibrations based on accelerometer readings. The drillstring undergoes a variety of dynamic forces during drilling. Further classification is based on prominent failure modes.

Lateral Acc		Lateral RMS Acc		Stick-Slip	
(g's)	Severity Level	(g's)	Severity Level	(-)	Severity Level
0-15	Normal	0-2.5	Normal	0-0.5	Low
15-35	Moderate			0.5-1	Moderate
35+	Severe	2.5+	Severe	1+	Severe

Figure 1-2 Severity level of vibrations based on accelerometer readings (Dushaishi et al., 2015)

Fatigue failure

A majority of drillstring failures fall under this category. Fatigue failure is characterized by weakening or crack propagation in a material due to cyclic loading (Lines, 2013). As seen in figure 1-2, estimating the severity of downhole vibrations helps understand the extent of stress loading in the system. Higher stresses often cause failure within low number of load cycles. Axial vibrations are longitudinal in nature causing cycles of tension and compression in the string (Millan et al., 2019). Stick-slip vibrations result in huge amplitudes of torsional oscillations in the drillstring. Bit RPM cycling is also very common with high amplitudes of fluctuation (Shen et al., 2017). This causes fatigue in drill downhole connections and drill collars.

Impact failure

Impact failure occurs in the form of deformations and fractures, often due to sudden shocks or collision in the system. Lateral vibrations are responsible for large lateral shocks between the BHA components and the wellbore. This can lead to tool failure and fractures in the BHA. Severe axial vibrations cause bit bouncing phenomenon which can lead to bit-formation collision damage, especially in hard formations. Spalling is another mode of impact failure that is observed in severe stick-slip vibrations when the bit rotation direction gets reversed for a short duration. This induces sudden stress development causing diamond to chip off from the cutter surface (Pastusek et al., 2007).

Bending failure

Bending failure is most observed in severe whirling conditions. Backward whirl, as explained in the previous section, causes the bit rotation axis to move in the opposite direction of the drillstring rotation. This induces high magnitude bending moment in the BHA (Christian, 2017). The bending moment occurs at both high frequency and amplitude causing flexural stresses in BHA components.

1.2 Problem Definition

Like every mechanical system, the process of drilling rock is not completely efficient. Drilling, being a destructive process is nature is accompanied by vibrations at the bit and along the drillstring. In the previous section, different modes of vibrations were introduced. However, the rest of the dissertation will focus on investigating stick-slip vibrations, a severe form of torsional oscillations. This section defines the problem at hand, which is stick-slip vibrations. An index to measure its severity is also defined.

1.2.1 Stick-slip vibrations

Stick-slip vibrations are essentially severe torsional oscillations. They occur when the rotational energy in the string is not sufficient to overcome the torque at bit. This phenomenon is called stick-slip vibrations because two distinct phases of bit sticking and slipping exist. While the top drive continues to provide rotational energy, the bottom section of the string stops momentarily due to high bit torque. This causes a buildup of torsional energy in the drillstring which is released suddenly causing a spike in bit RPM (Zhu et al., 2014). Figure 1-3 shows three cycles of stick-slip vibrations in which a period of stick, characterized by 0 RPM is followed by a period of slip, characterized by high RPM. In this case, bit RPM can be seen to reach 4 times the surface ROM. Interestingly, one can observe how stick-slip vibrations are rarely observed at surface making these vibrations extremely difficult to monitor. The surface RPM remains constant throughout the stick-slip cycles.

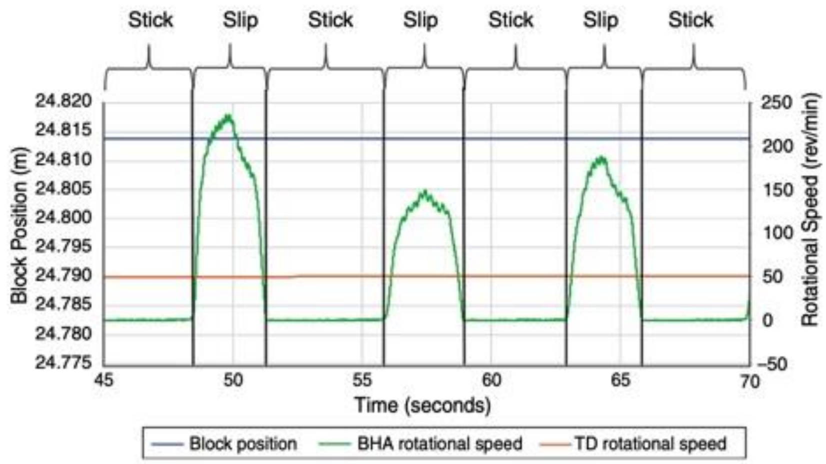

Figure 1-3 Successive stick-slip cycle events during off-bottom conditions (Cayeux et al.,2021)

If not monitored or diagnosed, stick-slip vibrations can lead to a variety of issues (Shen et al., 2017):

1. Damage to downhole tools, BHA components and bit
2. Loss in rate of penetration (ROP)
3. Drillstring fatigue failure due to constant torque loading and unloading cycles
4. Poor wellbore quality
5. Poor directional control
6. Increased overall drilling cost

1.2.2 Stick-slip severity

For stick-slip diagnostics and monitoring, the severity of the vibrations needs to be quantified. In context of torsional oscillations, two methods are popularly used for vibration severity estimation—accelerometer readings and Stick-Slip Index (SSI). Figure 1-2 helps distinguish the low and moderate (0.5 – 1g) vibrations from severe (>1 g) vibrations. However, accelerometer readings are not completely reliable since vibration modes are often coupled and have other sources of noise in the system.

Stick-Slip Index on the other side is an industry standard method that normalizes the RPM fluctuations over a time period and is defined as (Patil, 2013, Ertas, 2014):

$$SSI = \frac{Bit\ RPM_{max} - Bit\ RPM_{min}}{2 * Bit\ RPM_{avg}} \quad \text{.............................}(1\text{-}1)$$

As a result, when SSI = 1, it represents a pure stick-slip signal where the bit RPM fluctuates between 0 and at least twice the surface RPM. When $1 > SSI > 0.5$, this represents torsional vibrations and when $0 < SSI < 0.5$, weak torsional vibrations or smooth drilling are represented.

In conclusion, stick-slip vibrations are bad for drilling. Moreover, characterizing this severe mode of vibration is a complex task. The dissertation aims to provide a deeper understanding of stick-slip vibrations through an experimental, modeling and data driven approach. In doing so, the influence of drilling, drillstring and data acquisition parameters will be investigated in great depth. The stick-slip severity index will be used to compare effects of various influencing parameters.

1.3 Research Methodology

The ultimate objective of the study is to have a comprehensive understanding of stick-slip vibrations and the various influencing factors. The study focuses on pure uncoupled torsional vibrations. The various influencing parameters included for stick slip analysis are:

1. Rotational speed (RPM)
2. Weight on Bit (WOB)
3. Bit aggressivity (TOB/WOB)
4. Drillstring stiffness
5. Bit sticking period
6. Well configuration (vertical vs. horizontal)

The approach for stick-slip vibration investigation is divided into the following three methods:

1.3.1 Experimental analysis

While analytical and numerical modeling provide quick results, they come with a level of uncertainty (Ghasemloonia et al., 2015). Additionally, many input variables are unknown or not available while running the drillstring models. This has led to the development of experimental set ups that provide data for finetuning many bit-interaction models. Moreover, experiments, when properly scaled, provide a reliable estimation of downhole response to changing drilling parameter (Srivastava and Teodoriu, 2019). In this study, experiments are carried out in the drilling vibrations lab at the University of Oklahoma. This 15m setup is one of the largest downscaled experimental setups in the world dedicated for stick slip analysis. The setup is run with an advanced data acquisition system and continuously measures and displays data from surface and downhole sensors. The influencing factors in the experimental analysis include surface RPM, WOB, bit sticking frequency, bit torque, sampling rate for data acquisition, well configuration and drillstring stiffness. To account for the variations mentioned, approximately 1500 experimental tests have been planned and executed successfully throughout the duration of this study.

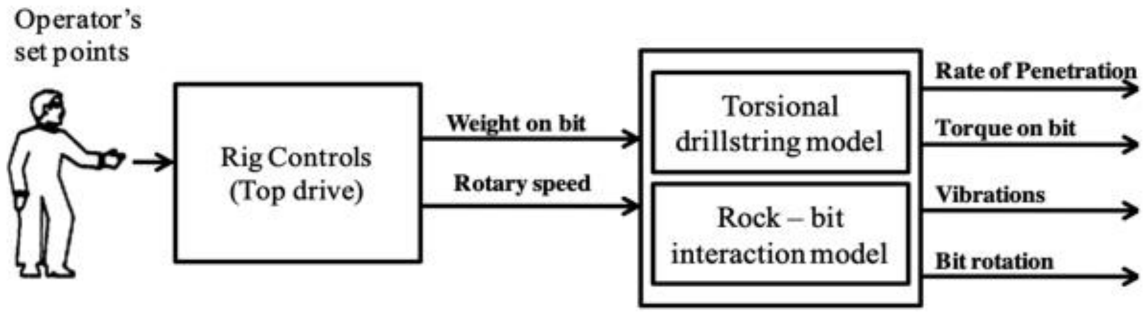

Figure 1-4 Modeling torsional vibrations (Patil and Teodoriu, 2013)

1.3.2 Modeling of drillstring vibration

Model based analysis is a widely used technique for investigating drilling dysfunctions (Márquez, 2015). In pre-drilling investigations, numerical studies can help estimate severity of downhole vibration, effect of BHA design on resonant frequencies and bending stress estimation to name a few. If vibration damping tools are to be utilized for drilling, modeling techniques can help finetune the tool parameters by quick sensitivity analysis. For this study, a lumped parameter model is used to replicate experimental parameters and confirm dependencies of drilling parameters like RPM, surface torque, drillstring stiffness and weight on bit on induced vibrations in the system. The model is solved in MATLAB Simulink. Figure 1-4 illustrated the model-based analysis that includes a motor drive, torsional pendulum drilling model and a rock-bit interaction model that provides a dynamic downhole response. Additionally, WellScan, a software for modeling drilling dynamics is utilized to model experimental parameters and run sensitivity analysis on process parameters like RPM, WOB, friction co-efficient, bit aggressivity and torsional stiffness. A combination of approximately 150 modeling tests were performed in WellScan throughout the course of this study.

1.3.3 Data driven analysis

Another popular and upcoming technique for drilling vibration analysis is the use of data driven models in field applications (Gupta et al., 2019; Ignova et al., 2019; Hegde et al., 2019; Srivastava et al., 2021). Although data acquisition has greatly advanced, we are still limited to post drilling analysis of huge datasets. This presents an exciting opportunity for training complex data driven methods for both classification and prediction of downhole vibrations. Using unsupervised machine learning techniques, drilling data can be clustered into groups based on downhole responses to characterize formations being drilled, vibration modes induced or simply to understand optimal drilling zones (Christian, 2017; Hegde et al., 2019). Classification of drilling vibration severity is also a popular machine learning task that helps identify the severity of downhole vibrations during drilling based on accelerometer readings (Ignova et al., 2019; Chen et al., 2020). In this study, classification of vibration severity is assessed using the comprehensive experimental datasets. The impact of data sampling, manual vs automatic labeling and choice of classifier on classification accuracy is analyzed. By estimating drilling vibration severity at a given depth, one can better understand reasons for BHA tool wear and damage (Srivastava and Teodoriu, 2020).

1.4 Research Objectives

With the approach of experimental, modeling and data driven analysis, the aim of this study is to investigate stick slip vibrations and the various influencing parameters. These parameters include surface RPM, WOB, drillstring stiffness, bit sticking frequency and well configuration. The research objectives of this study include:

1. To develop an experimental setup that helps in identifying the influence of process parameters on severe torsional vibrations and to reliably detect them at the surface for early diagnosis
2. To identify the effect of drillstring stiffness on severe torsional vibrations
3. To compare different data sampling rates for surface and downhole measurements and its effect on estimation of stick-slip severity
4. To finetune a mathematical model of the drillstring using experimental parameters and compare the results with experimental data
5. To classify vibration severity using machine learning algorithm on experimental data

1.5 Research Hypotheses

The research hypotheses include:

1. Higher sampling frequencies of measurement improves estimation of downhole stick-slip severity
2. Higher torsional stiffness drillstring provides more resistance to downhole vibrations

3. Horizontal well configuration is prone to higher self-induced bit sticking
4. Period of bit sticking and slipping has an impact on severity of stick-slip vibrations
5. Higher quality of drilling data improves classification of downhole vibration severity

1.6 Dissertation Outline

This study explores the research objectives listed above for a deeper understanding of stick-slip behavior. This chapter introduced drilling vibrations in general before diving deeper into defining stick-slip vibrations and its severity index. The research methodology was explained followed by the objective of the study. The next chapter provides literature on existing experimental setups for drillstring vibration analysis. In doing so, gaps in experimental studies are highlighted. Literature review is also provided on modeling of drilling dynamics ranging from simple-low fidelity models to complex-non-linear models. Chapter three introduces the experimental design and discusses the components of the experimental setup including sensors, data acquisition, drillstring material and the design of experiments in great detail. Chapter four presents the findings of the experiments and evaluates the influence of different process parameters by comparing the severity of torsional vibrations. Chapter 5 presents the results of modeling the system in MATLAB Simulink and WellScan. The results are confirmed by comparing it with the experimental data. Chapter six presents machine learning methods used for diagnosis of drilling vibrations and compares performance of different classifiers in identification of severity of stick-slip vibrations using experimental data. In doing so, the chapter addresses the importance of data collection, pre-processing, and model training. It also explores how high-resolution data, obtained from high sampling measurement helps in enhanced classifier performance. Chapter seven discusses the results from different approaches used in the study and presents important takeaways from the study. Lastly, chapter eight states the conclusions and future scope of work for this study.

Chapter 2: Literature Review

Torsional vibrations and its eminent impact on drilling performance has been the source of continuous diagnosis and investigations. In the last 50 years, stick-slip vibrations have been studied extensively (Raymond, 2008) using modeling techniques, field trials, experimental setups, vibration mitigation tools and now, through machine learning models. This section discusses the different approaches in literature for characterizing stick-slip vibrations in detail.

2.1 Experimental Studies on Drillstring Vibrations

The dynamics of drillstring vibrations are very complex. Numerical and experimental study of drilling dynamics has attracted interest since decades (Raymond, 2008). Significant progress has been made to improve the complexity of the drillstring models to incorporate dynamic interactions between the bit and the formation, drillstring bending and twisting, drillstring-wellbore friction to name a few. Such high-fidelity models have always required field data validation for finetuning. Experimental Rigs have existed in the past that were designed for isolating and testing of drilling phenomenon with full-scale parameters. For example, while other parameters can be estimated through literature, friction models need field data for accurate predictions (Pavone et al., 1994). However, in the long run, although field experiments helped in providing an insight into drill string's dynamic behavior, they proved to be costly, time consuming and difficult to carry out (Westermann et al., 2015). Laboratory experimental rigs provided an alternative opportunity to study downscaled drill-string dynamics (Westermann et al., 2015). The advantages of a laboratory downscaled setup included economic viability, easy repeatability of downhole testing conditions, increased safety due to lower spinning energy in the string and easy access to both downhole and surface parameter measurements (Srivastava and Teodoriu, 2019). This study aims at identifying and comparing the different components of an experimental test rig, evaluating the testing conditions for different vibration modes and finally, gaining an understanding of the need for accurate downscaling.

Understanding the various rig components is essential before comparing them. The components include the structural framework of the rig, the top drive or the motor, drill pipe, bottom hole assembly and the data acquisition system. The frame of the rig contains the top drive mechanism. The top drive includes an electric motor that transfers rotational energy to the drillstring. Based on the testing application, the system has various bottom hole assembly configurations. The data acquisition system integrates the various sensors in the top drive, drillstring and bottom hole assembly to help measure and analyze the dynamic properties of the vibrational modes. A summary of the downscaled test rigs used for vibrational study has been included in table 1 and 2. The reported parameters include drill string length and diameter, stiffness co-efficient, setup inclination, top drive, bottom hole assembly and rock-bit interaction mechanism. The following section discusses the components of the drill string in greater detail and presents a comparison between the test rigs discussed.

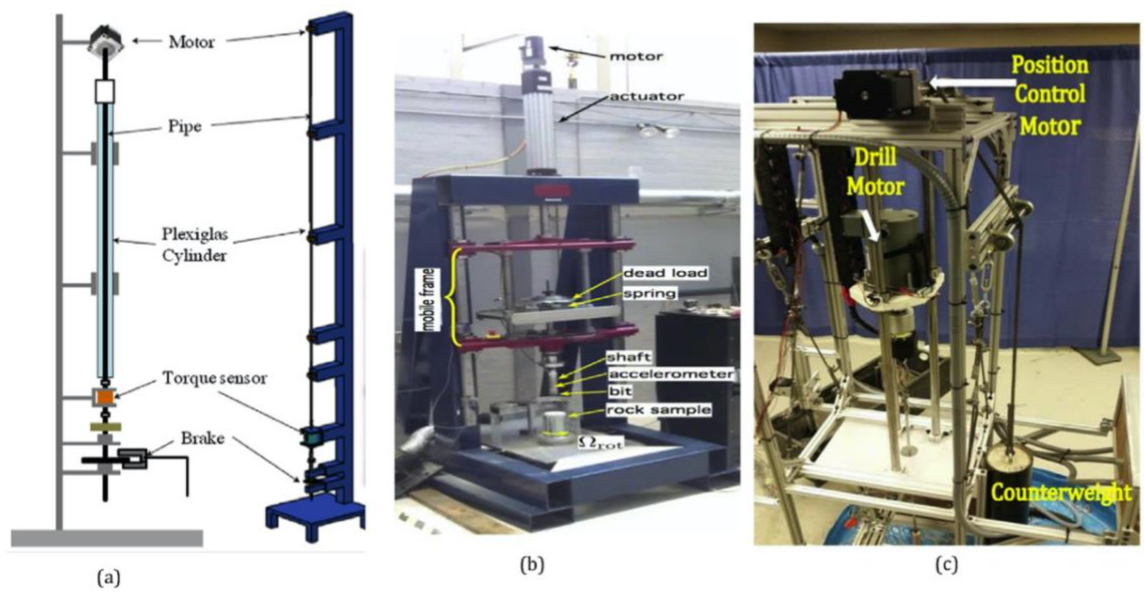

Figure 2-1 (a) Test rig for torsional vibrations (Patil and Teodoriu, 2013) (b) Torsional vibration study by drilling rock sample (Kovalyshen, 2014) and (c) Automated drilling dysfunction mitigation test rig (Bilgesu et al., 2017)

2.1.1 Structural framework of test rig

The different structural rig frameworks help study the drilling vibration mode of interest—coupled or uncoupled. Figure 2-1 displays the three different structural design configurations of test-rigs used for drilling vibration study. In case (a), a rigid frame is chosen to study torsional vibrations in the string by keeping lateral constraints on the string. In case (b), by using actuator run system, a rock sample is drilled by the rig and the torsional and axial measurements are recorded. In case (c), the position control system and motor are housed at the top of the rig to remove limitations of both axial and lateral vibrations. These design of vibration test-rigs are discussed further in the top drive section.

2.1.2 Top drive assembly

Top drive assembly is one of the most integral sections of a test-rig. It provides torque to the drill string through an electric motor as well as provides a weight on bit mechanism. Based on the literature study, DC motors, servomotors and positive displacement motors are chosen for providing the rotational energy to the string. The choice of top drive motor is integral to the study of drillstring vibrations. Rotary encoders are commonly used for precise downhole measurements. In such cases, to reduce system noise, a DC motor is preferred over others due to its smooth torque transfer capabilities. The characteristics of a DC motor is explained in equation 2-1 where the power provided by the torque remains constant. Since there is no holding torque in the system, the rotor is free to rotate unlike a stepper motor.

$$Power_{DC} = Torque\ X\ RPM = constant\ T \quad \ldots\ldots\ldots (2\text{-}1)$$

Servomotors provide a stepwise movement capability which is needed when dealing with actuators in the rig design as seen in figure 2-1 (b). This movement aids in the application of weight on bit on the system. A positive displacement pump is used for high power applications and its usage in a laboratory scale test rig is rare, as observed in literature review. However, there is an instance of using this kind of motor in literature for a slightly bulkier rig setup (Raymond et al., 2008). In terms of position control, an additional motor can also be utilized for controlling a counterweight that acts as a weight on bit device. In conclusion, the DC motors remain the most widely used electric motor for vibrational study of rotating drillstring.

2.1.3 Rig configuration

In the world of laboratory test rigs for study of drillstring vibrations, most configurations are vertical in nature. Out of these vertical setups, the longest setup is about 5 meters in length (Patil and Teodoriu, 2013). The size limitations are relaxed when horizontal/deviated setups are utilized for measuring vibrations. Up to 25 meters long horizontal setups exist for vibrational study (Lin et al., 2018). Longer strings help in maintaining a practical downscaling ratio. Since all wells nowadays have a fair amount of deviation in the well design (if not horizontal), there is need for laboratory test rigs that are more versatile than basic vertical setups. A few of the non-vertical test rigs are summarized in figure 2-2. Figure 2-2 (a) displays the 25 meters horizontal test-rig with 5-inch drill pipe. This system can measure all three modes of vibrations. In case (b), an interesting rig design is presented that aims to automate a laboratory scale rig. Issues of torque fluctuations, weight transfer, pressure losses with deviated wells are studied in this setup (Cayeux et al., 2017). While case (c) aims to study lateral vibrations for a highly deviated well design, case (d) helps investigate the torsional vibrations in a horizontal well profile. More information on the testing parameters, the rock-bit interactions and downscaling of the setups mentioned has been included in the next section.

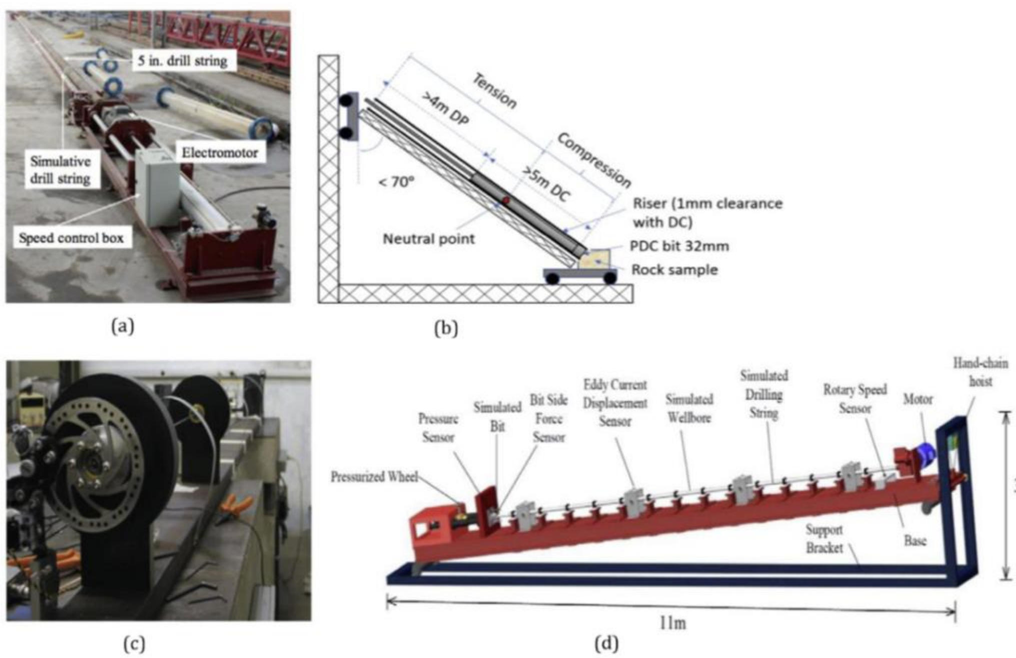

Figure 2-2 (a) 25 m horizontal test rig (Lin et al., 2018), (b) Automated test rig (Cayeux et al., 2017), (c) Torsional analysis in horizontal setup (Cayres, 2015) and (d) Lateral vibration study in 79^{O} deviated well (Wen et al., 2018)

2.1.4 Drill String

The drillstring's physical properties—length, material, torsional stiffness, diameter etc. play a pivotal role in drillstring vibrational analysis. The primary purpose of this comparison is to ensure a standard for downscaling and to analyze the effectiveness of choosing a drill string material for the vibration study.

Downscaling factor

One of the most overlooked yet important aspect of having results like field testing is to have a defined downscaling factor for the experimental design. In an ideal state, a complete similarity is needed between the field and laboratory testing conditions. A complete similarity includes defining a scaling factor for geometric, kinematic, and dynamic parameters of the drill pipe (Westermann et al., 2015). The downscaling factor n is defined as a geometric similarity ratio of length of experimental drill pipe to length of an actual drill pipe ($n = L_{exp} / L_{actual}$). Length of the drillstring can have an impact on the experimental outcome (Tang and Zhu, 2019). Maintaining an overall downscaling for parameters like moment of inertia of BHA, torsional stiffness of drill pipe etc. helps in reliable study of kinematic and dynamic properties of the drill pipe. In the case of laboratory test rigs that are downscaled from actual drilling, the limiting factor is often the diameter of the drill pipe. After careful evaluation of the drill pipe length used by various setups, downscaling 450m of actual drill pipes makes for a reasonable downscaling ratio. Downscaling drill pipe of length smaller than 450m would reduce drill pipe diameter to an unachievable value. Furthermore, if similar materials are used for downscaling, certain parameters like modulus of elasticity and density do not change. Other must be estimated using the principle of similarity. Figure 2-3 lists and compares the various downscaling factors of laboratory test rigs reported in literature for a drill pipe of length 450m. Ratios lower than 1:225 would make geometric downscaling close to impossible with respect to the drill pipe diameter requirement. Such thin pipes will fail to reciprocate the desired mode of vibration during experimental testing. As observed in figure 2-3, only a handful of experiments have a reasonable downscaling ratio, for

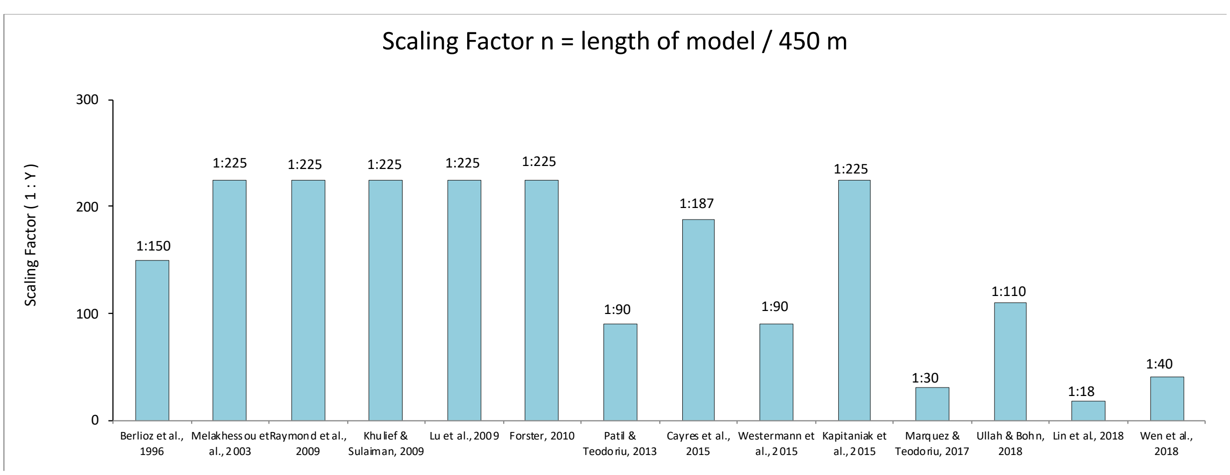

Figure 2-3 Comparison of downscaling factor of laboratory test rigs across the world (Srivastava and Teodoriu, 2019)

example, 1: 90 (Patil and Teodoriu, 2013; Westermann et al., 2015), 1:40 (Wen et al., 2018), 1:30 (Marquez and Teodoriu, 2017) and 1:18 (Lin et al., 2018). In conclusion, the reporting of downscaling factor as well as its reference field scale length should be encouraged in the experimental design section. In doing so, the objective of the experimental tests can be better understood. For example, when dealing with lateral vibrations, the need for accurate downscaling is essential because the nature of lateral vibrations is along the entire length of the string. In such cases, a one meter downscaled setup would not be able to reciprocate the slenderness of a long drill pipe undergoing severe whirling. Knowing that complete downscaling is extremely difficult to achieve, understanding and clearly stating the objectives of the experiment will help immensely in selecting the parameters for optimal downscaling.

Drill pipe material

The drill pipe material selection process depends upon the experiment's objective. Steel, aluminum, and PVC are three different reported drill pipe material in literature. Steel/aluminum drill pipes are often used when the experiment uses a bit to drill rock samples. In such cases, higher rigidity and stiffness of the material is needed. In cases when experiments are designed to study the dynamic behavior of the drillstring and use a brake system instead of actual drilling, the PVC material provides a more dynamic range of motion. Some experiments also opt to use interchangeable drill pipe materials for having a flexible testing condition (Kapitaniak et al., 2015). The study also utilizes a flexible shaft in the experiment made up of multiple wire layers that aid in better inter-string friction and overall torque transfer capabilities (Figure 2-4 (a)).

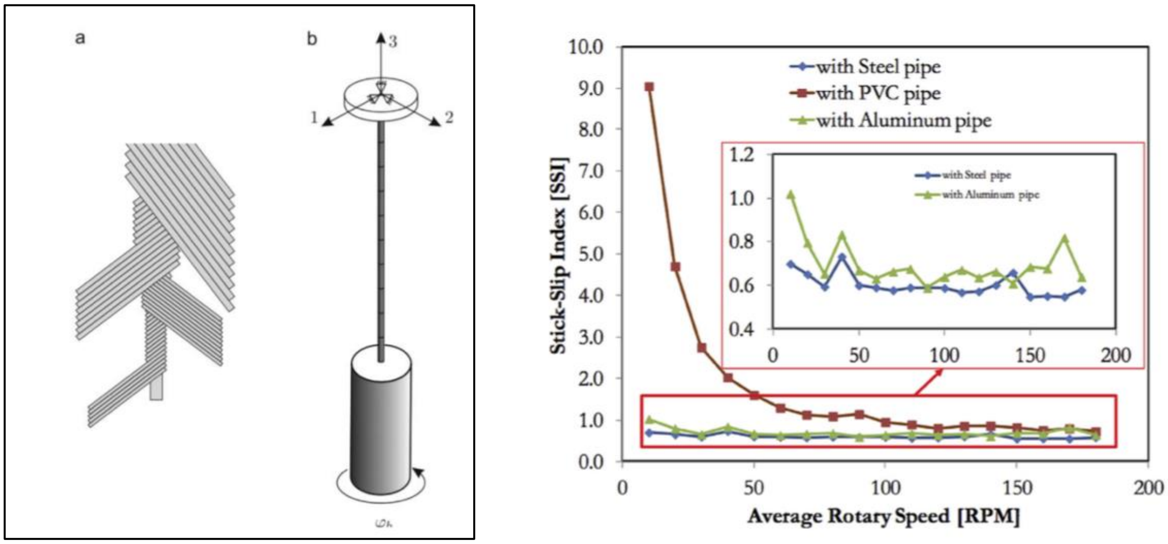

Figure 2-4 Using a flexible shaft (a) and shaft dampening for torsional vibrations (b) (Left) (Kapitaniak et al., 2015) and comparison of stick-slip index for steel, aluminum, and PVC (Patil and Teodoriu, 2013)

Playing with pre-tension in the string is also a proven method to enhance certain vibration modes. Increasing it can readily help induce torsional vibrations while decreasing it can induce axial vibrations in the system (Forster, 2011). Patil and Teodoriu (2013) presented an interesting evaluation of torsional vibrations by comparing three different drill pipe materials to relate the torsional stiffness of the material to the stick-slip index at varying rotational speed. The lower torsional stiffness material was more prone to torsional vibrations than materials with higher stiffness. PVC was preferred over aluminum and steel as seen in figure 2-4 (b).

2.1.5 Bottom hole assembly (BHA)

The bottom hole assembly chosen for experimental analysis of drilling vibrations goes in sync with the rock-bit interaction system. Early investigation included a programmed shaker as the BHA to understand the coupling between axial and lateral vibrations (Shyu, 1989). However, to get a holistic understanding of drillstring dynamics, experimental test rigs included conventional components like drill bits and collars. An inertial mass disc is used in almost all cases to represent the drill collars and/or bit and its moment of inertia. In some cases, a small degree of off-centered mass is preferred to study the unbalanced effect of BHA design (Melakhessou et al., 2013). The bit is added to the BHA when a drilling component is included in the experiment. PDC bits are most widely used with one instance of using roller cone and milling bit each (Lu et al., 2009;

Franca, 2010). In cases where there is no drilling, a brake system is used to induce torque at the bit/inertial disc. The braking system and its advantages are explained in detail in the torsional vibration section.

2.1.6 Sensors and data acquisition system

Data acquisition includes optimal measuring, conversion, and sampling of measured signals. The data acquisition system integrates the sensors in the system and presents the parameter control mechanism for testing. The sensors used in an experimental test rig include load cells for weight measurement, torque sensors, top and bottom rotary encoders for precise RPM measurement, accelerometer for vibration estimation and displacement sensors. In some cases, sensors are places below the drilled rock sample to get an accurate estimation of weight and torque applied at the bit in X and Y axis. The complete data acquisition workflow with sensor integration is presented by Sharma et al. (2020). The importance of sampling rate of signals is presented in the latter section of the dissertation.

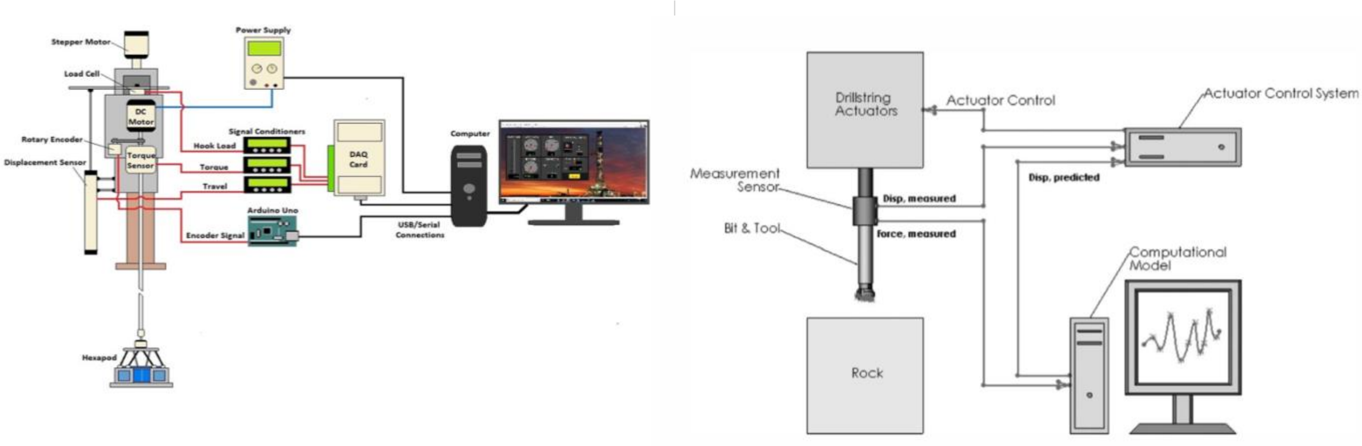

Figure 2-5 Examples of data acquisition and control systems for drilling vibration study (Sharma et al., 2020; Raymond et al., 2008)

Figure 2-5 (a) shows an example of system integration with a National Instrument DAQ and Arduino card. LabVIEW is chosen as the system design platform to collect, process and display sensor data through a human machine interface (drilling simulator). This enables a convenient control strategy for drilling parameter controls to support an elaborate testing matrix. Figure 2-5 (b) also shows a model-based control system for studying drilling vibrations. The heart of this system is the actuator control system. It accepts drillstring sensor measurements as input (displacement and force) to produce fast-acting actuator movement to simulate close to actual drilling conditions. The actuator response is controlled by the dynamic drillstring model.

2.1.7 Stick-slip Vibration Experiments

Since most of the included literature on drillstring vibration study includes analysis of torsional vibrations, the following section focuses on stick-slip experimental test-rig and its comparison. The rig components of a torsional setup are similar to the ones presented in the previous section.

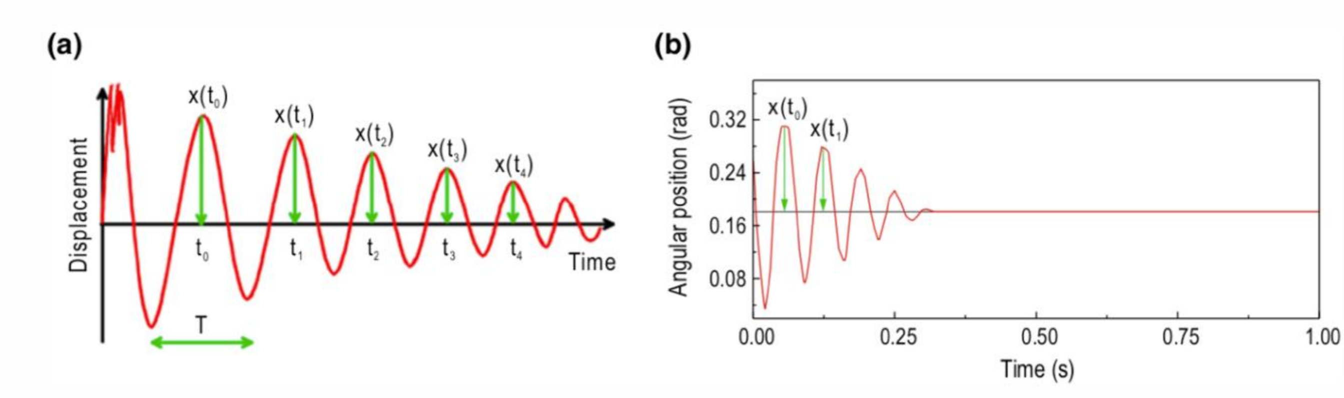

Figure 2-6 Decaying torsional oscillations (a) and angular position x(t) in radians (b)

The emphasis is more on the drill pipe material and its physical properties. The importance of having a proper downscaling of geometric and dynamic parameters has been emphasized before. The advantage of using PVC instead of steel or aluminum drill pipe for measuring stick-slip index has also been summarized in the previous section. Additional details regarding stick-slip experimental investigation include:

Parameter estimation

Estimating the parameters for a torsional vibration study is helpful in evaluating vibration response as well as testing under operational limit. The parameters that need determination include string damping constant, torsional stiffness, and torsion constants (Liu et al., 2017. A relatively flexible string is required for estimating these parameters. Hence, PVC or multiple layers of thin wire are suitable as the drill pipe material. Using a fast data acquisition system and a known torque, the angle of deformation as well as the decay of torsional vibrations is measured to calculate the essential parameters. The torsional oscillation decay is shown in figure 2-6 where x(t) represents the angular position of the bottom hole assembly shaft in radians. The calculated string properties are required to be in sync with the estimated string properties keeping the downscaled factor in mind. If not, the downscaling factor must be revised, and other parameters have to be adjusted accordingly. For example, as seen in Table 1, weight on bit is adjusted as $W_{real}/W_{exp} = n^{3.56}$. Thus, for a range of 0-50000lbf of real scale weight on bit, the experimental range is 0-0.275 lbf.

Rock-bit interaction for torsional vibrations

As discussed earlier, the rock-bit interaction system consists of either actual bits or a brake system. By using a random/controlled braking mechanism, a non-linear friction at bit is included in the experiment design. The braking mechanism used is either magnetic (non-contact) or friction induced (contact). In figure 2-7 (a), a magnetic brake is used. Magnetic brakes help in generating non-linear friction at bit (Khulief and Sulaiman, 2009). As seen in figure 2-7 (b), the rotating inertial wheel is subjected to brake pads, which is a dry friction breaking mechanism. The induced torque in the system introduces torsional vibrations. Using the same mechanism with lubrication between disc and brake pads, a smoother torque can be introduced in the system (Patil and Teodoriu, 2013; Mihajlovic et al., 2006). In case (c), a lubricated disc brake is utilized along with force measurements to control the friction at bit. In case of actual drilling, PDC, roller cone, milling and drag bits have been utilized to drill granite, limestone, sandstone, and wood (table 2 and 3).

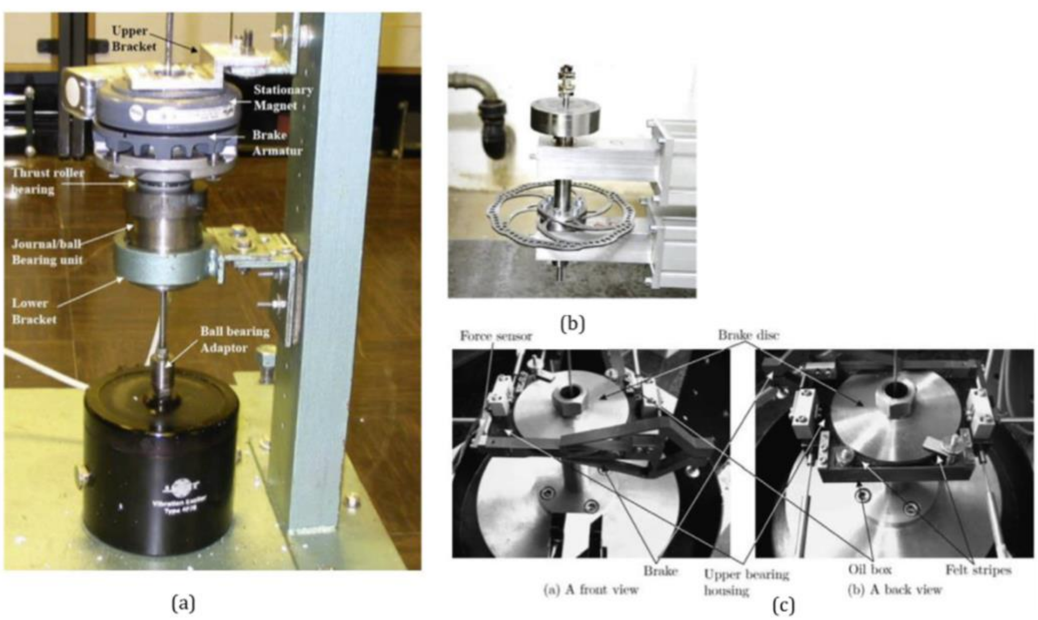

Figure 2-7 (a) Magnetic brake (Khulief and Sulaiman, 2009) (b) Torsional friction brake (Patil and Teodoriu, 2013) and (c) Lubricated disc brake (Mihajlovic et al., 2006)

The important lesson is here—although drilling a rock sample presents a closer to reality picture, the tests are not repeatable. It becomes extremely hard to single out any vibration mode for in-depth analysis. Magnetic or friction brakes on the other hand can be programmed and used for controlled testing.

Repeatability of testing conditions

Repeatability of experimental tests is crucial. It relates to measuring the deviation in vibration response under identical testing conditions. This requires standardization among procedures and optimizing error in sensor measurements. Operating parameters and drilling conditions must be maintained as well. In case of drilling of an actual rock sample, every test result is different. The task for analysis of drilling vibrations becomes cumbersome with multiple dependent variables, each with a margin of change. By ensuring repeatability, sensitivity analysis can be done on the setup by varying one or few dependent variables at a time. Furthermore, boundary conditions can be defined for the tests with a higher accuracy. This can help in finetuning a drilling optimization/advisory loop.

Ref	References	Research	Inclination	Scaling factor	Drillstring Length	Drillstring Diameter (OD)	Measured Vibrations	Testing Parameters	Stiffness Coeff	Top Drive	BHA	Rock - bit interaction
1	Shyu, 1989	To study coupling between axial force and bending vibrations	All inclinations		1 m	6.5 mm	Axial & lateral	N = 1.5 - 25 rps	-	Motor driven	Static cylinder	A function operated mini shaker
2	Antures, 1992	Analyzing rotatory shafts in dense fluid medium	Vertical		1.5 m	75 mm	Axial & lateral	N ≤ 700 rpm	-	Motor driven	Support plate	200N Electro mechanical shaker
3	Berlioz et al., 1996	Study lateral drilling vibrations	Vertical & Horizontal		3 m	2-7mm adjustable	Axial & lateral	N=150 rpm Axial τ = 0-10Nm Axial force 0-200 N	-	DC Brushless motor	Chuck assembly	Magnetic powder brake
4	Melakhessou et al., 2003	Study behaviour on contact of BHA will wellbore	Vertical		2 m	4mm	Lateral	N =180 rpm	Kr= 101.9 N/m Kt= 100N/m K_{TOR} = 1.371 N m/rd	DC Brushless motor	Inertial Disc R=10mm	Powder Brake
5	Mihajlovic et al., 2006	Friction induced limit cycling	Vertical		1.47 m	-	Torsional	20.5N ≥ Normal force at brake	K_{TOR} = 0.0775 N m/rd	DC motor	Inertial disc	Lubricated disc brake system
6	Raymond et al., 2009	Axial mode of drillstring dynamics	Vertical		≤ 2 m Actuator system	76.2 mm	Axial	N = 120-260 rpm W = 500 lb	26 compression springs * K=27lb/in	25 HP Positive displacement motor	Coring bit - 3-1/4 in with 3 PDC cutters	Drilling on white granite rock sample
7	Khulief and Sulaiman, 2009	Investigation of axial and torsional vibrations in both air and fluid filled annulus	Vertical		1-2 m	3 -10 mm	Axial & Torsional	N = 50-1000 rpm	-	DC motor with speed control	Drill string connected to brake armatur	Magnetic tension break and Vibration shaker both
8	Lu et al., 2009	Using WOB to control stick slip oscillation	Vertical		≤ 2 m	-	Torsional	W = 180N	K = 0.67 N m/rd	DC motor	Milling Bit	Drilling on cedar wood block
9	Forster, 2010	Study effect of compressive loading on AVDT tool	Vertical		2 m	5 mm	Lateral & Torsional	N = 330 rpm	-	12-30 V DC motor	Weighted block 1-3.5 kg	-
11	Franca, 2010	Drilling response of roller cone bit	Vertical		Actuator system	-	Axial	N = 10-400 rpm	-	Gearless & brushless servomotor	Roller cone bit	Limestone and sandstone rock samples
12	Forster, 2011	Investigation of axial excitation to reduce stick slip	Vertical		1.25 m	1 mm	Axial & Torsional	N = 100-150 rpm W = 5N	-	0-30 V DC motor	Inertial steel cylinder of D = 5 mm	Steel insert as well bore
13	Liao et al., 2011	Study drill string dynamics	Vertical		1 m	5 mm	Torsional	N = 400 rpm	K_{TOR} = 4.69 N m/rd	-	Drive motor	-
14	Esmaeilli et al., 2012	Investigation of drillstring dynamics	Vertical		0.524m Actuator system	40 mm	Axial	N = 120/240/360 rpm W = 80 Kg	-	5.2 kW Servo motor with pulley system	2in OD drill bit	Sandstone
15	Patil and Teodoriu, 2013	Study bit induced stick slip vibrations	Vertical		5m	4 mm	Torsional	N= 10-80 rpm	K_{steel}= 2.73 Nm/ rd K_{al}= 0.54 Nm/ rd K_{PVC}= 1.73 $X10^{-4}$ Nm/ rd	Stepper motor	Inertial disc	Torque braking system

Table 1 Summary of experimental test rigs for investigating drillstring vibrations

Ref	References	Research	Inclination	Scaling factor	Drillstring Length	Drillstring Diameter (OD)	Measured Vibrations	Testing Parameters	Stiffness Coeff	Top Drive	BHA	Rock - bit interaction
16	Kovalyshen, 2014	Understanding the cause of stick slip vibrations	Vertical		Actuator system	49 mm	Axial & Torsional	N = 10-400 rpm	K_{TOR} = 0.05 N m/rd	Servo motor	49 mm OD drag bit	Limestone
17	Cayres et al., 2015	Evaluation of dry - friction induced stick slip	Horizontal		2.4 m	3 mm	Torsional	N = 10-36 rpm	-	DC motor	Inertial wheel	Disc brake
18	Kapitaniak et al., 2015	Investigation of drillstring dynamics	Vertical		≤ 2 m	10 mm	Torsional	WOB = 0.85 - 2.19 kN N = 1370 rpm	Flexible shaft with K_{TOR}=5.2 Nm/rad	DC motor	Steel cylinder with PDC/tricone drill bit	Rock sample
19	Westermann et al., 2015	Measure wellbore contact force in a horizontal setup	Horizontal		5m	44.5 mm	Lateral, Axial & Torsional	RPM = 140	-	16W Drive motor	Steel cylinder	-
20	Bavadiya et al., 2017	Automated drilling rig	Vertical		0.9 m	9.5 mm	Lateral & Axial	WOB = 10-40 lfb N ≤ 850 rpm	-	1 HP DC motor	Two-blade PDC bit	Rock sample
21	Cayeux et al., 2017	Laboratory scale automated drilling rig challenges	Horizontal (< 70 deg)		1m	9.5 mm	Lateral & Torsional	W = 0.5 - 2.5 Kg	-	700W Stepper motor	PDC bit	Rock sample
22	Marquez and Teodoriu, 2017	Validation of torsional drillstring model	Vertical		15m	6-12mm	Torsional	RPM = 10-180	K_{TOR}=0.0001735 Nm/rad	Stepper motor	Inertial disk	Disc brake system
23	Bilgesu et al., 2017	Laboratory scale automated drilling rig challenges	Vertical		0.9 m	9.5 mm	Lateral & Axial	RPM = 200-900	-	375W DC motor	1.125" OD PDC bit	Rock sample
24	Ullah and Bohn, 2018	Surface control for reducing torsional vibrations	Vertical		4.1 m	6 mm	Torsional	-	-	Servo motor	Inertial metal disk	-
25	Zarate-Losoya et al., 2018	Mitigate downhole dysfunctions in automated drilling rig	Vertical		0.9 m	9.5 mm	Lateral & Axial	RPM ≥ 400		Motor driven	Two-blade PDC bit	Rock sample
26	Erik et al., 2018	Autonomous Laboratory drilling rig	Vertical		0.8 m	9.5 mm	Axial & Torsional	N ≤ 1500 rpm	-	DC Brushless motor	PDC bit	Rock sample
27	Lin et al., 2018	Study of vibration modes in horizontal drilling	Horizontal		25 m	12 mm	Lateral, Axial & Torsional	N = 200-500 rpm W =0.2 - 0.6 MPa	-	Motor driven	Cone bit	Rock sample
28	Real et al., 2018	Analysis of stick-slip vibrations	Vertical		≤ 2 m	-	Axial & Torsional	N = 300 RPM Torque = 8Nm	-	DC Brushless motor	Inertial disc + Concrete bit	Rock sample
29	Wen et al., 2018	Study lateral characteristics of drill string	Horizontal (79^0)		11 m	-	Lateral	N = 50-350 rpm W = 0.5 - 3 Kg	-	Motor driven	Simulated bit	Pressurized rock sample
30	Pires et al., 2019	Friction-Induced Vibrations in a Drill-String Experimental Set-Up	Horizontal		≤ 2 m	-	Torsional	N = 55 rpm Normal force = 35 N	Stiffness between disc and motor K=0.3659 Nm/rad	DC motor	Inertial disc	Disc brake

Table 2 (Continued) Summary of experimental test rigs for investigating drillstring vibrations

2.2 Modeling of Drillstring Vibrations

With advancement in MWD technologies, downhole data is readily available for real-time drilling parameter adjustment. However, downhole tools are both expensive and often subjected to severe drilling vibrations that lead to tool failure. This calls for using sophisticated drillstring vibration models that help in pre-drilling system analysis as well as downhole vibration control (Ghasemloonia, 2015). This report introduces soft string and stiff string models that are comprehensive torque and drag models used in the industry. The focus is then shifted towards popular methods used primarily for drilling vibration study. However, due to mud dampening, unpredictable rock-bit interaction, coupled vibrations, formation properties, friction etc., vibration models undergo a tradeoff between complexity and computational speed. Naturally, early models were uncoupled vibrations models to save computational time.

One of the first torque and drag model was developed by Exxon in 1980's (Johancsik et al., 1984). Popularly called 'soft string model', the model assumed zero bending stiffness in the string. As a result, the physics behind the model is based on continuous contact of drillstring with the wellbore. Rotation and axial movement of the string caused drag in the system. This can be observed in figure 2-8. Being fast and simple, the model is still being widely used in the industry. Major criticism for the soft string model—absence of radial clearance between the drillpipe and the wellbore. Assuming continuous contact, the model ignores the diameter variance between tool joints and different BHA components. As a result, no well bore contact calculations are made for buckling, fatigue, and stress failures.

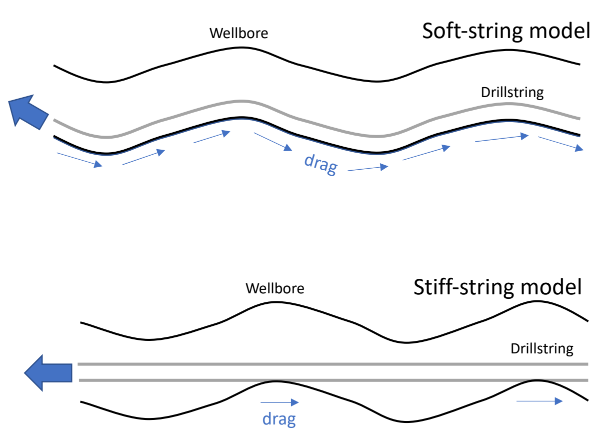

Figure 2-8 Soft string and stiff string model

To overcome these shortcomings, stiff-string models were developed. Initial models included addition of stiffness in BHA, while assuming the drill pipe to still be in continuous wellbore contact. Advanced models were developed that assumed stiffness in the entire drillstring by considering a beam element. The drillstring also considered no wellbore contact. The model calculated contact points for further dynamic analysis (Menand et al. 2006). The interaction of axial, lateral and torsional vibrations are also calculated in the model. However, the stiff-string models are currently limited to steady state motion of the drillstring. Dynamic transient motion, for example stick-slip vibrations are neglected (Tikhonov et al., 2013). However, stiff-string models are not widely used in the industry. Their biggest drawback is the model's computational complexity as even the fastest models require considerable computation time for each operation.

For investigation of drilling vibrations, simpler models were required that could provide insight into both uncoupled and coupled vibrations. In broad terms, drillstring vibration models are divided into two broad groups (Marquez et al., 2015).

Distributed parameter models

The drillstring is considered a beam undergoing dynamic forces. The resultant wave equations have been successfully managed by appropriately defining boundary and initial conditions. Solution to such models requires solving partial differential equations

Lumped parameter models

The drillstring consists of mass, spring and dampener components with dependent variables that are a function of time alone. The solution to the governing equation of motion is ordinary differential equation. The model can support one or more degrees of freedom.

The following section contains an example of both distributed and lumped parameter modeling It also presents an example of a high-fidelity dynamic model that considers all modes of vibrations and their interactions.

Distributed Parameter Modeling

Modeling uncoupled axial vibrations is an example of distributed parameter modeling. The basis of modeling axial vibrations is solving a wave equation for a flexible metal bar subjected to undamped longitudinal oscillations. Bailey and Finnie (1960) helped derive axial natural frequencies of the drillstring using wave equations for undamped oscillations. As seen in Figure

2-9, a flexible bar of length L and cross section s_o is assumed. Variables q(x,t) and T(x,t) are displacement and tension of point x at time t.

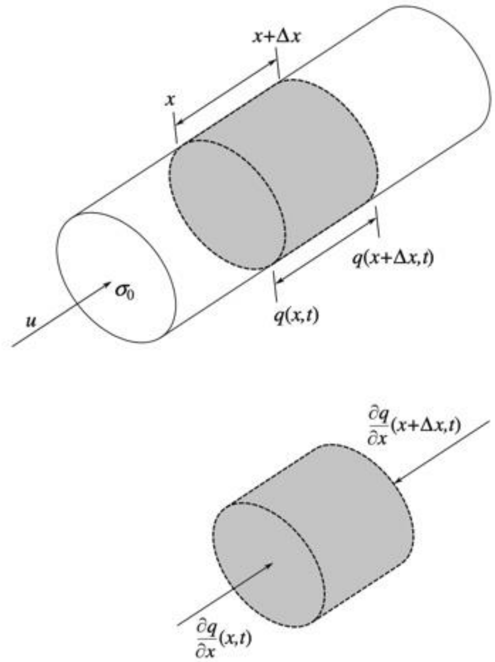

Figure 2-9 Tension on short section of flexible bar (Marquez et al., 2015)

Using fundamental law of elasticity, the model can be written as:

$$\frac{\partial^2 u}{\partial t^2}(x,t) = c^2 \frac{\partial^2 u}{\partial x^2} \text{ ………………………….(2-2)}$$

Where propagation speed $c = \sqrt{\frac{E_o \sigma_o}{\rho_o}}$, ρ_o is mass/unit length and E_o is the young modulus. Further complexity to the axial vibration models was added by studying damped axial wave equations (Dareing and Livesay, 1968; Li et al., 2007) as well as including dynamic phenomenon such as tripping motion, weight on bit fluctuations, mud damping, tool joint stiffness etc. (Dunayevsky et al., 1993)

2.2.1 Lumped parameter models

Torsional oscillations are the most appropriately modeled by lumped parameter models. Stick-slip vibrations are modeled mathematically by treating the drillstring as a simple torsional pendulum with one or more degrees of freedom. Preliminary torsional pendulum models were developed by

Kyllingstad and Halsey (1988) with one degree of motion. Damping coefficients and effect of weight on bit was included to improve understanding of stick-slip vibrations (Spanos and Payne, 1992).

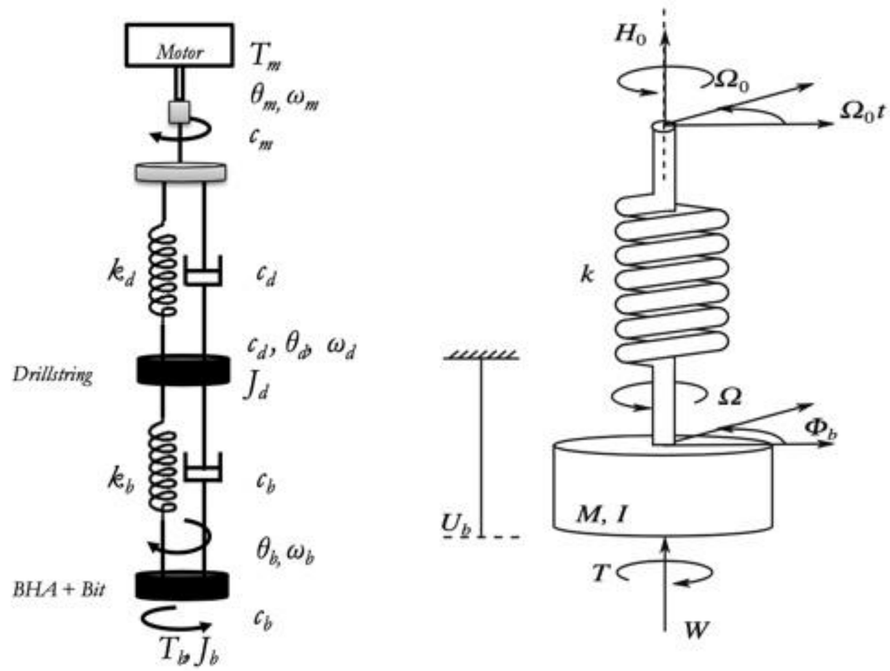

(a) (b)

Figure 2-10 Two rotational degree of freedom in torsional spring model (Patil and Teodoriu 2013) and (b) Simplified axial and torsional (2 DOF) model (Marquez et al., 2015)

Navaro and Lopez (2004), proposed a two degree of freedom model driven by a top drive motor that assumes non-linear friction as rock-bit interaction. Patil and Teodoriu (2013), summarized this model as seen in figure 2-10 (a).

The equation of motion can be summarized as:

$$J_d \ddot{q_d} - c_d(\dot{q_m} - \dot{q_d}) - k_d(q_m - q_d) + c_b(\dot{q_d} - \dot{q_b}) + k_b(q_d - q_b) = 0 \text{ ………(2-3)}$$

$$J_b \ddot{q_b} - c_b(\dot{q_d} - \dot{q_b}) - k_b(q_d - q_b) = -T_b \text{……… (2-4)}$$

Where θ_m, θ_d and θ_b represent the angular displacement of the motor, drill string and the bit. c_m, c_d and c_b represent the damping coefficient of the motor, drill string and bit. J_d and J_b represent the mass moment inertia of the drill string and the bit. k_d, k_b, w_d and w_b represents the torsional stiffness and angular velocity of the drill string and bit. T_b the torque at bit.

The reactive non-linear torque T_b is defined below:

$$T_b(w_b) = c_b.w_b + T_{fb}(w_b) \text{ ………(2-5)}$$

Here $c_b.w_b$ is the component that represents the drilling fluid damping at bit and T_{fb} represents the reactive non-linear torque due to bit-rock friction (Navarro-Lopez, 2009). Figure 3-3 (b) represents an axial and torsional (2 DOF) model. The torsional pendulum stays the same and the BHA and drillstring are assumed lumps of mass M. The equation of motion is summarized as:

$$J\ddot{\phi}_b + k(\phi_b - \phi_{bo}) = T_o - T \text{ ………(2-6)}$$

$$M\ddot{U}_b = W_o - W \text{ ………(2-7)}$$

Where ϕ_b and U_b are vertical and angular bit position. M is the lumped mass and T and W stand for torque and weight on bit. To and Wo stand for stationary values of the same. J is the moment of inertia and k is the spring stiffness of the drillpipe.

2.2.2 High-fidelity discrete model

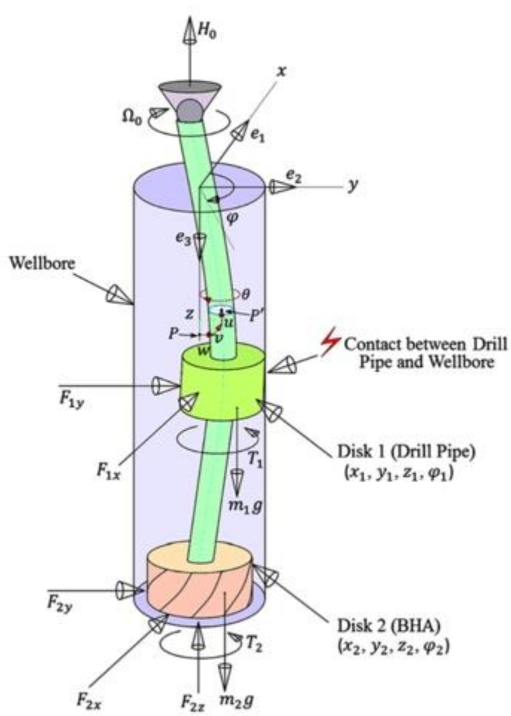

Figure 2-11 Discrete model with representation of dynamic forces and torque (Liu et al., 2012)

An eight degree of freedom model is represented in figure 2-11, where discretization of the drillstring component is used for numerical and analytical studies. Drill pipe is lumped as disc 1 and BHA and its components have been lumped as disc 2. The disc dynamics include 1 DOF for axial, 1 DOF for torsional and 2 DOF for lateral vibrations. The coordinates of both discs are defined in axial, lateral and torsional components as (x, y, z, j), with j representing the positive inclination in z axis. Angular displacement q is defined in (z, t) coordinates. The equation of motion for the system is summarized below (Liu et al., 2012).

$$\left.\begin{aligned}
m_1\ddot{x}_1 + c_l\dot{x}_1 + 2k_l\left(x_1 - \tfrac{x_2}{2}\right) &= m_1 e\dot{\varphi}_1^2\cos\varphi_1 + F_{1x}\\
m_1\ddot{y}_1 + c_l\dot{y}_1 + 2k_l\left(y_1 - \tfrac{y_2}{2}\right) &= m_1 e\dot{\varphi}_1^2\sin\varphi_1 + F_{1y}\\
m_1\ddot{z}_1 + c_a\dot{z}_1 + k_a\left(z_1 - z_2\right) &= m_1 g - H_0\\
J_1\ddot{\varphi}_1 + c_t\dot{\varphi}_1 + k_t\left(2\varphi_1 - \varphi_2\right) &= -T_1 + k_t\Omega_0 t\\
m_2\ddot{x}_2 + c_l\dot{x}_2 + k_l\left(\tfrac{x_2}{2} - x_1\right) &= m_2 e\dot{\varphi}_2^2\cos\varphi_2 + F_{2x}\\
m_2\ddot{y}_2 + c_l\dot{y}_2 + k_l\left(\tfrac{y_2}{2} - y_1\right) &= m_2 e\dot{\varphi}_2^2\sin\varphi_1 + F_{2y}\\
m_2\ddot{z}_2 + c_a\dot{z}_2 + k_a\left(z_2 - z_1\right) &= m_2 g - F_{2z}\\
J_2\ddot{\varphi}_2 + c_t\dot{\varphi}_2 + k_t\left(\varphi_2 - \varphi_1\right) &= -T_2
\end{aligned}\right\} \quad (2\text{-}8)$$

Here *m*, *J* and *e* are mass, moment of inertia and eccentricity for disc 1 and 2. k and c represent the stiffness and damping in the system with a, t and l subscript for axial, lateral and torsional parameters. The reactive forces and torque in the system is represented by F and T where F_1 and T_1 represent drillpipe and wellbore interaction and F_2 and T_2 represent BHA and formation interaction. The model assumes coupling of vibration modes in the system.

2.2.3 Analytical solution

Investigation of drilling vibrations needs consideration of natural frequency of a drillstring. The following section provides an analytical solution to the beam equation presented earlier. However, the model does not include any damping in the system. Moreover, lateral vibrations are ignored, and independent torsional and axial motion are considered. Since both axial and torsional vibrations are exactly analogous, the equation of motion of torsional vibrations are described below. Lateral vibration equation of motion can be derived by changing parameters like shear force to axial force, shear modulus to Youngs modulus, axial displacement to angular displacement etc. The equation of motion for torsional motion is expressed as:

$$\frac{\partial^2\theta}{\partial x^2} = \frac{1}{c_\theta{}^2}\frac{\partial^2\theta}{\partial t^2} \text{ ....(2-9)}$$

Where $\theta = \theta$ *(x,t)*: is a function of time *t* and *x* is a spatial variable, c_θ is a real non-negative coefficient, which is the speed of propagation of shear waves in the system. The general solution to the equation is:

$$\theta(x,t) = (A\sin\frac{w}{c}\ x + B\cos\frac{w}{c}\ x)(D\sin wt + E\cos wt) \text{ ....(2-10)}$$

Where w = angular velocity, A, B, D and E are constants, wx/c_θ is a dimensionless number that characterizes the wave in x direction or defines the wavelength of vibration as W. The boundary conditions for the model are described for angular position with respect to time and position. The lower boundary condition is defined at x = 0 and the upper boundary condition is defined for x = x_{12} where x_{12} is the lowest section of the drill collar. The boundary conditions are defined below as:

$$\theta_1 = C_1\sin\frac{w}{c}x\sin wt \text{ ....(2-11)}$$

$$\theta_2 = C_2\sin\left(\frac{w}{c}x + e_{12}\right)\sin(wt + \acute{e}_{12}) \text{.........(2-12)}$$

Where e_{12} and $\acute{e}_{12}$ are constants that balance the boundary conditions and C_1 and C_2 are amplitude of torsional vibration. In conclusion, The C_1/C_2 ratio is defined as:

$$\frac{C_2}{C_1} = f\ (I,\Omega) = \frac{C_2}{C_1}(\frac{I_2}{I_1},\frac{w}{c_\theta}\ x_{12}) \text{ ....(2-13)}$$

Where I_2/I_1 is the ratio of polar moment of inertia, $(w/c_q)\ x_{12}$ is the phase angle and $C2/C1$ is the amplitude ratio of torsional rotation. The author provides a graph-based solution to find $C2/C1$ ratio based on phase angle and ratio of polar moment of inertia across change in cross section of pipe. The phase change is calculated as DW = (w/c_q). L where c_q is the shear wave's speed of propagation for a system running at angular velocity w for a fixed length L. The phase change is written as a function of n, the natural frequency of the system. Using figure 2-12, a back calculation is made with the range of amplitude ratios to identify the phase change that relates to a resonant frequency of the system. The study also provides a calculation for torsional displacement and stress in the system.

In conclusion, the calculations presented are an example of an analytical solution of drilling vibrations. The model assumes steady conditions with no damping or vibration coupling in the system. Adding that complexity makes finding analytical solutions almost unachievable. This calls for numerical techniques where discretizing the string into finite elements can help introduce complexities in the model.

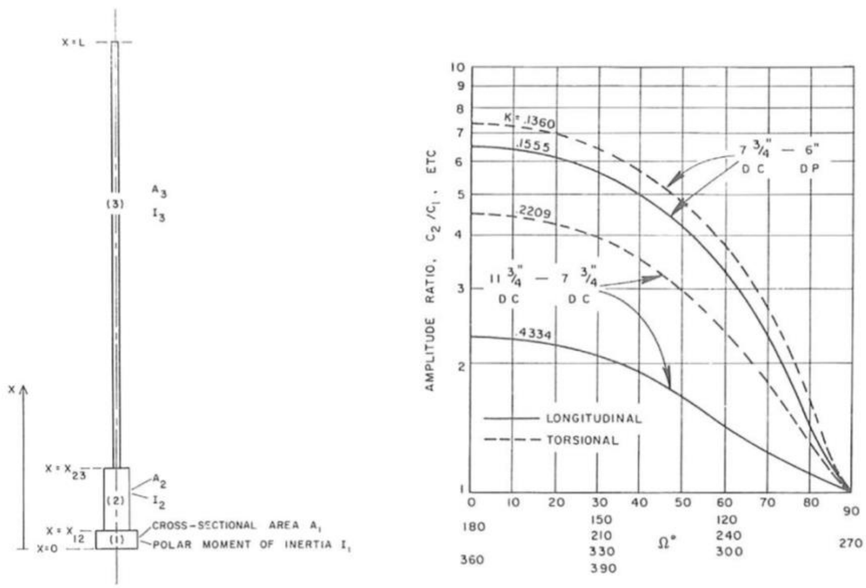

Figure 2-12 Drill string with step change in diameter (Bailey and Finnie, 1960)

2.2.4 Numerical modeling vs. experimental testing

As observed in section 2.2, drillstring vibration models, especially dynamic models, contain ordinary and partial differential equation of motion. Finite element and finite difference methods are popularly used numerical techniques in the industry. Numerical methods offer a tradeoff between model complexity and computation time. Experimental setups are used extensively for validating numerical models and for a downscaled study of drilling dynamics. This section compares the numerical and experimental study of drilling vibrations.

Numerical methods are often simplistic in design with a lot of underlying assumptions that include exclusion of drillstring friction, mud damping effects, wellbore deviation etc. In exchange for low fidelity, they offer a quick and approximate idea of what to expect downhole. With advancement in numerical techniques, sophisticated drilling models have been developed that offer better understanding of downhole conditions. Finite element method (FEM) is used to provide numerical solutions to partial differential equations by breaking down the model into smaller finite elements or meshes. Higher mesh count results in higher accuracy. Naturally, there is a tradeoff between the mesh count and the computation time of the model. Furthermore, modeling rock-bit interaction, friction along drillstring and top-drive motor needs experimental verification. Without including this validation process, the accuracy of numerical models is hindered (Pavone, 1994). When properly downscaled, experimental test rigs provide an accurate prediction of drilling dynamics. They provide a variety of testing conditions and an opportunity to isolate a drilling dysfunction for an in-depth analysis.

Figure 2-13 (a) shows the results obtained from experimental testing of torsional vibrations, particularly stick-slip vibrations by plotting bit RPM vs time. Rotary encoders are used for accurately measuring angular velocity. The surface RPM is 100 and aluminum is used as the drillstring material. Similarly, figure 2-13 (b) shows the estimated downhole RPM for the same drilling conditions using a numerical model with downscaled parameters that match the experimental configuration. The numerical result sees a buildup of torsional vibrations in the system with onset of high frequency stick-slip conditions after 2.5 seconds of rotation. The experiment result shows distinct low frequency stick-slip cycles. Every stick phase leads to a buildup of torsional energy in the string that is released during the slip phase. The peak of rotational speed is almost 800 RPM in experiment measurement while numerical models predict a peak of 250 RPM. Furthermore, the experiment results show the occurrence of negative RPM as a reaction to sudden RPM increase in the slip phase. This phenomenon is not observed in numerical results. Therefore, the inability of numerical models to include dynamic forces is a major drawback (Baumgartner and Oort, 2014).

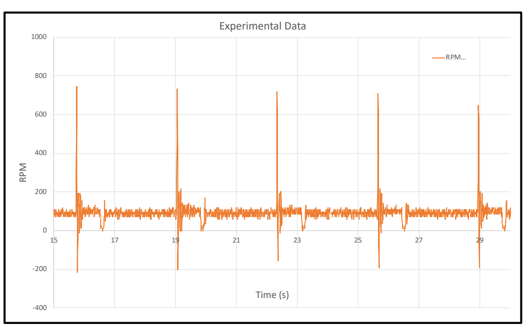

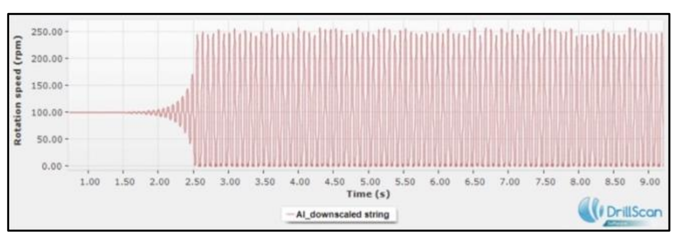

(a)

(b)

Figure 2-13 (a) Bit RPM vs time for experimental test of stick-slip vibrations and (b) numerical model result for downhole RPM for stick-slip conditions

Numerical methods have a few advantages over experimental methods. Once a numerical model has been configured, it provides a convenient interface with quick results. Experimental testing on the other side requires planning and in-person monitoring. In cases of emergency, numerical estimations can be performed remotely. Another big advantage of numerical solutions includes its versatility for sensitivity analysis. Testing different BHA configurations, stabilizer placement, bit aggressiveness etc. are easy variations while using numerical models (Pavone, 1994). These changes are very cumbersome for experimental testing and in many cases not possible. In conclusion, numerical methods provide an amazing tool for pre-drilling estimation of downhole conditions. (Bailey and Gupta, 2008). They can be finetuned with experimental/field data for more accurate predictions. However, they have their limitations. They should be used as guidelines with real-time measurement validation.

2.3 Drillstring Vibration Mitigation

In the previous sections, experimental and modeling studies on torsional vibrations have been reviewed extensively. Even though the understanding of torsional vibrations has improved significantly, it cannot be completely avoided. In this section, stick-slip vibration mitigation techniques have been discussed. This section aims at classifying vibration mitigation techniques into four broad categories that include traditional and upcoming techniques.

2.3.1 Vibration analysis during design stage

The concept behind this strategy is to adjust the design of the bottom hole assembly and other components in the drillstring to avoid the resonant frequency vibration during drilling. This was proposed as early as 1984 when BHA design changes were recommended to avoid violent vibrations downhole (Dareing, 1984). Studies have shown that adding stabilizers to the drillstring to provide additional constraints/damping helps reduce BHA vibration (Mahyari et al., 2010). Extensive research has also been done on BHA redesign. Changing BHA length affects the neutral point in the string. This changes the resultant vibration wave propagation in the drillstring. Changing the stiffness of the BHA is also proposed in literature to cure stick-slip vibrations (Pastusek et al., 2005). Figure 2-14 shows the WOB and RPM dependency for PDC bits. Analyzing vibration amplitudes, high frequency torsional vibrations occur at high WOB and high RPM values. This stability map is used for redesigning bit aggressivity. Changing bit aggressiveness (TOB and WOB ratio) is a key factor in reduction of stick-slip vibrations (Dao et al. 2019). Newer bits on the market include DOCC (depth of cut technology) to limit the depth of cut while drilling. This reduces the resultant reactive torque. Using such technology, torsional vibrations are kept in check by making the bit aggressive when needed (softer formations) and limiting its aggressiveness in other situations (harder formations). During the design phase, bit aggressiveness can be adjusted to find rate of penetration for a formation with least torsional vibrations.

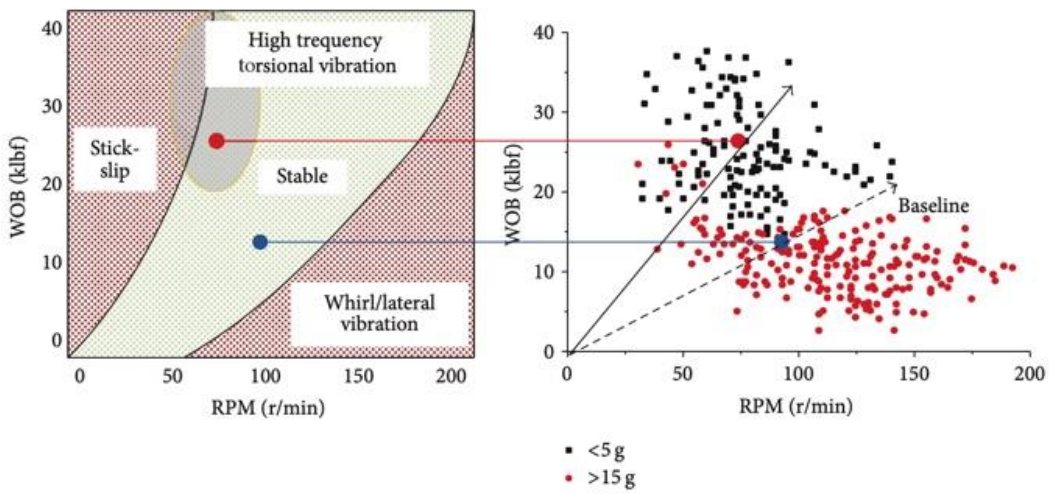

Figure 2-14 Stability map for PDC bits (Dong and Chen, 2016)

A powerful tool for redesigning drillstring for reducing drilling vibrations is performing sensitivity analysis on dynamic models to find an optimal BHA design that sees a reduction in downhole vibrations (Ghasemloonia et al., 2015). This technique is used to optimize stabilizer placement, balancing BHA components, adjusting bit aggressivity and to estimate the friction in the wellbore with help of prior drilling data. The models are numerically solved and provide a quick and reliable estimation of downhole vibrations.

2.3.2 Passive control techniques

Passive control mechanism uses systems and components that do not need external energy requirement and work on the system energy already available. The utilization of shock absorbers has been widely accepted in the industry as an effective, passive technique for vibration mitigation. They are usually installed below the MWD and LWD tools and above the bit. Furthermore, they help in lowering the drillstring’s natural frequency (Ghasemloonia et al. 2015).

Popularly called shock subs, shock absorbers can be further classified into axial and rotational kind (Dong and Chen, 2016). Axial shock subs use disc springs to absorb the sudden increment in WOB during its compression stroke. The shock sub then smoothly adjusts the WOB by releasing the compression energy. They can work up to 300 hours at 231° C in all well profiles (Dong and Chen, 2016). Studies have been done to finetune the stiffness of shock sub springs for an optimized mitigation of axial and resultant lateral vibrations in the drillstring (Brett et al., 1998). Hydraulic subs use hydraulic oil instead of springs to dynamically adjust the WOB changes.

Rotational shock subs have become increasingly popular. In this mechanism, an increased TOB is absorbed as compression energy by the torsional springs in the system. The working mechanism of an AST (Anti stall tool) tool is shown in Figure 2-15 (a) where an abrupt torque M_2 is absorbed by the springs through compression, which is slowly released as F_2 at bit. Figure 2-15 (b) also shows the stroke length of a popular AST tool used in the field to give an idea of the tool effectiveness to mitigate both torsional and axial vibrations through compression and elongation.

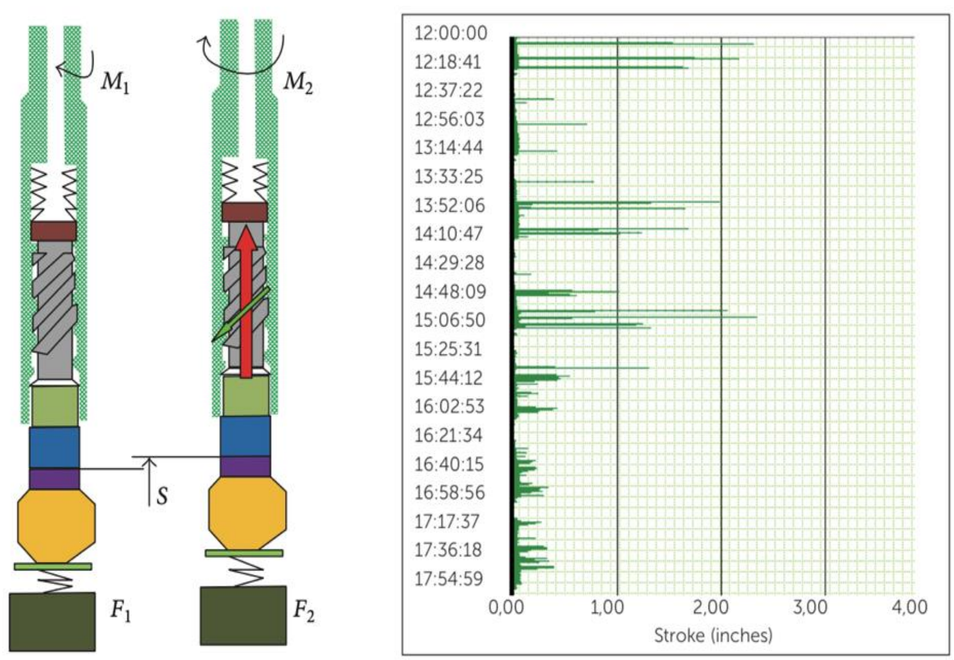

(a) (b)

Figure 2-15 (a) Anti stick tool working mechanism (Dong and Chen, 2016) and (b) Stroke travel length for a popular AST tool (Vromen et al., 2019)

2.3.3 Active control techniques

Active control techniques focus on dynamic application of a reactive forces to compensate for the forces induced by the drillstring due to vibrations. Based on input of disturbances in the system and output of changes in control parameters, control systems are divided into open-loop or closed-loop feedback systems. Figure 2-16 (a) shows the working principle of open and closed loop systems—control function is independent on output (open-loop) and dependent on output signal (closed-loop). Open-loop systems work towards mitigation of external forces in the systems (WOB, RPM control) and closed loop systems effectively change drillstring damping and stiffness to reduce vibration amplitudes.

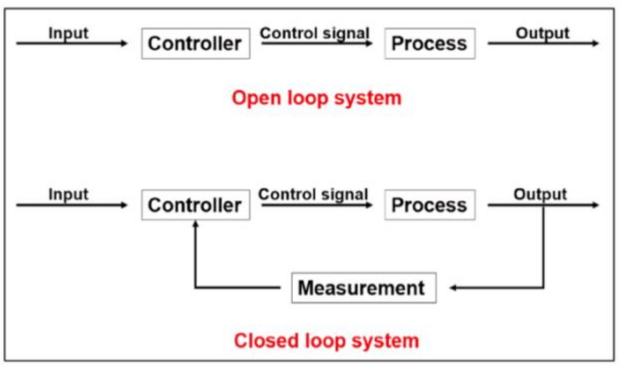

(a)

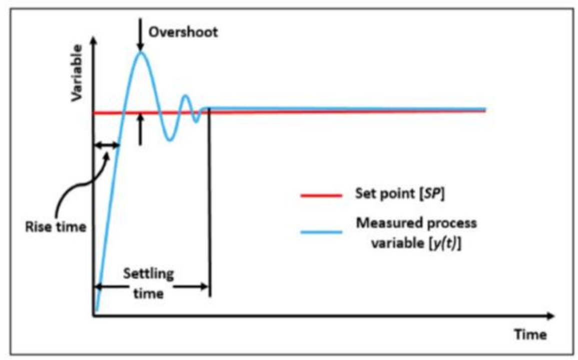

(b)

Figure 2-16 (a) Open loop vs closed loop system (Gurjao et al., 2018) and (b) PID controller in action (Ogata, 2010)

Damping of stick-slip vibrations at the surface, specially the first few modes of vibrations was one of the early active control techniques developed (Jansen et al., 1995). Usage of PID became more popular where only simple servo-motor controlled systems were adjusted to avoid stick-slip situations (Pavone, 1994). However, this system needed better damping of downhole vibrations. Better adaptive PID controllers have been developed and widely used (Li et al., 2011). Figure 2-16 (a) shows an example of a developed closed-loop control loop system which used WOB as a control variable to optimize the tradeoff between WOB and rate of penetration to mitigate drilling vibrations. STRS (Soft torque rotary system) is another improved torque feedback system. Instead of using torque measurements, the system uses motor current as a control variable (Jansen et al., 1995). Figure 2-16 (b) shows the working of the STRS systems in which the motor current was used to control torsional oscillations in the system. This is achieved by damping the top drive to absorb the torsional energy.

2.3.4 Real-time vibration optimization

Real time vibration control requires optimizing drilling parameters to avoid drillstring resonant frequencies. Wu et al. (2010) presented a relation between WOB and RPM to highlight the drilling dysfunctions and suggested a theoretical optimum drilling zone where drillstring vibrations were minimum. Figure 2-17 (b) shows the optimum drilling window was a stable drilling zone. The zone depends on the bit used as well as the formation to be drilled. Utilization of SCADA systems to adjust WOB and RPM during drilling based on real-time data acquisition has proven to be an effective solution (Chapman et al., 2012). An accurate parameter control workflow can be developed by monitoring the MWD obtained drilling parameters like accelerometer, TOB and bit RPM measurements. Although this strategy can be most efficient, we are restricted from obtaining real-time downhole data due to mud telemetry bandwidth constraints (Zha, 2018).

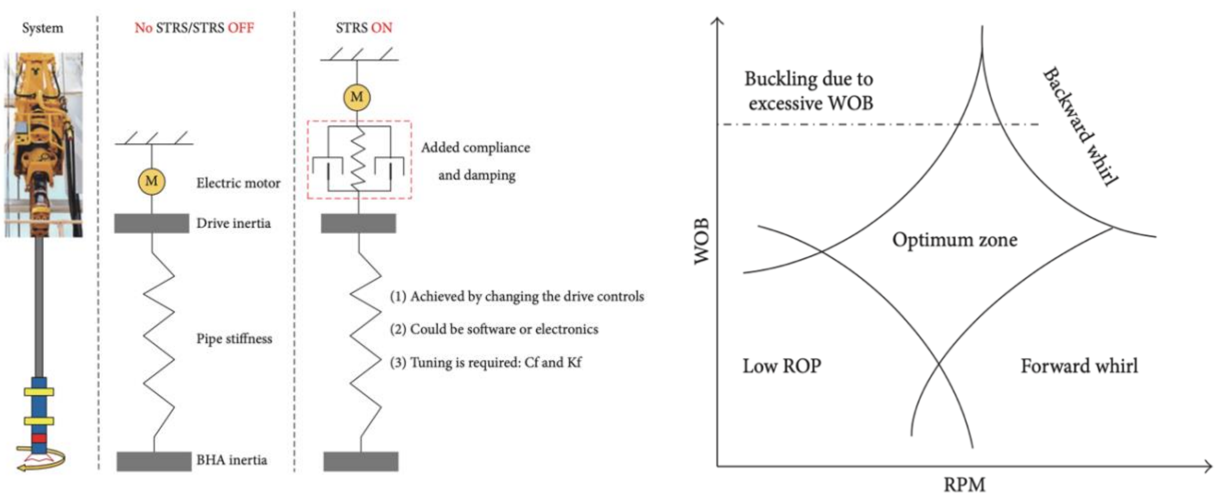

(a) (b)

Figure 2-17 (a) STRS working principle (Dong and Chen 2016) and (b) Optimum drilling zone as a relation between WOB and TOB (Wu et al., 2010)

For lateral and torsional vibrations that cannot be identified from surface parameters, indirect methods like monitoring MSE (Mechanical Specific Energy) have been proven to be an effective technique for field applications (Dupriest et al., 2005). MSE is defined as the ratio between system input energy and the rate of penetration. It quantifies the efficiency of the drilling process.

Assuming the same formation and drilling parameters, a drop in MSE correlates to energy being lost as vibrations. This helps in changing WOB and/or RPM to cure the drilling dysfunction.

2.4 Data Acquisition and Sampling

Drillstring vibrations are defined based on direction of appearance in three distinct categories namely, axial, lateral and torsional (Lopez et al., 2004). The modes of vibration are summarized in Figure 2-18 along with their respective characteristic frequency. However, with better downhole tools and data acquisition methods, the understanding of downhole vibrations has changed drastically. For example, while stick slip is seen as a low frequency vibration mode, torsional oscillations along the drillstring have been characterized up to 500Hz (Patil and Ochua, 2020). While high-frequency torsional oscillations and stick-slip vibrations may originate independently, multiple sources of vibrations have been identified that are coupled in nature. For example, coupled axial and stick-slip vibrations and bit chatter. Dong and Chen (2016) present a detailed summary of possible classifications of drillstring vibrations.

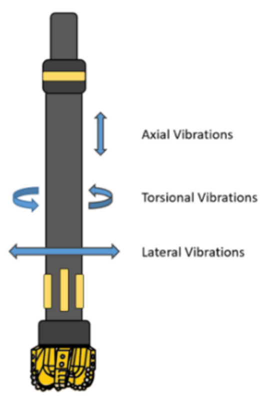

Vibration	Mode	Vibration frequency
Stick-slip	Torsional	≤ 2 Hz
High Freq. Torsional Oscillations	Torsional	100-500 Hz
Bit/BHA Whirl	Lateral	5-100 Hz
Bit-Bouncing	Axial	1-10Hz

Figure 2-18 Major vibration modes and associated characteristic frequencies (Marquez et al., 2015, Patil and Ochua, 2020)

Interestingly, data acquisition tools and sensors have adapted to high-frequency downhole measurements by utilizing downhole data storage solutions. Currently, in the industry, downhole tools exist that can acquire and store downhole parameters such as weight on bit, downhole torque, bit RPM, bit acceleration, temperature, pressure etc. at incredible sampling rates of up to 5120 Hz (Li et al., 2021). While such high-resolution data is immensely helpful for research and post drilling scrutiny, the tools do not provide real-time feedback, are expensive to run and require data management solutions. One possible answer is to develop downhole processing of data that helps in summarizing a large volume of data into unique statistical parameters for early vibration detection. Another solution is to develop an optimal sampling strategy that is adequate for real-time monitoring of downhole conditions. This can be applied at both the surface and bit level. Figure 2-19 presents a review of sampling frequency literature used in field and laboratory setting for surface and downhole measurements. The Y-axis in figure 2-19 represents the sampling frequency (in logarithmic scale). The suggested minimum requirement for successfully detecting different modes of drill string vibrations have also been marked. While high sampling frequencies help in detecting all modes of vibrations in the drillstring, not all vibration modes cause severe damage/loss of performance. A broad spectrum of sampling frequency is used in the industry, as seen in figure 2-19. Ultimately, the choice of sampling frequency should be based on vibration mechanism being analyzed. Table 3 provides further insight regarding downhole sensors and data acquisition methods utilized.

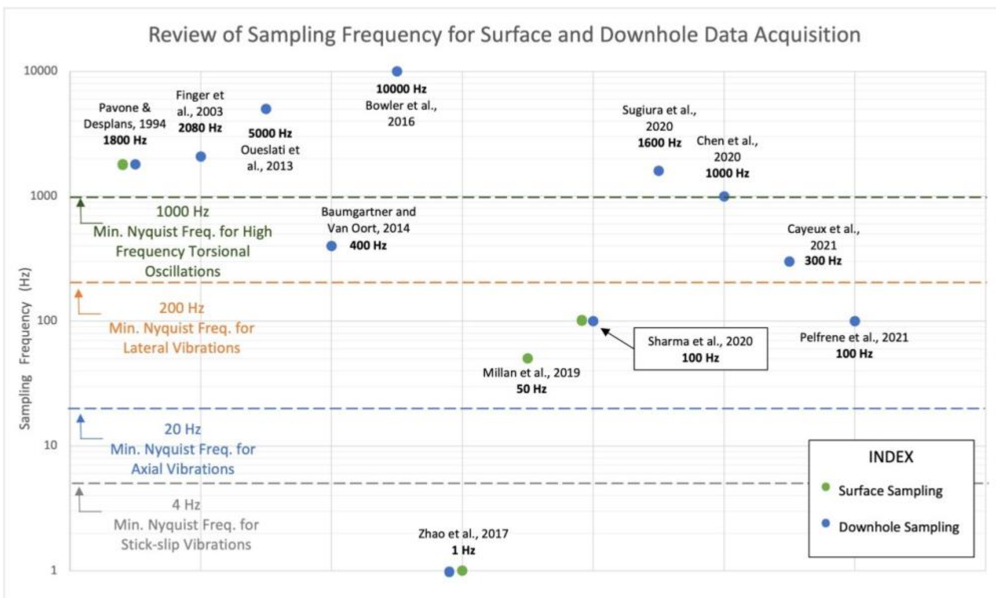

Figure 2-19 A review of sampling frequency for surface and downhole measurements with associated limits for detecting drill string vibrations

Drilling is a dynamic process which involves multiple process parameters including weight-on-bit (WOB), torque, drillstring RPM, rate-of-penetration (ROP) annular pressure, annular temperature, etc. Continuous measurement and analysis of drilling parameters plays a crucial role in carrying out a safe and efficient drilling operation. In the past, downhole measurements made using wireline measurement systems could not be utilized for real-time drilling optimization. With the introduction of measurement while drilling (MWD) tools, it became possible to measure drilling parameters and use them in process control. Today, with the advancements in technology, state-of-the-art data acquisition systems (DAQ) are used to monitor and analyze drilling operations. This has helped in optimizing drilling, which in turn has resulted in cost reduction and reduced non-productive time (NPT) (Ouselati et al., 2013).

Reference	Tool	Data Acquisition Location		Sampling Freq.	Data Acquisition, Transmission and Storage
		Surface	Downhole		
Pavone and Desplans, 1994	Downhole sub with accelerometer, magnetometers, temperature, pressure, and weight on bit sensors	✓		1800 Hz	Continuous transmission Wired drillstring
Finger et al., 2003	Sub equipped with accelerometers, magnetometers, pressure sensor, load sensor, torque sensor and temperature sensor.		✓	65 - 2080 Hz	Real-time wired drillstring
Oueslati et al., 2013	Vibration sensor at bit		✓	1400 Hz (Field), 5000 Hz (Lab)	Not reported
Baumgartner and Van Oort, 2014	Radially oriented accelerometer at bit		✓	Up to 400 Hz (in bursts)	Not reported
Bowler et al., 2016	Sub equipped with accelerometers, magnetometers, gyroscopes, inclinometers, pressure sensor, load sensor, torque sensor temperature sensor.		✓	10000 Hz	Data stored downhole
Zhao et al., 2017	Not available	✓	✓	0.5 - 1Hz	Not reported
Millan et al., 2019	Downhole shock sensors	✓	✓	10 -50 Hz	Not reported
Sugiura et al., 2020	Hockey-puck-shaped sensor package with accelerometers, magnetometers, gyroscopes, and temperature sensor installed at the bit		✓	20-1600 Hz	Burst/Continuous data storage
Chen et al., 2020	Sub equipped with accelerometers, magnetometers, gyroscopes, inclinometers, and a temperature sensor		✓	1000 Hz	Data recorded and stored downhole
Pelfrene et al., 2021	Sensor package with accelerometers, gyroscope, and temperature sensor installed in the bit shank or BHA		✓	100 Hz	Data storage
Cayeux et al., 2021	Sub equipped with three-axis accelerometers, gyro, and magnetometers		✓	200Hz, 300 Hz	Data recorded and stored downhole

Table 3 Summary of vibration detection tools

2.4.1 Data Acquisition System

Data acquisition (DAQ) systems are electronic/computer systems that are used to measure and acquire real-world physical signals and convert them into digital data that can be processed by a computer. A standard DAQ system consists of four basic components as shown in figure 2-20.

- Sensors/Transducers: Sensors detect the changes in the physical environment and generate a corresponding electrical signal. In a drilling system some of the sensors used are gyroscopes, accelerometers, and magnetometers (to measure RPM, vibrations, inclination etc.); load cells (to measure system load, WOB); pressure sensors; torque sensors etc.
- Signal Conditioners: The raw signals from the sensors must be conditioned/cleaned before they can be processed. Signal conditioners are used to filter the unwanted noise out of the signals. Thus, achieving a desired signal-to-noise ratio. They can also be used to amplify very-low voltage signals i.e. signals from a strain gauge-based sensors often have very low voltage output (millivolts (mV) range) which must be amplified before it can be processed. Signal scaling is another common signal conditioning application.
- Analog-to-Digital Converter (ADC): The analog signals from the sensors are digitized so that they can be interpreted by a computer. ADCs are electronic systems that perform quantization and sampling on the analog signal to convert it to a digital signal.
- Computer: This is the final component of the DAQ system and it's where all the incoming digital data is integrated with software. The data can be stored in memory for future analysis or can be used in real-time to display the process parameters or as input/feedback to control loops in the system.

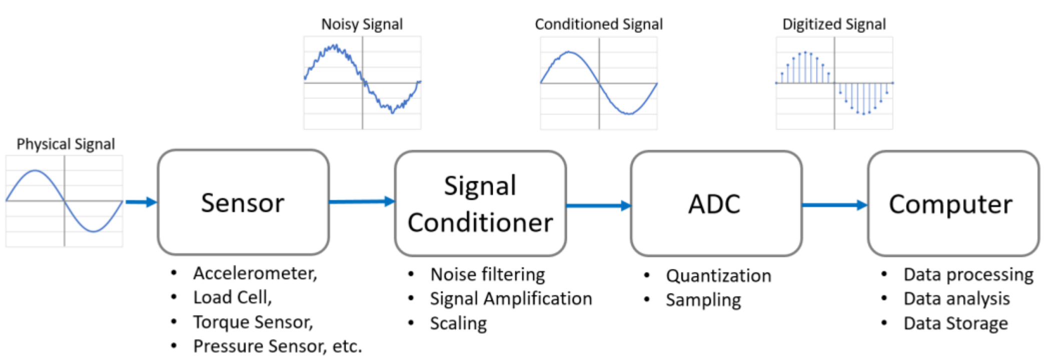

Figure 2-20 A standard DAQ system

2.4.2 Sampling Theory

The world we live in is analog. All the physical quantities we perceive or measure around us in nature, like sound, pressure, temperature, voltage etc., are analog i.e., they are continuous in time. A variety of sensors/transducers can be used to acquire these physical quantities and convert them into electrical signals containing useful information and data. These electrical analog signals must be digitized to make them accessible for computers to process the data contained in them and this is where the concept of data sampling comes into play.

Sampling is the process of digitizing an analog/continuous signal in time by acquiring discrete amplitude values (samples) of the signal at regular intervals of time. Sampling frequency, measured in hertz (Hz), is the number of samples collected every second. For example, digital audio is sampled at rate of 44,100 Hz, this means the analog audio signal from a device like a microphone is sampled 44,100 times a second or 44,100 discrete samples are recorded every second at fixed intervals of time. This time interval is called the sampling interval (t_s) and is the inverse of the sampling frequency.

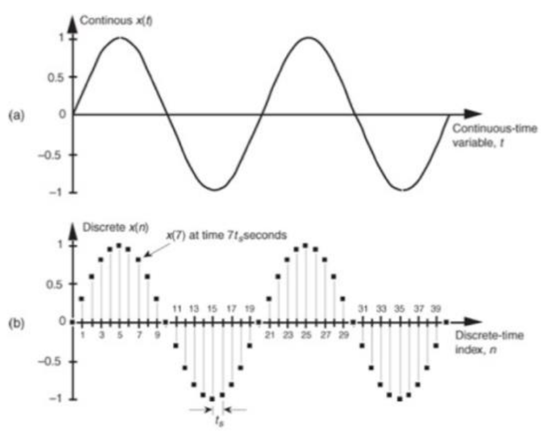

Figure 2-21 (a) A continuous time domain sine wave, (b) discrete sample representation (Ploennigs, 2010)

This approach of sampling analog signals uniformly over constant time intervals is a more traditional method of sampling. Other non-uniform or irregular sampling techniques also exist and are advantageous in situations where power and/or memory consumption are constrained (Shannon, 1948, Sharma et al., 2020)

2.4.3 Nyquist-Shannon sampling theorem

Claude Shannon's work at the Bell Labs in 1948 built upon the work of others like Harry Nyquist and Edmund Taylor Whittaker. It formalized the concept of periodic sampling as we know it today. In his 1948 article titled 'A Mathematical Theory of Communication', Shannon stated:

> *If a function of time f(t) is limited to the band from 0 to W cycles per second it is completely determined by giving its ordinates at a series of discrete points spaced* $\frac{1}{2W}$ *seconds apart.*
>
> *Let f(t) contain no frequencies over W. Then*

$$f(t) = \sum_{-\infty}^{\infty} \left(X_n \cos \frac{sin\, \pi(2Wt-n)}{\pi(2Wt-n)} \right) \ldots\ldots\ldots (2\text{-}14)$$

> *where,*

$$X_n = f\left(\frac{n}{2W}\right) \ldots\ldots\ldots (2\text{-}15)$$

> *and,* X_n *is the* n^{th} *sample*

This is the basis of the Nyquist-Shannon sampling theorem which states—to avoid aliasing and loss of information, the sampling rate required to sample an analog signal must be at least twice the highest frequency (bandwidth) of the signal. This minimum required sampling rate is known as the Nyquist rate.

2.4.4 Over-sampling and Under-sampling

According to the sampling theory, to retain all the information in a band-limited analog signal, the signal must be sampled at a frequency which is at least double the highest frequency component of the signal. Sampling an analog signal below the Nyquist rate results in loss of information, also known as signal aliasing. Figure 2-22 (a) shows a sine wave sampled with adequate sampling frequency, thus preserving the information in the signal. On the other hand, in figure 2-22 (b), the same sine wave is under-sampled, and the resultant sampled signal has a frequency component much lower than the original signal, therefore the signal is aliased.

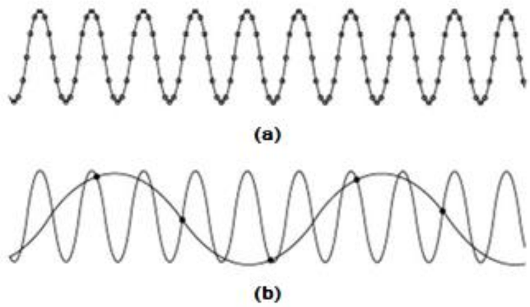

Figure 2-22 (a) Adequately sampled sine wave, (b) Under-sampled sine wave

With the advancements in technology, the capabilities of data acquisition systems have increased exponentially over the years, it possible to sample data at higher and higher rates. When a signal is sampled at a rate higher than the Nyquist rate, the signal is said to be over-sampled. It is known to improve the signal to noise ratio and resolution and help in overcoming aliasing but on the other hand it requires more power and memory to process the incoming signals.

2.5 Summary of literature review

In conclusion, a comprehensive review of existing literature on experimental and modeling studies for drillstring vibrations has been presented along with literature on vibration mitigation techniques. A review of data acquisition tools used in the industry is presented along with a discussion on the need of optimal sampling frequency for capturing drilling vibrations.

- In terms of experimental studies, there is a need for standardized downscaling factor and parameter estimation. Every setup is downscaled, but the degree of downscaling varies across setups and across parameters adjusted. While geometric downscaling is straightforward, dynamic, and kinematic downscaling is more complex and needs standardization and experimental estimation. Additionally, there is a need for more horizontal experiments for drilling vibration study. Considering that every well in the US contains a deviated profile, there is a need for investigation of drilling vibrations under these conditions. The additional contact points change the dynamic behavior of the string. In case of torsional vibrations, wellbore contact acts as source of non-linear friction and in turn produce a damping effect on the induced torsional vibrations (Patil and Teodoriu, 2013).
- In terms of modeling drilling vibrations, there are a multitude of available models with varying levels of complexities. When considering complex models with non-linearities

included, the modeling results need to be tied back to experimental results. Additionally, very few models for horizontal well profile are available, as seen in table 1 and 2.

- A drilling system incorporates excellent data handling capabilities and experimental setups do not mention or elaborate on it. Moreover, while high sampling measurement tools are available and readily used, there is limited literature on the side-effects of undersampling or oversampling when trying to observe a particular phenomenon. Data collected at adequate sampling rate can help verify complex models and compare with experimental results successfully.

Chapter 3: Design of an Experimental Test Rig for Torsional Vibrations

Experimental studies play a pivotal role in isolating and investigating drilling vibration related dysfunctions in a downscaled setup, validating mathematical models, and testing vibration mitigation algorithm and tools in a controlled environment. Each experimental test rig is unique based on its application and constraints. A review of different components of an experimental test rig has been provided in chapter 2. This chapter aims to describe the design of the experimental test rig at the University of Oklahoma's drilling vibration lab which is used extensively for stick-slip vibration analysis. The experimental setup is capable of both vertical and horizontal configuration. A schematic of the 15m long vertical experimental setup is shown in figure 3-1. The sensors at the top drive include the displacement sensor, load cell and a rotary encode. The bottom hole assembly includes a rotary encoder for RPM measurement and an electromagnetic brake. The sensors are connected to the data acquisition device (DAQ). The data collected by the DAQ card is processed in LabVIEW, which is used to control and monitor the system using a human machine interface (HMI). The design of the experimental setup can be broken down into the mechanical and electrical components.

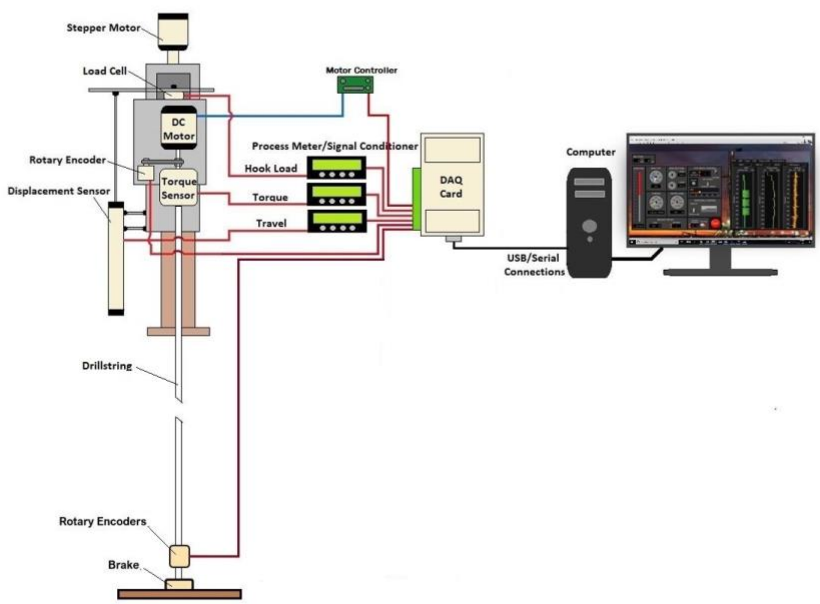

Figure 3-1 Schematic of the vertical experimental setup (Sharma et al., 2020)

3.1 Components of an Experimental Setup

This section contains the mechanical, electrical and data acquisition components of the experimental test rig.

3.1.1 Top Drive Assembly

The top drive assembly of the test rig can be seen in figure 3-2. A stepper motor provides hoisting and weight control of the drill string using a lead screw mechanism. Additionally, an 18V DC motor is utilized to provide rotational energy to the drill string. The DC motor helps in providing a smooth torque output to the drill string. The sensors at the top drive include the displacement sensor, load cell and torque sensor. The sensors are discussed in detail in the latter sections of this chapter.

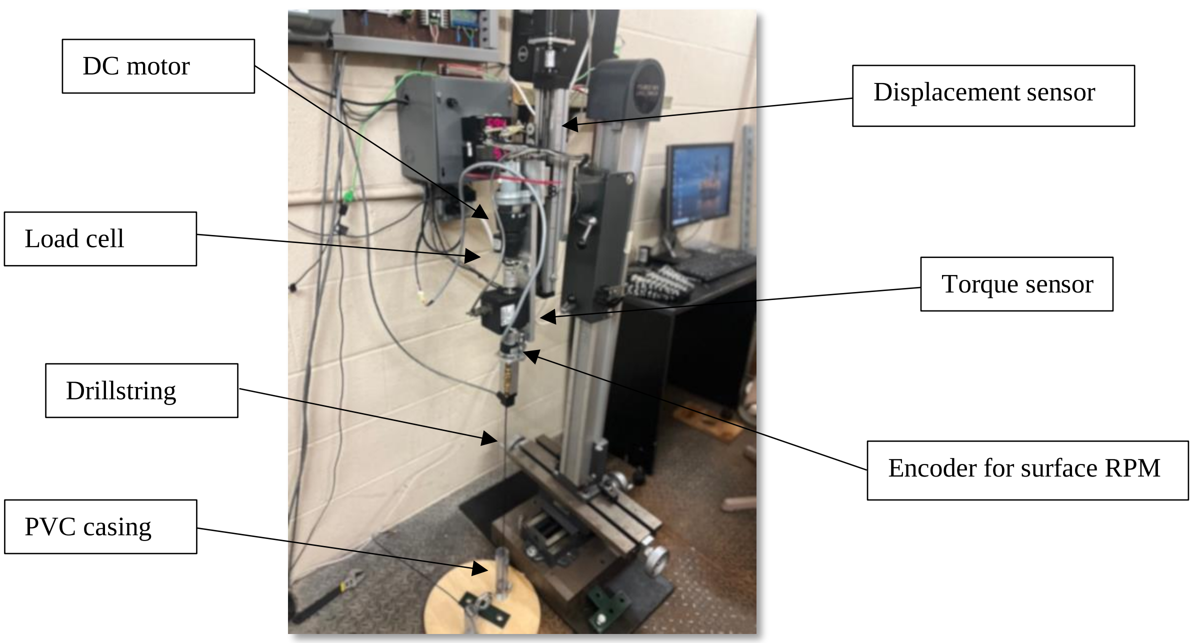

Figure 3-2 Top drive assembly of experimental setup

3.1.2 Drill String

The drill string is integral in transferring rotational energy from the surface to the bit. In the case of this experimental analysis, choosing a suitable drill string is critical to reproduce torsional vibrations in a downscaled setup. The mechanical properties of the drill string are closely considered while making a choice. This section talks about the need for proper downscaling, choosing the right material and performing preliminary torsional stiffness experiments.

Downscaling

The importance of proper downscaling has been discussed before in chapter 2. In this section, the downscaling values for the experimental setup have been calculated. Achieving geometric similarity is the first step in conversion of a large mechanical system to a smaller experimental setup. While geometric similarity considers all angles in the system to be the same, the scaling factor is a function of the length of both systems.

$$Scaling\ factor\ n = \frac{L_{real}}{L_{model}} \text{………(3-1)}$$

In the case of laboratory test rigs that are downscaled from actual drilling size, the limiting factor is often the diameter of the drill pipe. After careful evaluation of the drill pipe length used by various setups, downscaling 450m of an actual drill pipe makes for a reasonable downscaling ratio. Downscaling drill pipe of length smaller than 450m would reduce drill pipe diameter to an unachievable value. Furthermore, if similar materials are used for downscaling, certain parameters like modulus of elasticity and density do not change. Other values must be estimated using the principle of similarity.

Parameters	Variable	Downscaling	Real Value	Lab Scale Values
Length	L	$L_{real} = n \times L_{model}$	450 m	15 m
Diameter	D	$D_{real} = n \times D_{model}$	5″	0.125″
Angular Velocity	ω	$\omega_{real} = \omega_{model}$	50–200 RPM	50–200 RPM
Density	ρ	$\rho_{real} = n^{0.56} \times \rho_{model}$	8.05 g/cm^3	1.2 g/cm^3
Elasticity	E	$E_{real} = n^{2.79} \times E_{model}$	20×10^{10} Pa	15×10^6 Pa
Motor Torque	τ	$\tau_{real} = n^{3.56} \times \tau_{model}$	34–68 × 10^6 mNm	200–1300 mNm
Torsional Stiffness	K_{TOR}	$K_{TORreal} = n \times {}^{3.56}K_{TORmodel}$	2.76 Nm/rad	0.000015 Nm/rad

Table 4 Downscaled design parameters for PVC drill pipe (Srivastava and Teodoriu, 2019)

Table 4 gives a calculated estimate of the drilling parameters under torsional vibration investigation. For the sake of an example calculation, a PVC drill pipe is chosen for an experimental design. Using the downscaling factor of 1:30, a string length of 15m and diameter 0.125” is calculated. Furthermore, the values for drill string torque and stiffness have been calculated. Figure 3-3 lists and compares the various downscaling factors of laboratory test rigs reported in literature for a drill pipe of length 450m. Ratios lower than 1:225 would make geometric downscaling close to impossible with respect to the drill pipe diameter requirement. Such thin pipes will fail to reciprocate the desired mode of vibration during experimental testing. As observed in figure 3-3, only a handful of experiments have a reasonable downscaling ratio, for example, 1: 90 (Patil and Teodoriu, 2013; Westermann et al., 2015), 1:40 (Wen et al., 2018), 1:30 (Marquez and Teodoriu, 2017) and 1:18 (Lin et al., 2018).

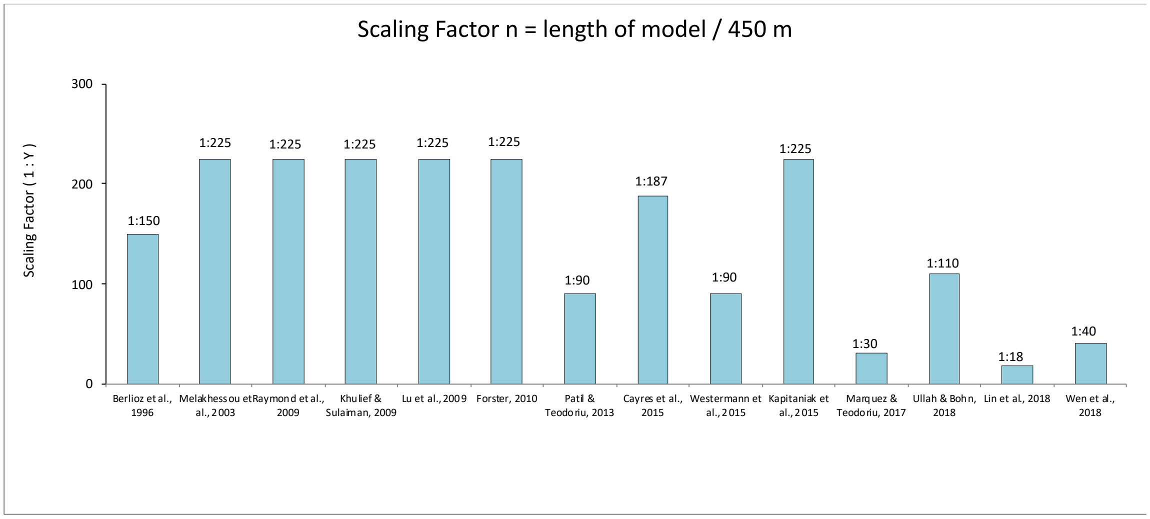

Figure 3-3 Comparison of downscaling factor of laboratory test rigs across the world (Srivastava and Teodoriu, 2019)

Material Choice

Choosing the appropriate drill string material is important. The torsional stiffness of the drill string should be appropriate to study the torsional vibration phenomenon. Four different strings are considered as options, namely, polyethylene, steel, nylon, and aluminum. Basic properties of the string are shown in table 5. Theoretical calculations for the stick-slip period and frequency are performed assuming that the drill string behaves like a simple pendulum under torsional oscillations (Kyllingstad and Halsey, 1988). The calculations explore the relationship between the rotary speed and drill string properties. Figure 3-4 plots the results for the stick-slip period calculation for different rotary speeds. Interestingly, high stick slip periods are observed at lower rotary speeds. This can be explained by the increased friction in the system at lower rotary speeds that cause self-induced bit sticking. Sticking period reduces with increasing rotary speed, a phenomenon commonly understood in real world drilling. Polyethylene has the lowest shear modulus and highest stick slip period. It is fair to state that the torsional rigidity of polyethylene is lowest among the materials considered. Polyethylene seems the most appropriate choice for drill string material as it readily undergoes sticking.

	Den.(kg/m3)	G (Pa)	OD (m)
Polyethylene	950	7.50E+08	0.0031
Steel	7890	8.14E+10	0.00159
Nylon	1150	4.10E+09	0.00443
Aluminum	2700	2.40E+10	0.0031

Table 5 Summary of drill string materials and their properties

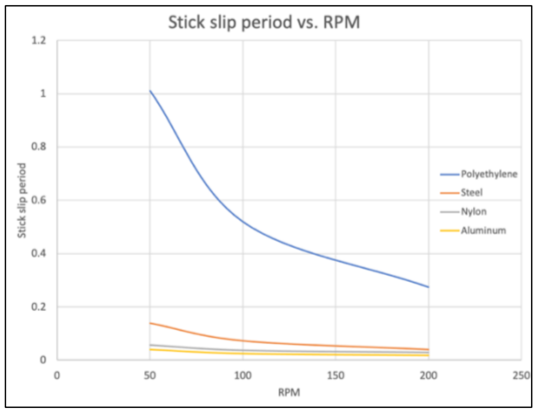

Figure 3-4 Stick-slip period calculation vs. RPM for different strings

Due to their higher torsional stiffness, nylon, aluminum, and steel are not considered appropriate drill string material choices. Further tests have been performed in this section to experimentally verify the stick-slip theoretical calculations. Although the shear modulus of steel is the highest, its stick slip period is greater than nylon and aluminum. this is due to the smaller OD size of the steel string as compared to nylon and aluminum.

Drill string stiffness experiment

For any object undergoing rotational torque, it is important to measure the objects' ability to resist torsion or twisting. In the case of drilling, we are concerned with the torsional stiffness of the drill pipe. In simple words, torsional stiffness is defined as the resistance offered by the drill pipe to the shear stress generated through rotational torque, in torque per radian. Since torsional stiffness is a material property, experimental analysis is the best way to estimate it. The experimental setup can be observed in figure 3-5.

The equation for torsional stiffness is defined as:

$$k = \frac{T}{\theta} = \frac{GJ}{L} \quad \text{.........}(3\text{-}2)$$

Where k = Torsional stiffness (Nm/radian),

θ = Angle of twist (radian)

T = Torque applied (Nm)

G = Shear modulus/modulus of rigidity (Pa)

J = Polar moment of inertia (m^4)

L = Length of drill pipe (m)

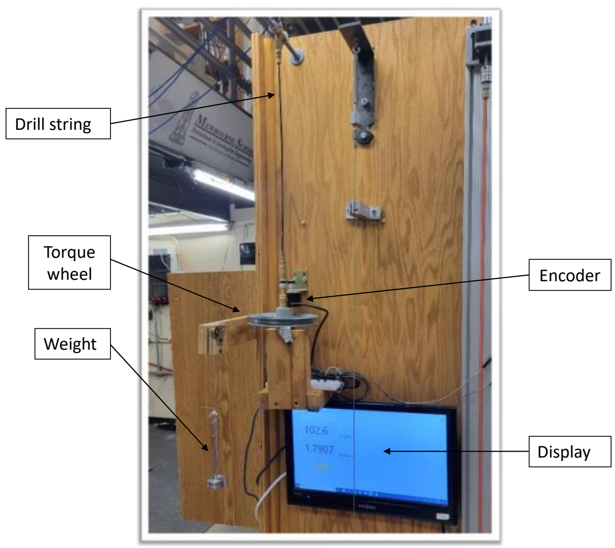

Figure 3-5 Torsional stiffness laboratory experiment

A small section (0.38m) of the drill string is used to test the torsional stiffness. The top section of the string is kept rigid while a torque wheel is utilized to apply shear stress on the string. An encoder is used to measure precise twist angles. The stored torque in the string is measured and plotted against the angle of twist for the three different strings. Aluminum, soft, and hard polyethylene are used as string materials.

The torsional stiffness of different strings is calculated as slopes of the individual plots in figure 3-6. The values are:

- Soft polyethylene (OD – 3.1mm): Torsional stiffness k = *0.0185 Nm/rad*

- Hard polyethylene (OD – 3.29 mm): Torsional stiffness $k = 0.053\ Nm/rad$
- Aluminum (OD – 3.29mm): Torsional stiffness $k = 0.505\ Nm/rad$

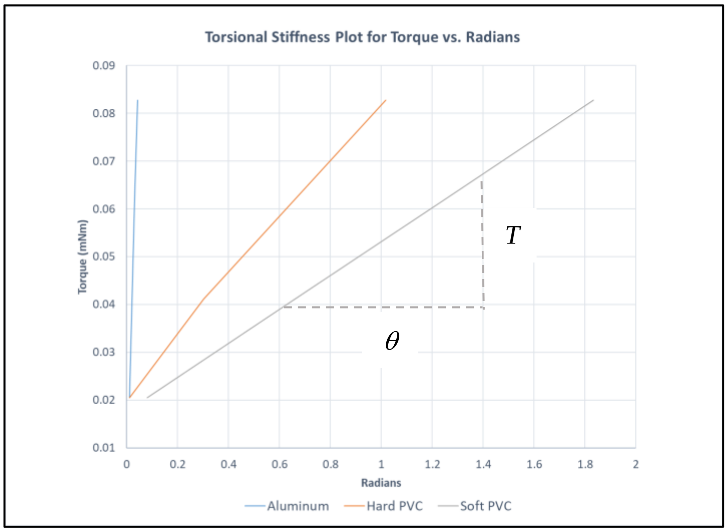

Figure 3-6 Experimental results for torsional stiffness tests

Comparison with drilling data

To validate the experimental setup and the drill string material and stiffness, a comparison is made with actual drilling data using the stick-slip index (SSI) defined in equation 1-1. The drilling data is plot in figure 3-7. Both surface and downhole data are measured at 1 Hz. Bit sticking of close to 1 second along with negative bit RPM is observed in figure 6-2. Experimental data is plot from figure 3-8 to 3-13 for 1 second bit sticking with 6 different strings. SSI is calculated for each case and reported.

$SSI_{drilling\ data} = 1.42.$ – *figure 3-7*

$SSI_{string\ 1}$ *(polyethylene1) = 1.15* – *figure 3-8*

$SSI_{string\ 2}$ *(steel wire) = 2.5* – *figure 3-9*

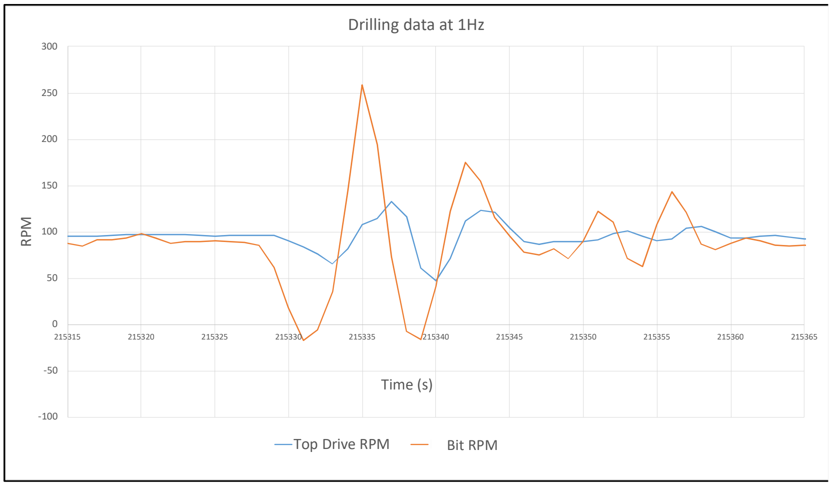

Figure 3-7 Bit sticking of 1 second observed in drilling data sampled at 1Hz

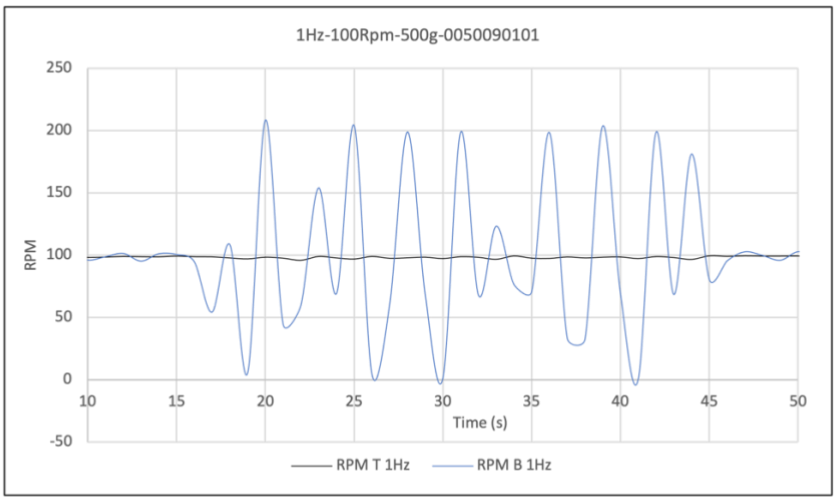

Figure 3-8 Experimental test reproducing 1 second sticking at 1 Hz with string 1 (polyethylene 1)

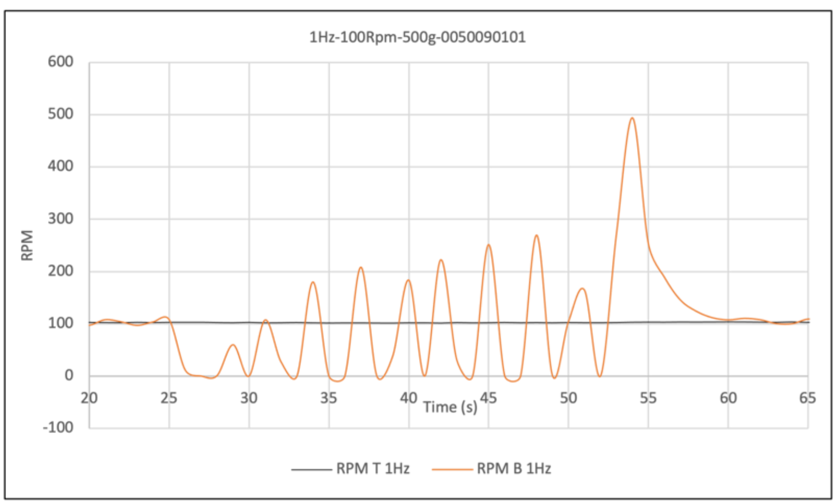

Figure 3-9 Experimental test reproducing 1 second sticking at 1 Hz with string 2 (steel wire)

$SSI_{string\ 3} = 1.275$ – *figure 3-10*

$SSI_{string\ 4} = 1.45$ – *figure 3-11*

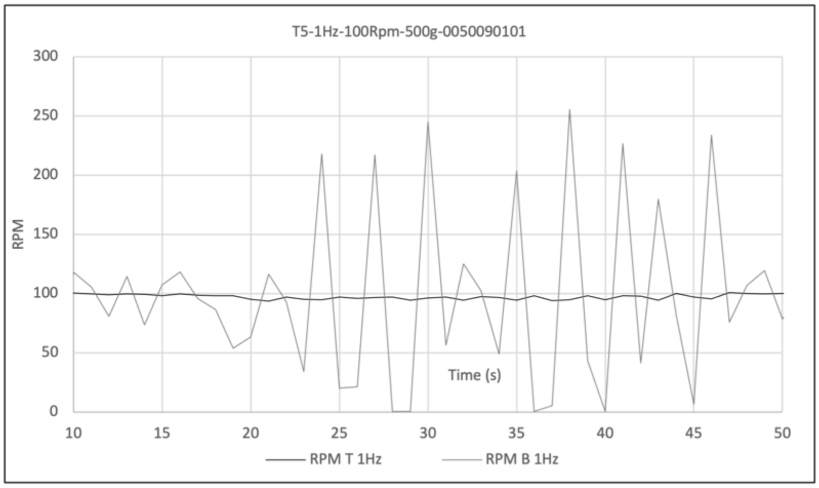

Figure 3-10 Experimental test reproducing 1 second sticking at 1 Hz with string 3 (nylon)

-

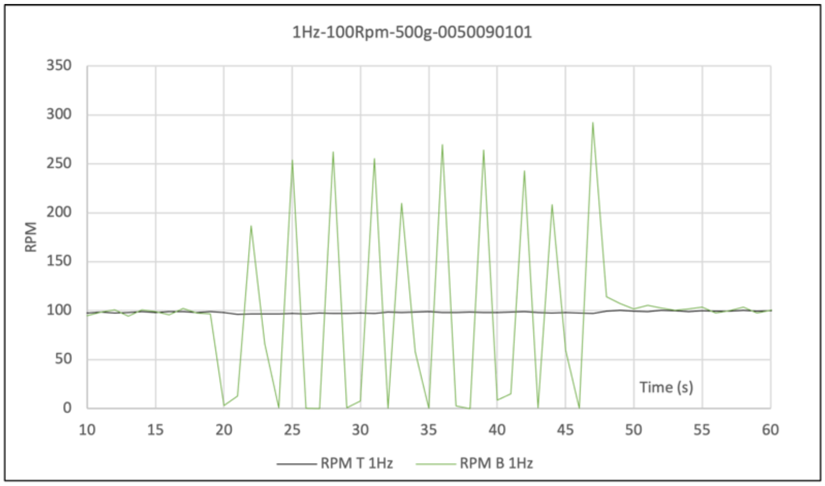

Figure 3-11 Experimental test reproducing 1 second sticking at 1 Hz with string 4 (polyethylene 2)

$SSI_{string\ 5} = 0.42$ – *figure 3-12*

$SSI_{string\ 6} = 0.2.$ – *figure 3-13*

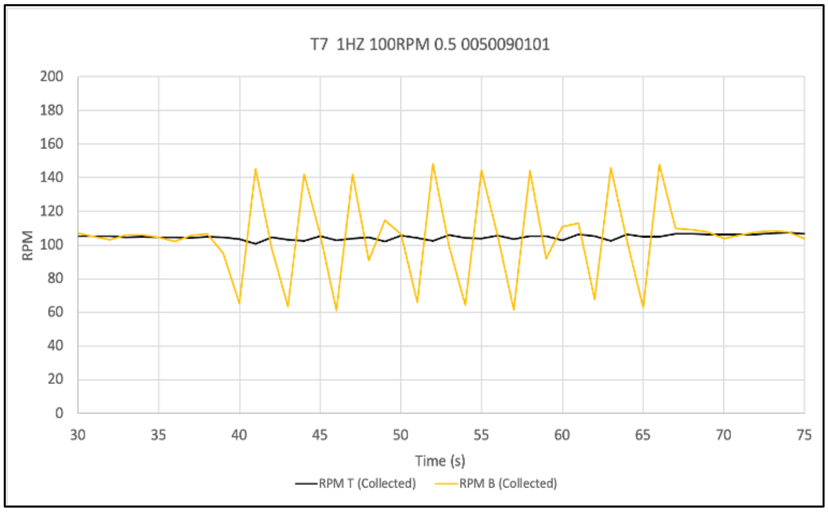

Figure 3-12 Experimental test reproducing 1 second sticking at 1 Hz with string 5 (polyethylene 3)

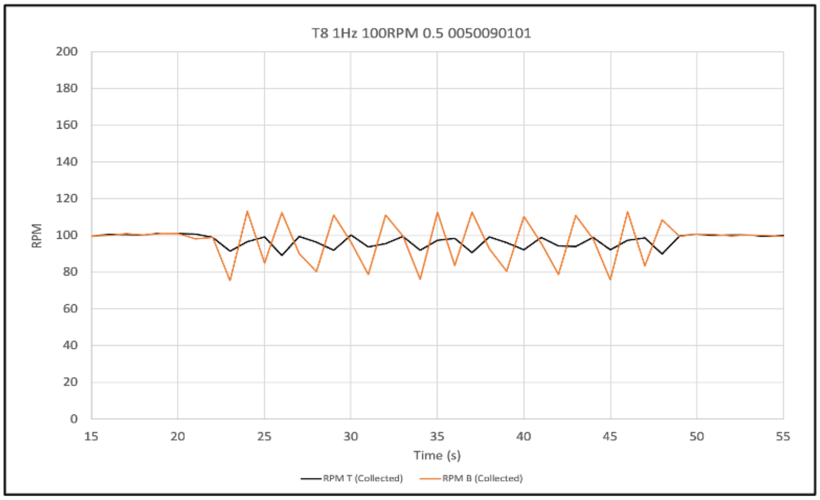

Figure 3-13 Experimental test reproducing 1 second sticking at 1 Hz with string 6 (aluminum)

The closest match to drilling data, in terms of SSI is observed in figure 3-11 with string 4 (polyethylene). SSI of drilling data is 1.42 whereas SSI = 1.45 for string 3. On the other hand, Aluminum has the lowest SSI of 0.2 as seen in figure 3-13. This makes sense as aluminum has one of the highest stiffness among the lot. The SSI of steel wire is relatively high, but this is because of its small OD as compared to other strings.

3.1.3 Rock-bit interaction

The BHA includes an electromagnetic brake for rock-bit interaction. An electromagnetic brake is preferred instead of an actual bit and rock due to predictability and repeatability of testing conditions. The electromagnetic brake induces a non-linear frictional torque at the bit when activated. In doing so, it opposes the motion of the drillstring. Figure 3-14a shows the electromagnetic brake being used in the BHA. Figure 3-14b displays the performance curve of the brake which is used to calculate the torque acting at the bit.

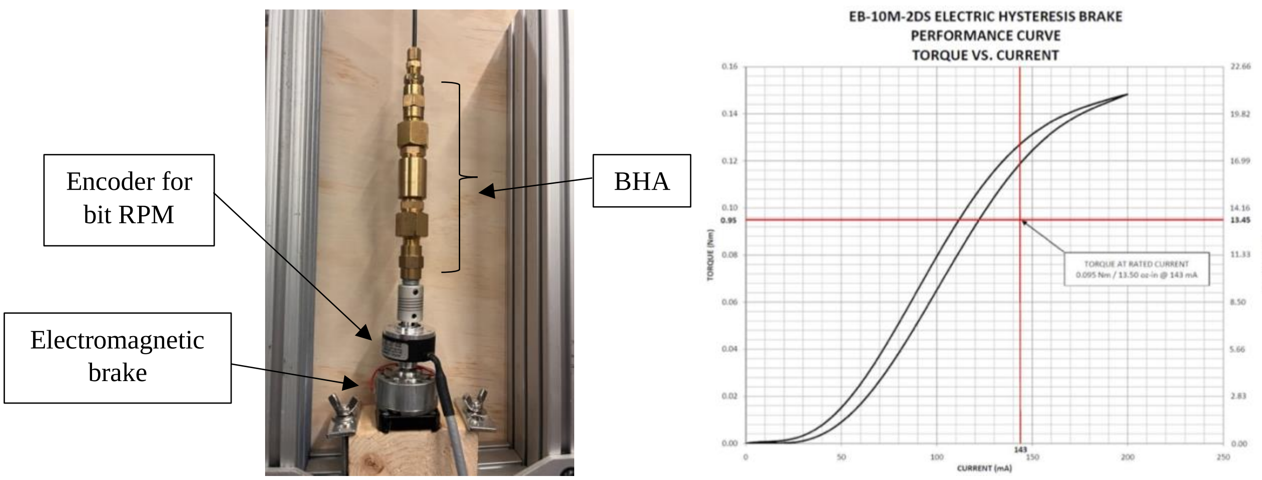

(a) (b)

Figure 3-14 Electromagnetic brake (a) and its performance curve (b)

3.1.4 Vertical to horizontal configuration

The experimental setup features a vertical to horizontal configuration adaptability. While the top drive assembly remains fixed, the drill string kicks off at 5m to build a 4m long horizontal section as seen in figure 3-15. The drillstring passes through a PVC pipe in the vertical and horizontal sections. The BHA and bit system in the horizontal configuration is the same as the one used in the vertical configuration. The top drive and BHA can be observed in the schematic diagram in figure 3-15. The objective of adding the horizontal section is to see the impact of well configuration on stick-slip vibrations as the well friction co-efficient changes drastically due to added points of contact in the horizontal setup.

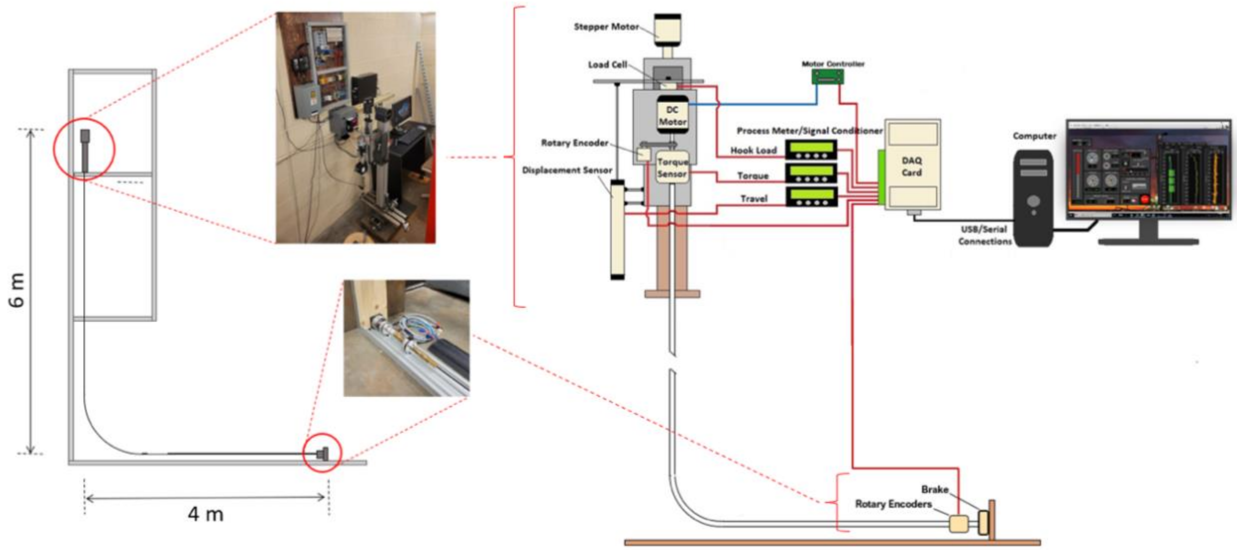

Figure 3-15 Schematic diagram of the horizontal well configuration

3.1.5 Electrical Sensors

The following section lists the three most important sensors used in the experimental setup namely, torque sensor, load cell sensor and displacement sensor.

Torque sensor calibration

The torque sensor is a strain gauge based bridge transducer that sits below the top drive system and measure the torque being supplied to the drillstring. The sensor has been calibrated using the experiment shown in figure 3-16, where a known amount of torque is applied to the string using the disc with weights. The details of the sensor include:

- Limit of torque sensor: 200 in oz
- Display unit for experiment: in lbf
- Maximum load calibrated: 10.57 mN

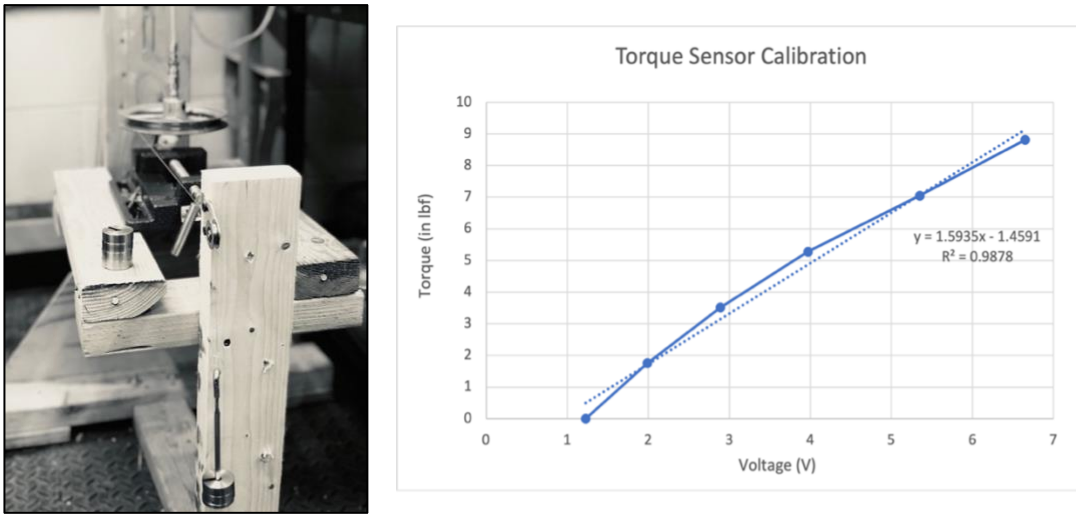

Figure 3-16 Experimental calibration of torque sensor

Displacement sensor calibration

The displacement sensor is a potentiometer-based sensor that is used to measure the vertical distance covered by the drillstring hoisting. Figure 3-17 shows the calibration and location of the displacement sensor on the top drive.

- Limit of displacement sensor: 300mm
- Display unit for experiment: mm
- Maximum distance calibrated: 250m

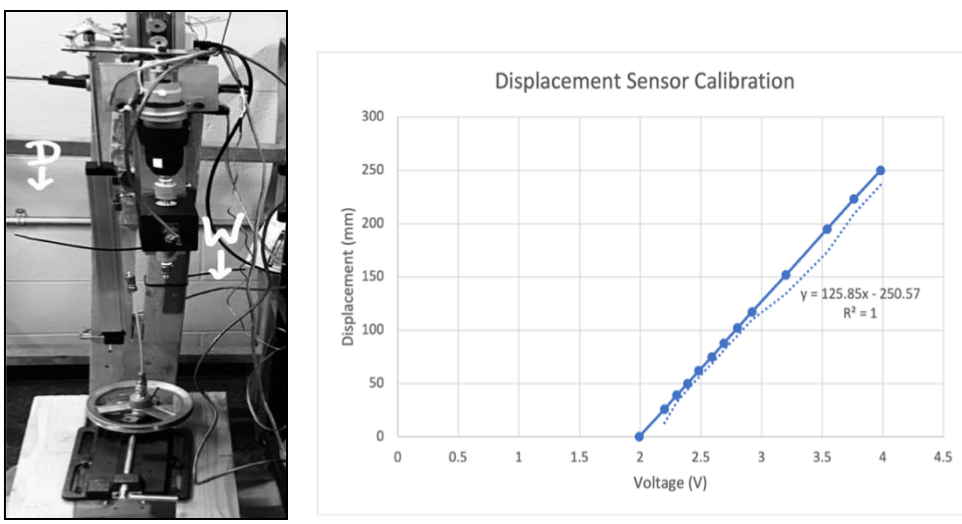

Figure 3-17 Experimental calibration of displacement sensor

Load cell sensor calibration

The load cell sensor is also a strain gauge-based bridge transducer that is calibrated to measure the weight acting on the bit. The calibration of the sensor is seen in figure 3-18. The details of the load cell sensor include:

- Limit of load cell: 12.5 Kg
- Display unit for measurement: gm
- Maximum load calibrated: 2000 gm

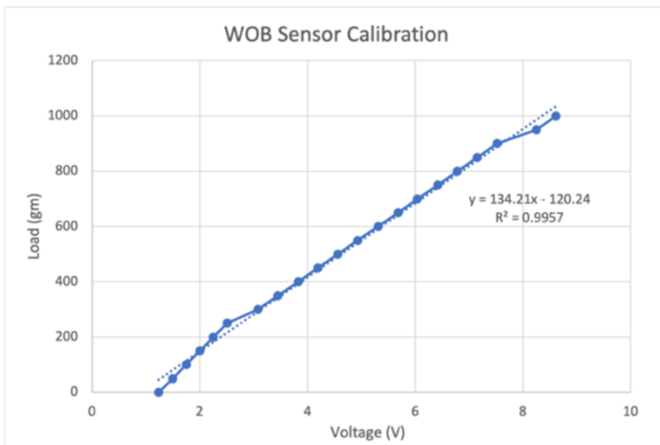

Figure 3-18 Experimental calibration of load cell sensor

3.1.6 Data acquisition and HMI (Human machine interface)

The hardware and software components of the experimental setup have been integrated into the HMI design. The interface closely mimics a drilling simulator design as drilling simulators offer a great academic learning opportunity (Srivastava et al., 2018). Figure 3-19 shows the HMI design developed for the experimental setup. The HMI features a simple design to incorporate the real-time process parameters and display them. It includes indicators and gauges to display surface and bit RPM, surface torque, hook load, WOB and angular position. To control the surface RPM, a motor control slider can be used. The HMI also features a unique sampling rate toggle that can be used to vary the sampling rate of the measurements. Adjustments to the WOB is done by changing the string tension using the position control. The user also has the option to save the generated data by switching the 'Save Data' switch on.

Figure 3-19 A snippet of the HMI (Human machine interface) for the experimental setup

3.2 Experimental design

The experimental tests have been carried out with 6 different materials as described in the previous chapter. The torsional stiffness of the viable material options has been estimated experimentally. The drill strings are connected to the top drive and made to pass through a PVC plexiglass with OD 33.5mm and ID 23.3mm. Rotational speeds from 50 to 200 RPM have been tested at different weight on bit values. The novelty of the experimental setup is in the programmable brake at the BHA. The electromagnetic brake controls the frictional force acting on the bit. Different sticking periods have been tested in combination with different slip periods to measure surface and downhole response accordingly. The data acquisition systems are integrated via LabVIEW into the human machine interface where sensor measurements are monitored, and the process parameters are controlled. The procedure of a stick-slip test is described below:

1. A string is chosen for analysis and is connected to the top drive and BHA via compression fitting through the PVC plexiglass
2. Connection to all sensors is verified and a safety inspection is performed on the experimental setup

3. The LabVIEW VI is used for controlling the process parameters. Before switching on the system, an appropriate sampling rate of measurement (1, 10 or 100Hz) is chosen and the option to save data is selected
4. The string is rotated by toggling the surface RPM, WOB to a desired value
5. When the system is stable, a test is performed by activating the electromagnetic brake that provides a programmed torque at bit
6. The HMI (Human machine interface) is monitored to verify surface and downhole response to the stick-slip test
7. The tests are repeated for 1, 10 and 100 Hz sampling before moving to a different torque at bit sequence
8. Steps 5 to 7 are performed repeatedly for different RPM and WOB combinations
9. The string is changed once all tests have been recorded successfully

3.2.1 Test matrix

Since there are multiple parameters that can be adjusted in a torsional stick-slip test, the experimental design is illustrated in figure 3-20 and 3-21 for both vertical and horizontal configurations. The different strings used in the experimental analysis help understand the effect of torsional stiffness on severe torsional oscillations. String 1, 4 and 5 are different polyethylene strings. String 2 is a steel wire, 3 is nylon and 6 is aluminum. Only string 4 is used in the horizontal configuration. The bearing torque is the static friction in the system. As mentioned earlier, the tests are repeated for the different sampling frequencies. Combinations of stick and slip periods help investigate different vibration related scenarios. A total of 1500 tests have been performed approximately.

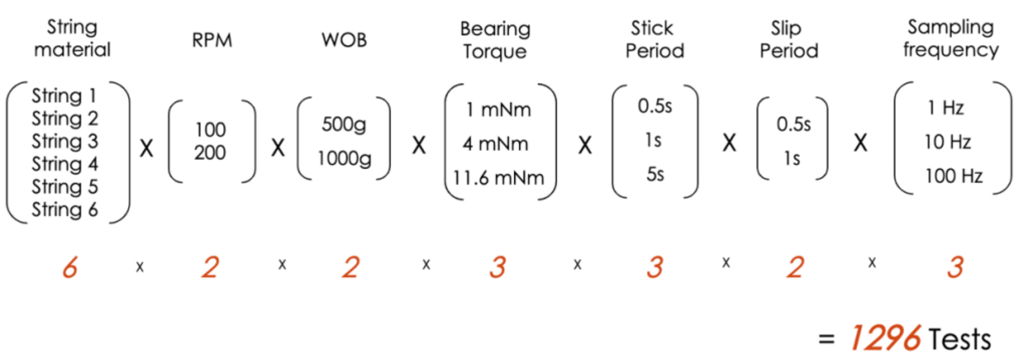

Figure 3-20 Experimental design of torsional stick-slip test (Vertical configuration)

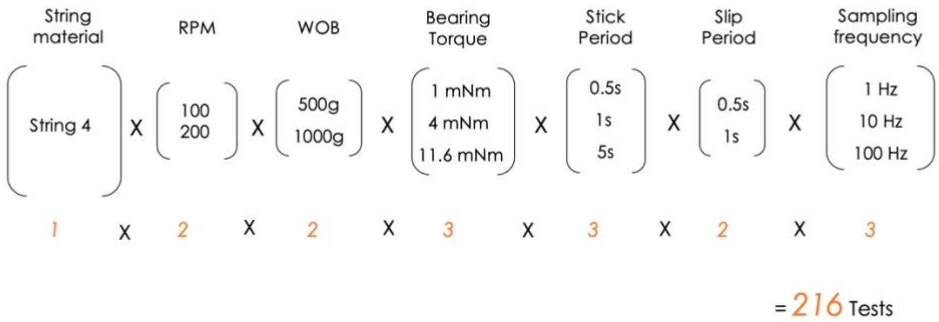

Figure 3-21 Experimental design of torsional stick-slip test (Horizontal configuration)

When talking about the duration of bit sticking, two kinds of bit sticking phenomenon are highlighted:

Severe stick-slip vibrations

Also called low frequency vibrations, this phenomenon includes longer bit sticking periods of 2-3 seconds or higher. These vibrations can be identified by a characteristic frequency of ≤ 0.02 Hz. These vibrations are considered severe in nature because longer bit sticking duration causes high torsional energy storage in the string. Ultimately, the enormous energy buildup is released violently in the slip phase through sudden bit acceleration and resultant downhole damage.

Mild stick-slip vibrations

Also called high frequency vibrations, these vibrations are characterized by abrupt bit sticking cycles of one second or lower. The characteristic frequency of this vibration is approximately 1 Hz. Since the period of sticking is smaller, the resultant peaks in bit RPM are lower than severe stick-slip vibrations.

3.2.2 Severity estimation

To compare experimental results based on different process parameters, the severity of torsional vibrations needs to be quantified. Currently, a statistical function is used to define this severity index. The severity index is often referred as stick-slip index (SSI) or stick-slip severity (SSS). It is defined as:

$$Stick - slip\ index\ (SSI) = \frac{RPM_{max} - RPM_{min}}{2 * RPM_{ref}} \quad \text{.........(3-3)}$$

Where, RPM_{max} and RPM_{min} are maximum and minimum bit RPM. RPM_{ref} is the reference RPM which is either the surface RPM (Ritto and Tehrani, 2018) or the average bit RPM (Patil, 2013). Another index used for torsional vibrations (Ertas, 2014) is defined as:

$$Torque\ Severity\ Index\ (TSE) = \frac{RPM_{max} - RPM_{avg}}{RPM_{avg}} \quad \text{………(3-4)}$$

Where, RPM_{max}, RPM_{min} and RPM_{avg} are bit RPM measurements. Effectively, TSE or SSI are calculated to be similar in values. Values of 1 indicate pure sticking conditions where the bit RPM drops to 0 due to sticking and fluctuates to at least twice the reference RPM or twice the average bit RPM. Values between 0.5 and 1 indicate mild torsional oscillations and values under 0.5 indicate normal drilling conditions. For the sake of uniformity, SSI will be used as a basis of comparison for all experiments. Additionally, a new index is defined called the Surface Torque Index (STI) that considers the fluctuation of surface torque due to severe torsional oscillations. It is defined as:

$$Surface\ Torque\ Index = \frac{Surf.T_{max} - Surf.T_{avg}}{Surf.T_{avg}} \quad \text{………(3-5)}$$

3.3 Summary of experimental design

This section presents the detailed approach taken in designing and constructing an experimental setup for stick-slip investigation. The physical and electrical aspects of the setup have been discussed. Emphasis is given to the downscaling ratio of the experimental setup as well as to the choice of drillstring material. The appropriate material is chosen by experimental analysis and comparison with real world vibration data. The procedure for conducting a stick slip test has also been provided. Most importantly, the various influencing parameters in the investigation of stick-slip vibrations have listed in the final experimental design. A test matrix of 1300 tests has been designed for the vertical string alone. Since quantification of stick slip vibrations is important for comparison of independent influencing parameters, indexes used in literature for measuring vibration severity have been defined. The next chapter focuses on results from the experimental setup.

Chapter 4: Experimental Results

This section presents the experimental results obtained from the stick-slip tests performed. The experimental procedure and test matrix has been described in section 4.2. By varying the influencing process parameters for the stick-slip tests, approximately 1500 tests have been performed using 6 drillstring materials in the horizontal and vertical well configuration. Mild stick slip tests relate to high frequency sticking with less than 1 second of bit sticking where severe stick-slip tests induce bit sticking for up to 5 seconds. For the sake of brevity, test results from string 4 (polyethylene) are presented in this section as the drillstring material closely imitates vibrations seen in field drilling. The section covers the following results

1. Effect of sampling rate for mild vs severe stick-slip vibrations
2. Effect of drillstring stiffness for mild vs severe stick-slip vibrations
3. Effect of RPM and WOB on mild vs severe stick-slip vibrations
4. Effect of well configuration on self-induced bit sticking
5. Effect of well configuration on mild vs severe stick-slip vibrations
6. Effect of bit sticking and slipping time-period on vibration response

Additionally, the results are compared using the SSI (stick slip index) and STS (surface torque severity) index.

4.1 Effect of sampling rate for mild stick-slip vibrations

For this experiment, sampling measurements are toggled between 1, 10 and 100 Hz. For each sampling rate, a set of mild and severe stick-slip tests are conducted. The tests remain identical for the different sampling rates. For each test, the surface torque, surface, and bit RPM are plot vs time. Additionally, each test is conducted at 100 RPM and 0.5kg WOB.

4.1.1 High frequency bit sticking / Mild stick-slip vibration results

The three test cases for high frequency bit sticking at 1, 10 and 100 Hz are plotted from figure 4-1 to 4-3. Interestingly, the vibration signature is different for all the three cases of sampling frequency. Overall, the test in figure 4-1, sampled at 1 Hz looks smooth with low noise interference whereas test case in figure 4-3 has the most noise due to higher sampling frequency.

With respect to surface and bit RPM, a few interesting observations can be made for high frequency stick-slip phenomenon. Peaks in bit RPM during stick-slip vibrations is commonly observed. This phenomenon is not caught by the 1 Hz sampling rate test (figure 4-1). Peaks in bit RPM up to 5 times the surface RPM can be observed in both 10 and 100 Hz sampling rate tests (figure 4-2 and 4-3). RPM peaks at bit represent sudden bit acceleration that has potential to damage downhole tools. Furthermore, negative bit RPM can be observed during bit sticking but only in the 100 Hz sampling test (figure 4-3). In comparison to low frequency bit sticking, the increment in surface torque and bit RPM is not significant and hence can be interpret as mild stick-slip vibrations.

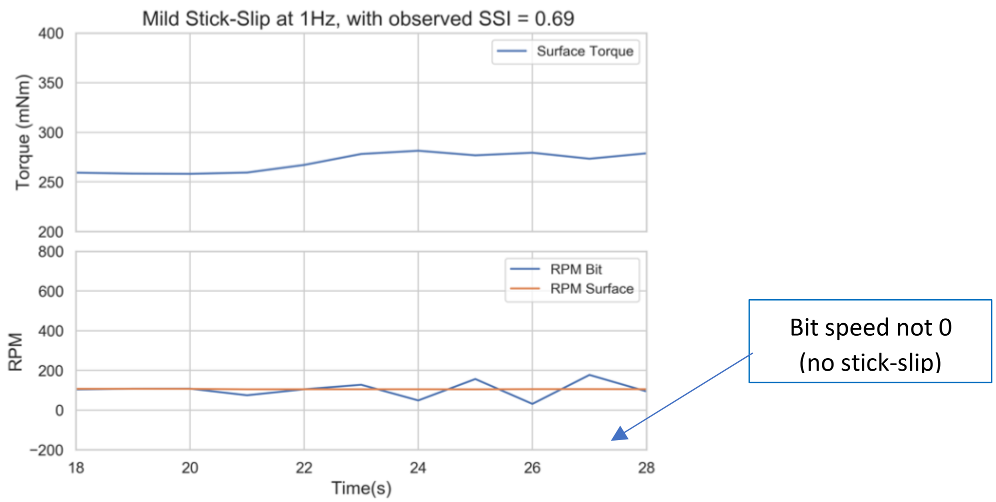

Figure 4-1 Mild stick-slip test, measured at 1 Hz sampling

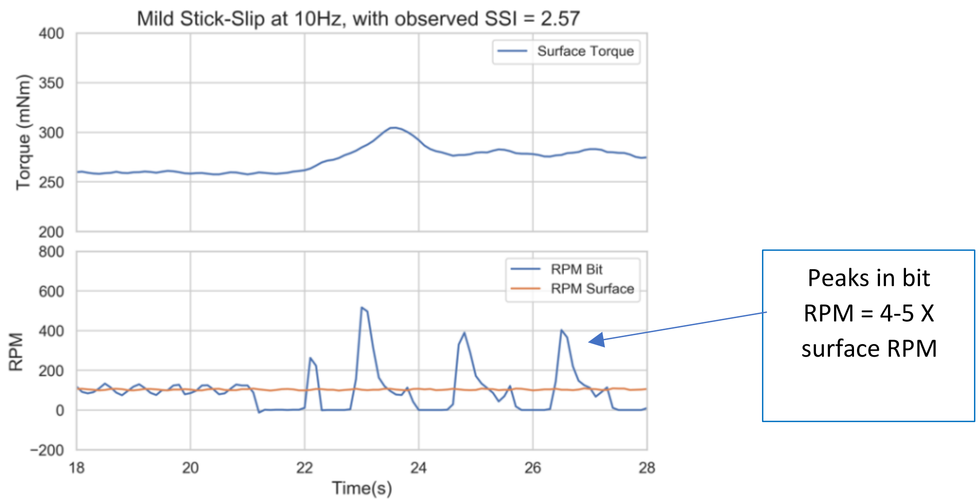

Figure 4-2 Mild stick-slip test, measured at 10 Hz sampling

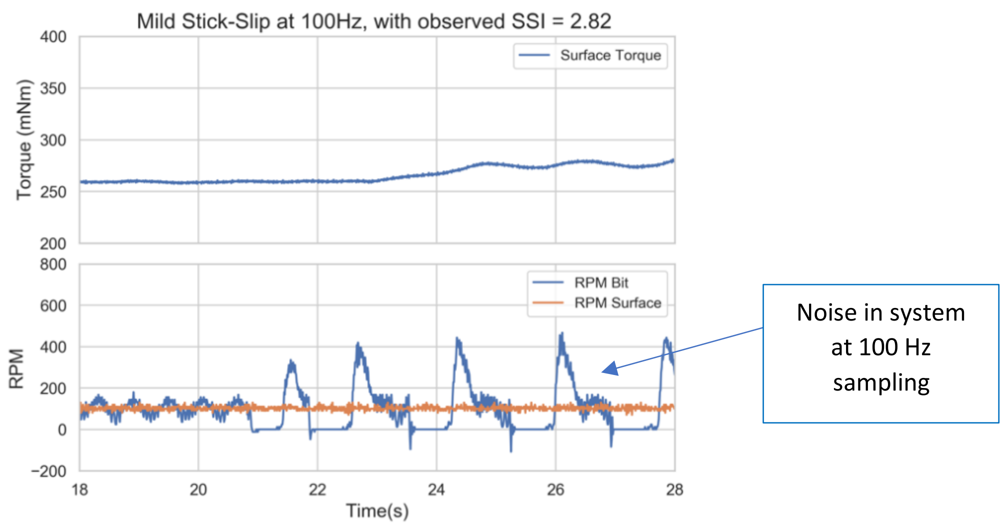

Figure 4-3 Mild stick-slip measurements, sampled at 100 Hz

With respect to bit sticking, as observed in figure 4-1, bit RPM does not completely stop in 1 Hz case. However, this does not confirm the absence of bit sticking as bit sticking can be observed in 10 and 100 Hz sampling case at approximately 21 second mark. The bit sticking period is observed to be lower than 1 second, confirming the characteristic frequency of high frequency stick-slip vibrations at around 1 Hz. The sudden reduction in bit RPM during bit sticking is compensated by an increment in surface torque, as observed in all cases. The increment in surface torque can be seen around 10-15 % in the three cases. Interestingly, a similar delay in surface torque response to bit sticking can be observed in all cases which confirms that a similar time is taken for the disturbance wave at the bit to reach the surface. The delay is approximately 2 seconds and is a function of the drillstring stiffness and length.

4.1.2 Low frequency bit sticking / Severe stick-slip vibration results

Characteristics of low frequency bit sticking include high torque and RPM fluctuations and longer period of bit sticking. As seen in figure 4-4 to 4-6, bit sticking of up to 5 seconds can be observed in all cases. Higher bit sticking period in the stick phase results in higher energy buildup and consequently, a higher bit acceleration in the slip phase. 1 Hz sampling frequency is not sufficient in estimating vibrations severity as seen in figure 4-4, bit RPM up to 15-20 times the surface RPM can be observed in both 10 and 100Hz sampling tests (figure 4-5 and 4-6) leading to severe downhole shock and vibrations. Sudden high RPM peaks create a rotational inertia in the drillstring which is compensated by negative rotations. This is only observed in the 100 Hz sampling test, as seen in figure 4-6. Additionally, surface RPM is constant in all three cases proving that it is not an indicator of downhole vibrations. With respect to torque response, similar torque swings are observed at the surface in all cases of sampling frequency. This proves that high frequency sampling is not required for measuring surface measurements to understand bit sticking severity. Vibrations originating from bit sticking produce waves of disturbance that travel upwards in the drillstring. Unlike high frequency bit sticking, increments of up to 80% can be observed in surface torque response due to severe bit sticking.

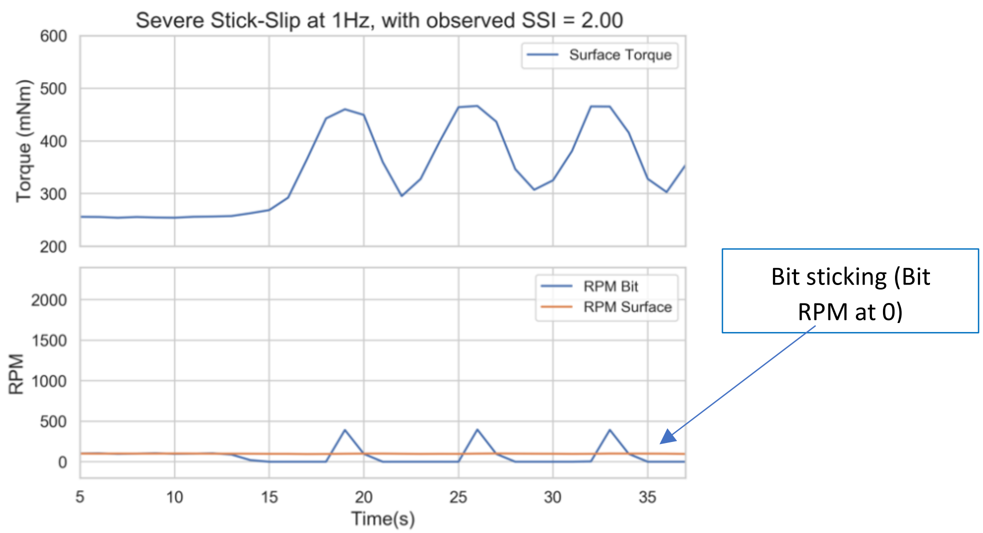

Figure 4-4 Severe stick-slip measurements, sampled at 100 Hz

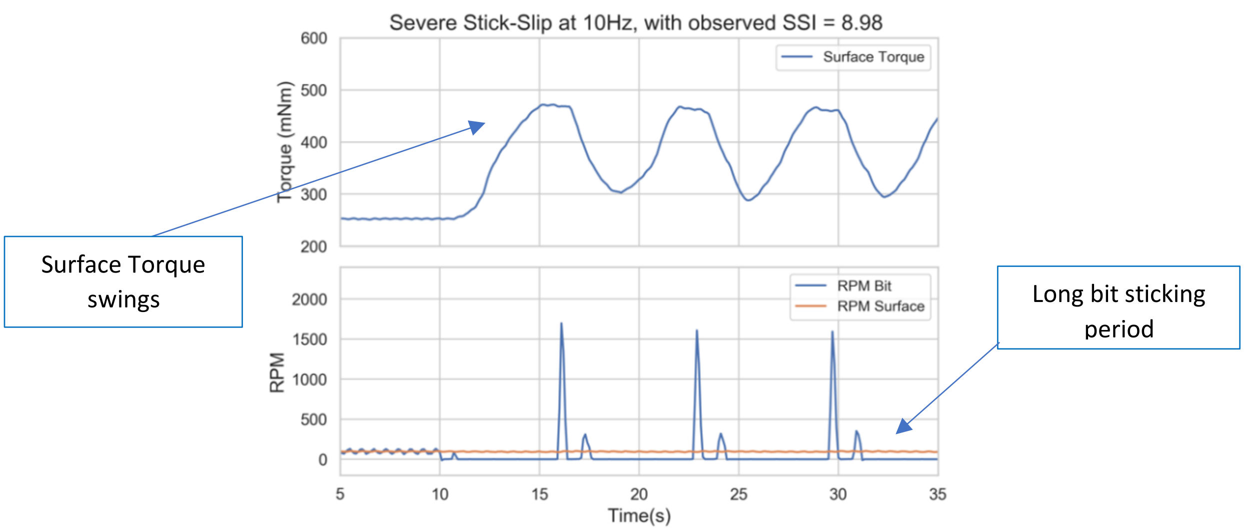

Figure 4-5 Severe stick-slip measurements, sampled at 10 Hz

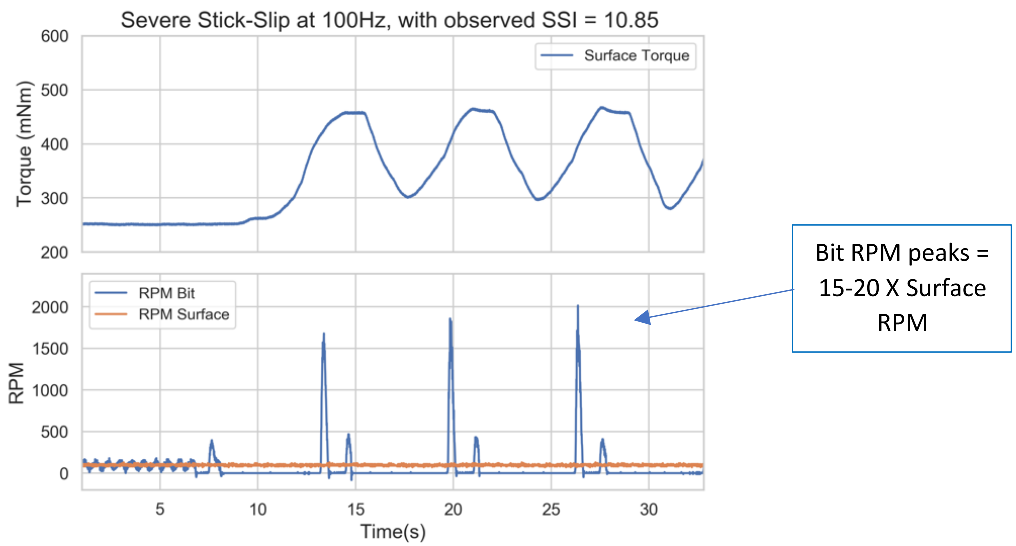

Figure 4-6 Severe stick-slip measurements, sampled at 100 Hz

4.2 Effect of drillstring stiffness for mild vs severe stick-slip vibrations

The extent of torsional oscillations in a drillstring is dependent on multiple factors including system friction, wellbore trajectory and drillstring properties (Cayeux et al., 2020). Amongst drillstring properties, torsional stiffness is an important metric that helps understand the behavior of torsional vibrations along the drillstring. The torsional stiffness of BHA is often optimized to dampen torsional oscillations, as explained in 2.3.1. This section discusses the results for mild vs severe stick slip vibrations for 4 different string materials, polyethylene, aluminum, nylon, and aluminum. Nylon string has the thickest OD followed by aluminum, polyethylene, and steel. Nylon and aluminum strings have higher/comparable stiffness than the steel wire which is significantly thinner. Both RPM and surface torque response have been plotted vs. time.

4.2.1 Mild stick-slip at 100 RPM

The results for mild stick-slip vibrations at 100 RPM can be seen in figure 4-7. A common sticking period begins around the 19th second mark when RPM values drop to 0. Aluminum is seen to offer more resistance to bit sticking torque resulting in quicker stabilization. When looking at surface torque response in figure 4-8, highest index can be observed in aluminum. Due to its high torsional stiffness, there is less energy stored in the system and the wave of disturbance is swiftly transferred to the surface.

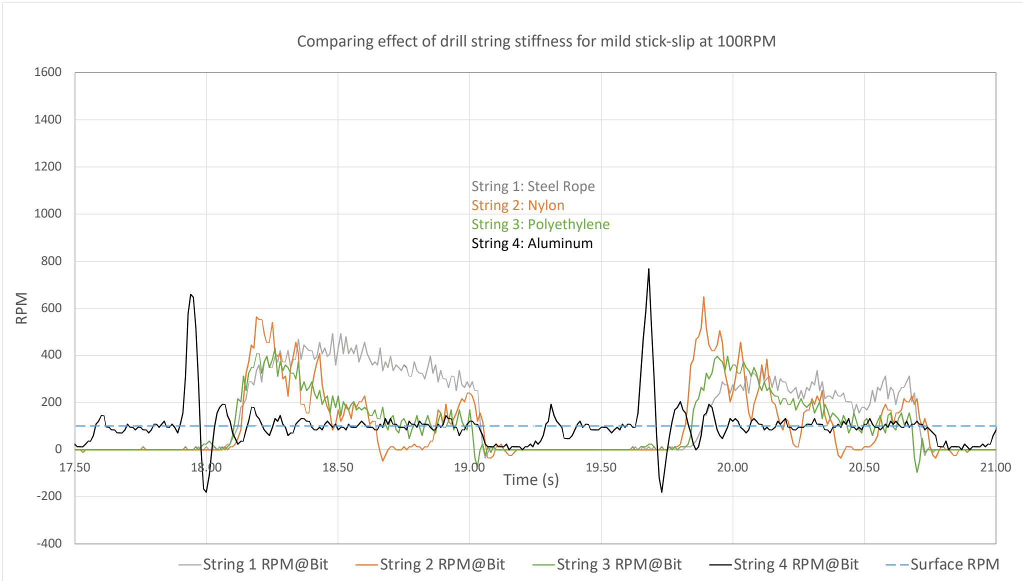

Figure 4-7 RPM response for mild stick-slip vibrations at 100RPM

In figure 4-8, it is observed that the surface torque variation in the steel rope is the lowest, followed by the polyethylene string.

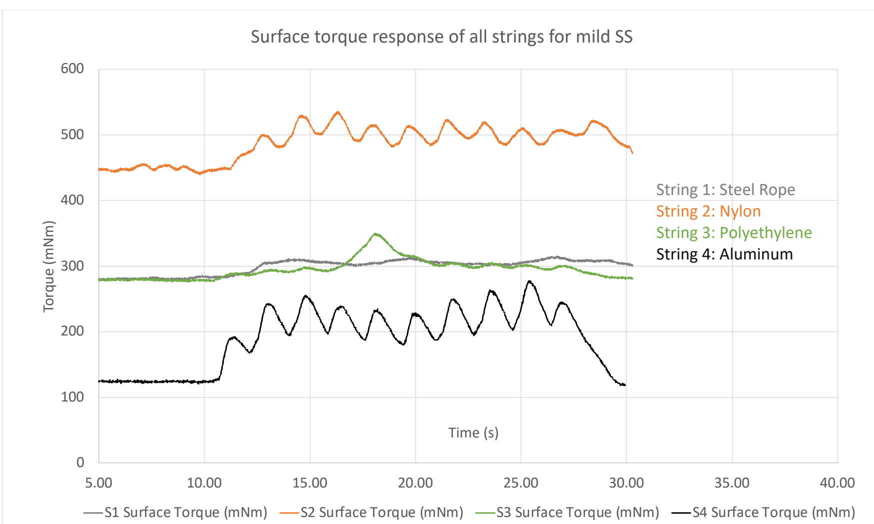

Figure 4-8 Surface torque response for mild stick-slip vibrations at 100RPM

4.2.2 Severe stick-slip at 100 RPM

The results for severe stick-slip vibrations at 100 RPM is presented in figure 4-9 and 4-10. While all strings are made to stick for 5 seconds, the nylon string is only made to stick for 2 seconds due to surface torque limits regarding nylons high inertia. The aluminum string only undergoes torsional oscillations indicating that the bit torque is not sufficient to induce sticking. In the case of severe vibrations, most energy is stored in the polyethylene string during the stick phase as its resultant RPM peak is the highest.

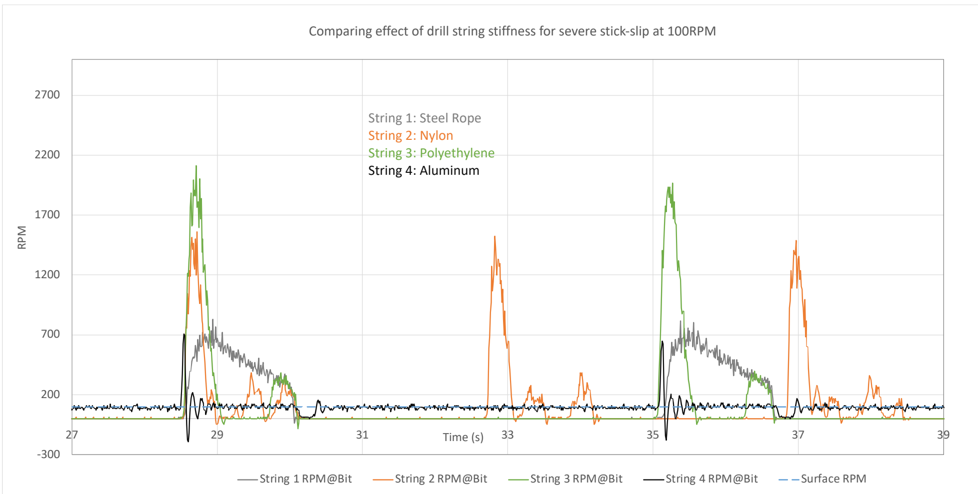

Figure 4-9 RPM response for severe stick-slip vibrations at 100RPM

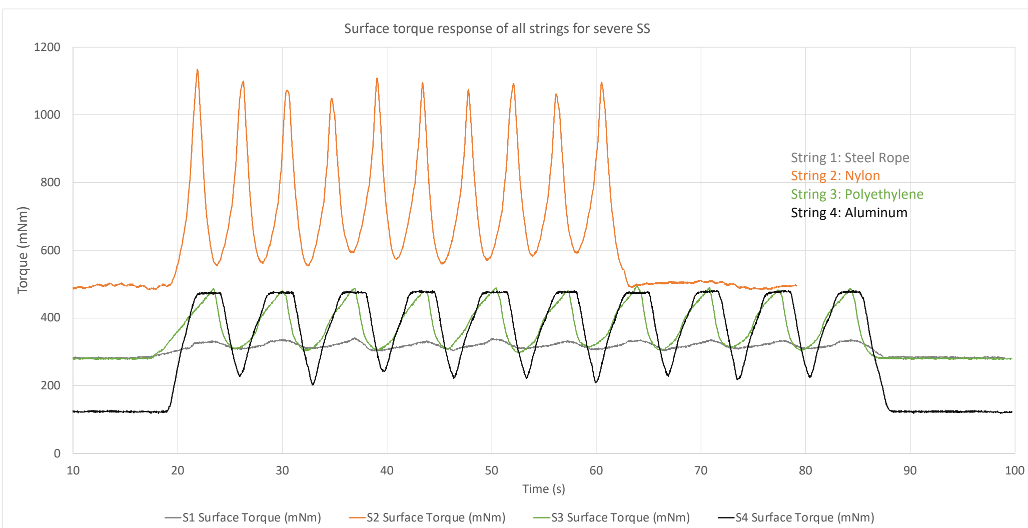

Figure 4-10 Surface torque response for severe stick-slip vibrations at 100RPM

The surface torque response as seen in figure 4-10 indicates the highest variation for nylon followed by aluminum indicating stiff string behavior. The least torque variation is seen in the case of steel wire followed by polyethylene.

4.2.3 Mild stick-slip at 200 RPM

The mild stick-slip test from section 4.2.1 is repeated at 200 surface RPM for the four strings. Results are seen in figure 4-11 and 4-12. The behavior of the strings stays similar to the previous experiment at 100RPM. The aluminum string only undergoes torsional oscillations while the other strings stick for 0.5 seconds. Interestingly, the nylon string reacts the fastest to the bit torque release at the 23.5 second mark. This can be attributed to its higher torsional stiffness.

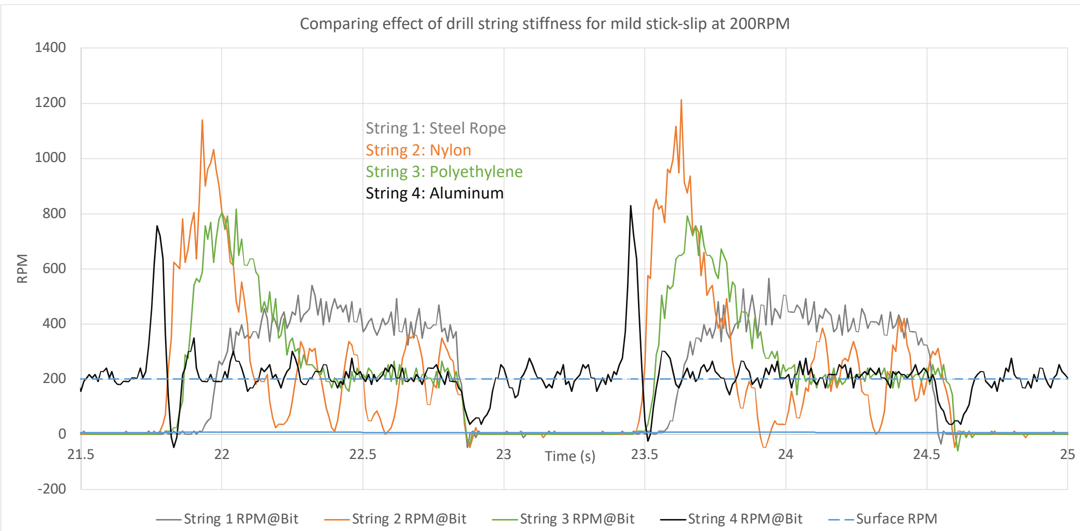

Figure 4-11 RPM response for mild stick-slip vibrations at 200RPM

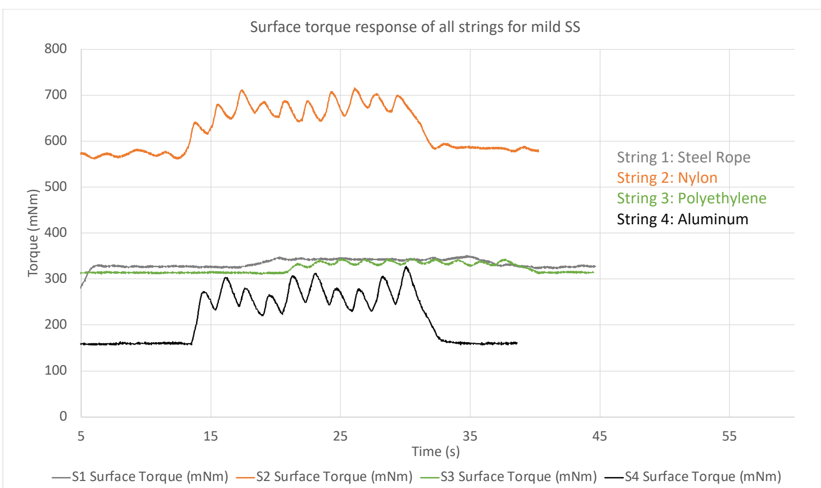

Figure 4-12 Surface torque response for mild stick-slip vibrations at 200RPM

The torque response is similar to the previous mild stick-slip experiment at 200RPM.

4.2.4 Severe stick-slip at 200RPM

In case of severe stick-slip vibration at 200 RPM, the vibration response remains very similar to the 100 RPM case (figure 4-13). Polyethylene is seen to store the most energy during the sticking phase with aluminum storing the least energy as aluminum only undergoes torsional oscillations and not bit sticking. The surface torque response is displayed in figure 4-14.

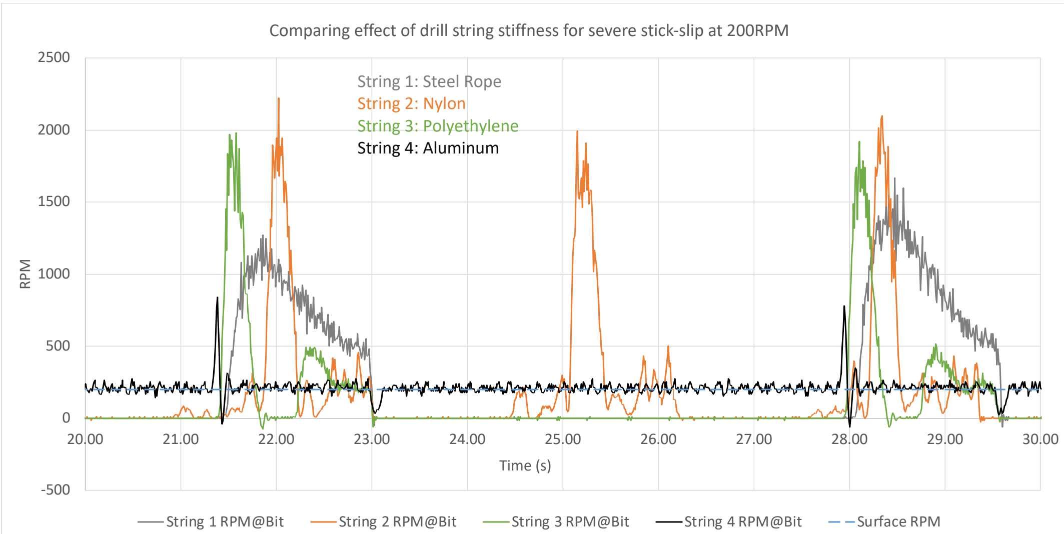

Figure 4-13 RPM response for severe stick-slip vibrations at 200RPM

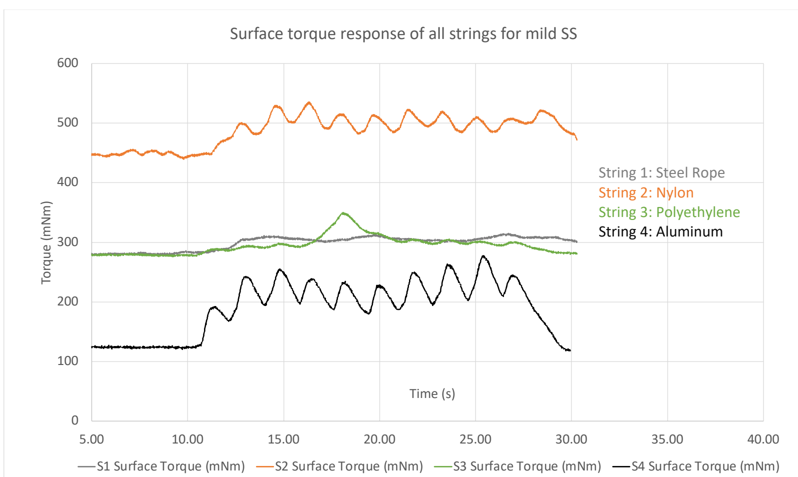

Figure 4-14 Surface torque response for severe stick-slip vibrations at 200RPM

4.3 Effect of RPM and WOB on mild vs severe stick-slip vibrations

In this section, the effect of weight on bit (WOB) and surface RPM on severe and mild stick-slip vibrations have been examined. The resultant plots are shown below.

4.3.1 Mild vs severe SS at WOB-0.5 Kg and RPM-100

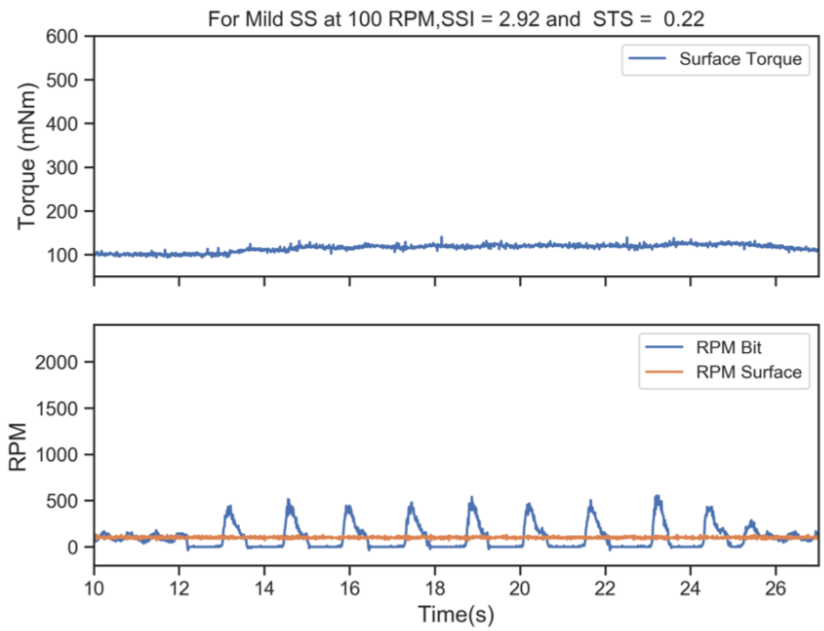

Figure 4-15 Mild stick slip at 0.5 kg WOB and 100 RPM

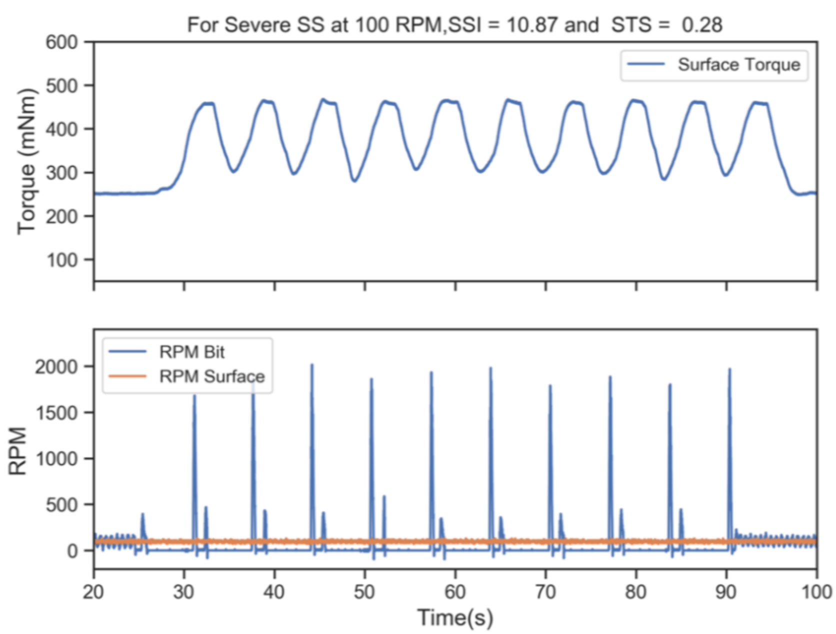

Figure 4-16 Severe stick slip at 0.5 kg WOB and 100 RPM

4.3.2 Mild vs severe SS at WOB-0.5 Kg and RPM-200

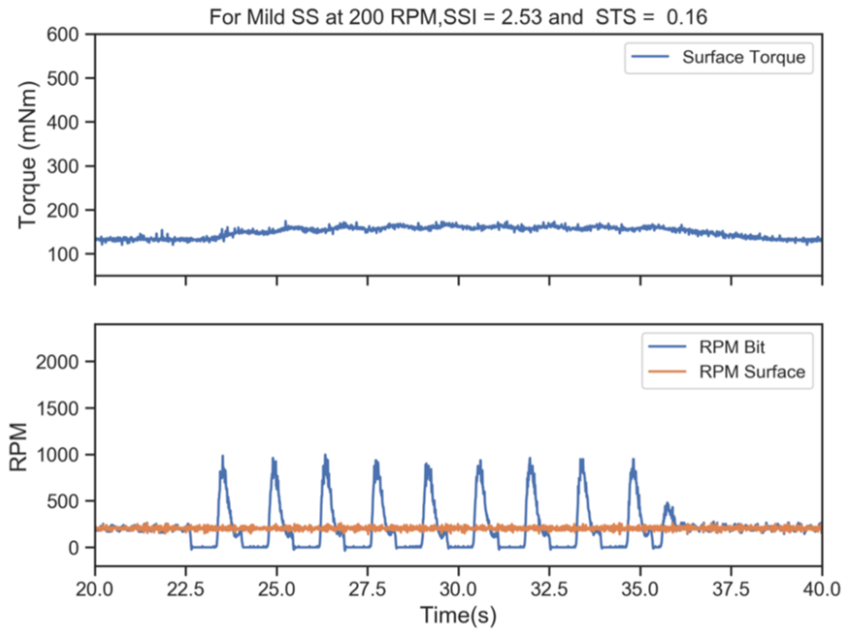

Figure 4-17 Mild stick slip at 0.5 kg WOB and 200 RPM

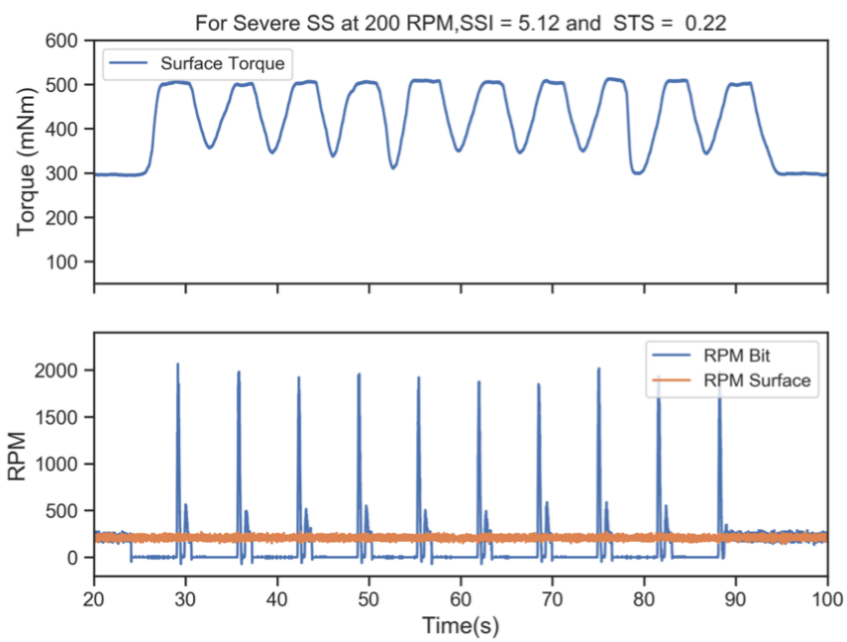

Figure 4-18 Severe stick slip at 0.5 kg WOB and 200 RPM

4.3.3 Mild vs severe SS at WOB-1 Kg and RPM-100

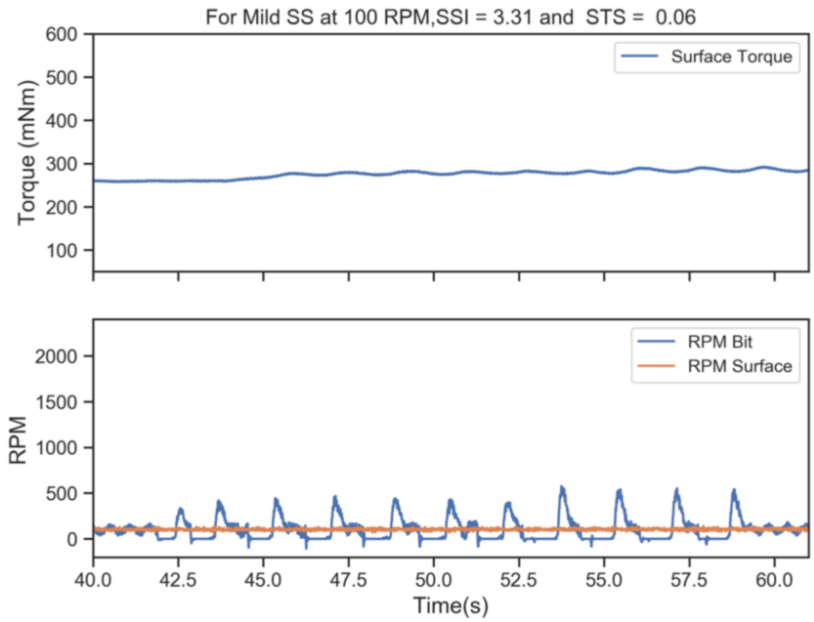

Figure 4-19 Mild stick slip at 1 kg WOB and 100 RPM

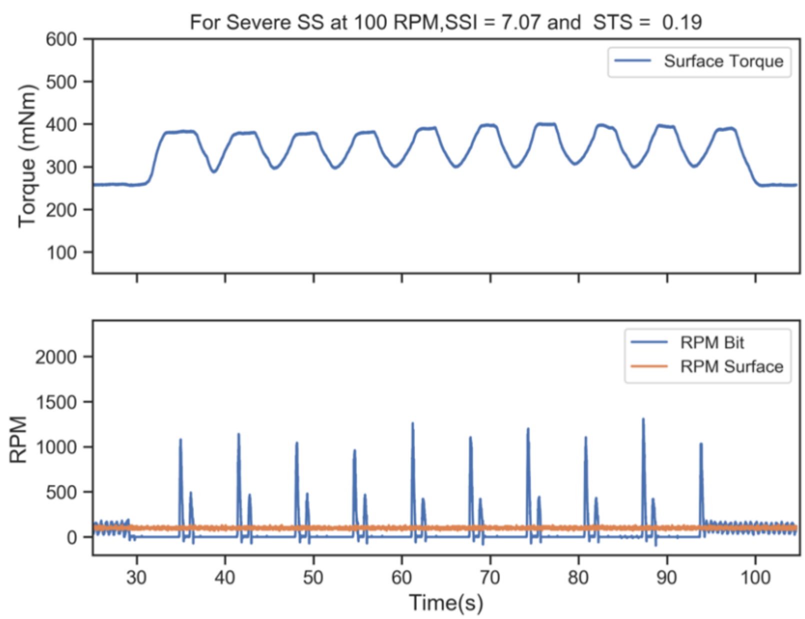

Figure 4-20 Severe stick slip at 1 kg WOB and 100 RPM

4.3.4 Mild vs severe SS at WOB-1 Kg and RPM-200

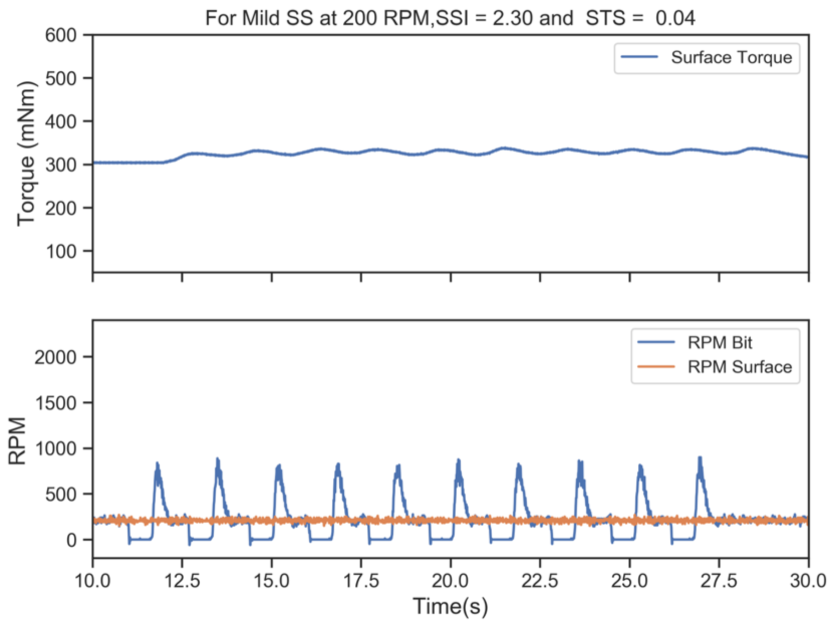

Figure 4-21 Mild stick slip at 1 kg WOB and 200 RPM

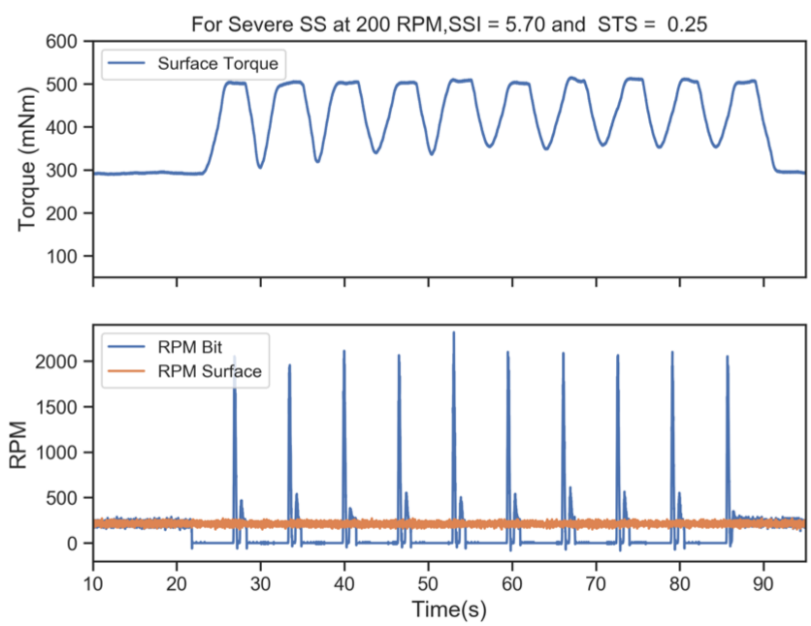

Figure 4-22 Severe stick slip at 1 kg WOB and 200 RPM

4.4 Self-Induced Bit sticking

Self-induced bit sticking is a huge problem in the drilling industry, especially when the drillstrings starts rotating at lower speeds. At lower speeds, the static friction along the drillstring is higher which can result in accumulation of torsional energy and subsequent higher rotation speeds. It has been documented that stick-slip can be observed both off and on-bottom at lower speeds (Cayeux et al., 2020). This examines self-induced bit sticking by varying operating RPM from 0-200 for both horizontal and vertical well profile, as seen from figure 4-23 to 4-26.

4.4.1 Horizontal well configuration

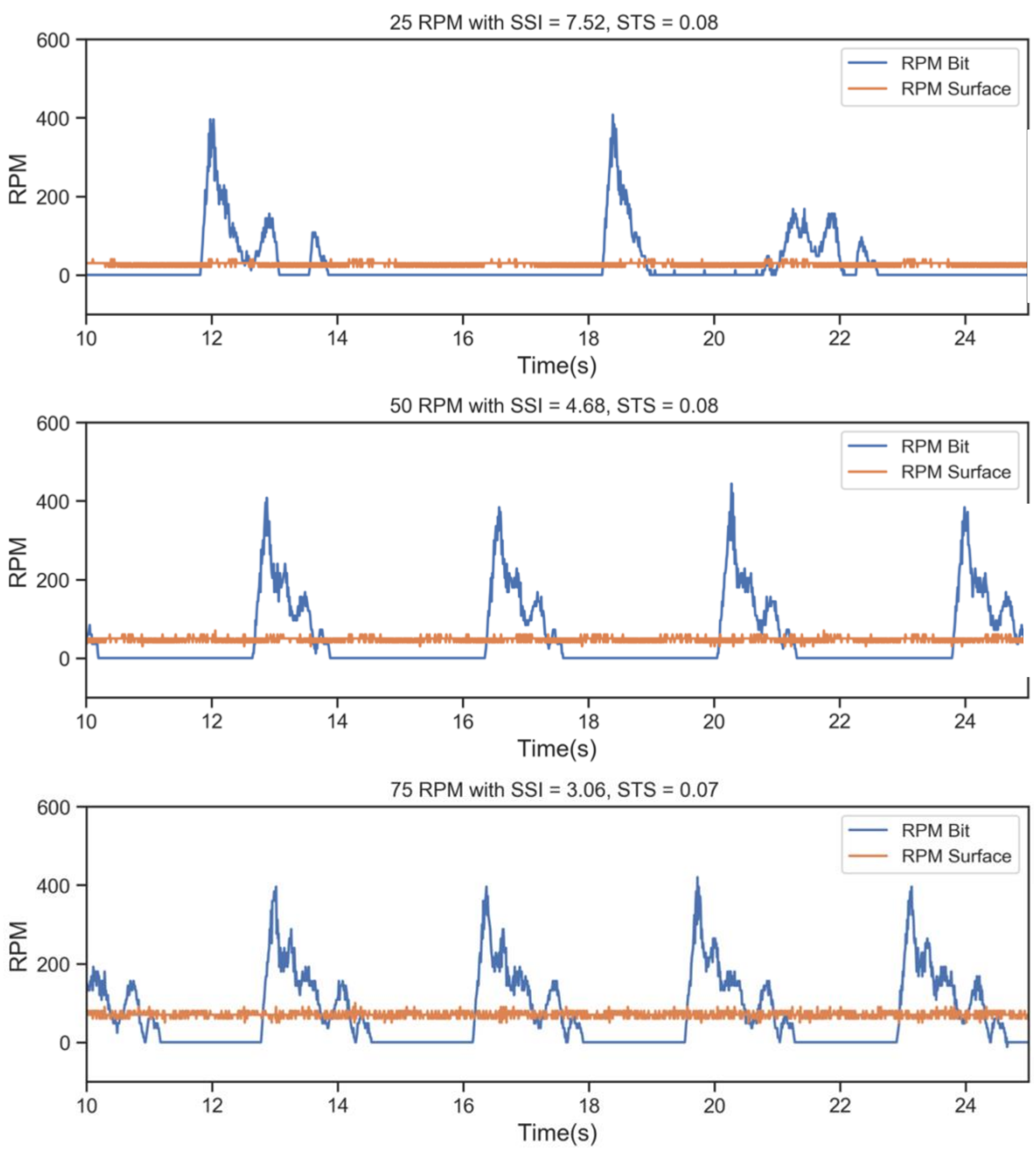

Horizontal, 25 RPM

Horizontal, 50 RPM

Horizontal, 75 RPM

Figure 4-23 Self-induced vibrations for horizontal setup from 25-100RPM

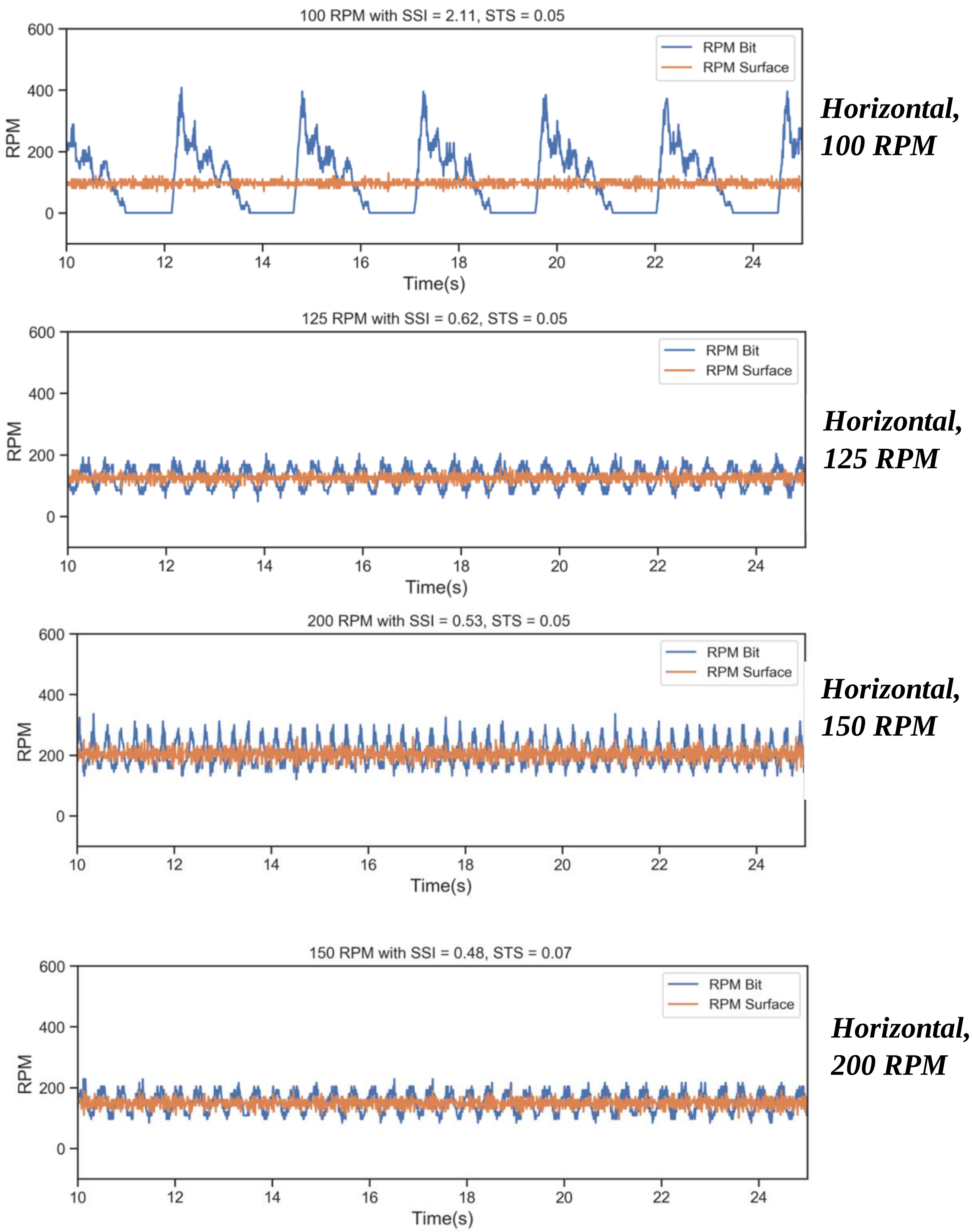

Figure 4-24 Self-induced vibrations for horizontal setup from 125-200RPM

4.4.2 Vertical well configuration

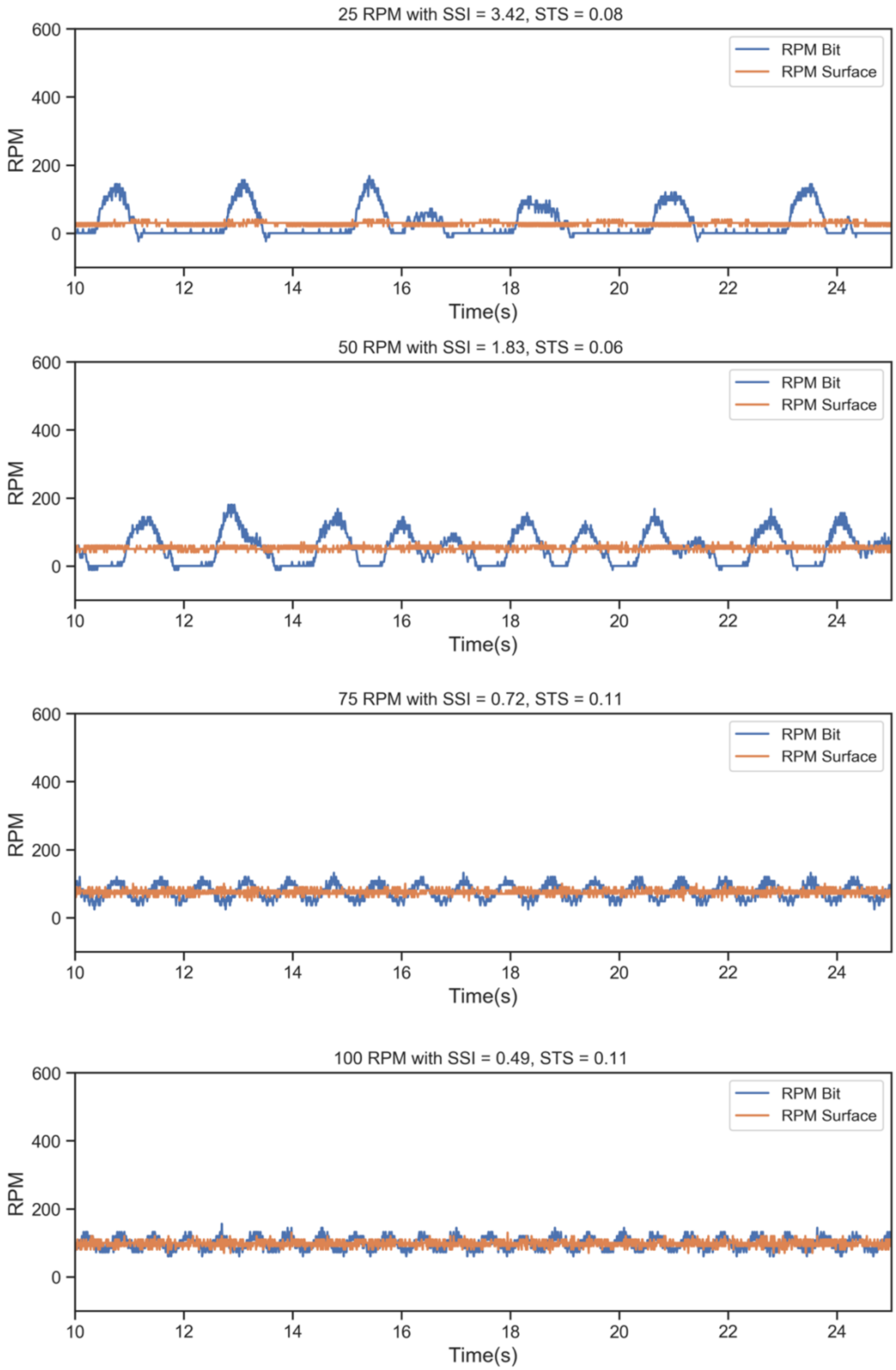

Vertical, 25 RPM

Vertical, 50 RPM

Vertical, 75 RPM

Vertical, 100 RPM

Figure 4-25 Self-induced vibrations for vertical setup from 25-100RPM

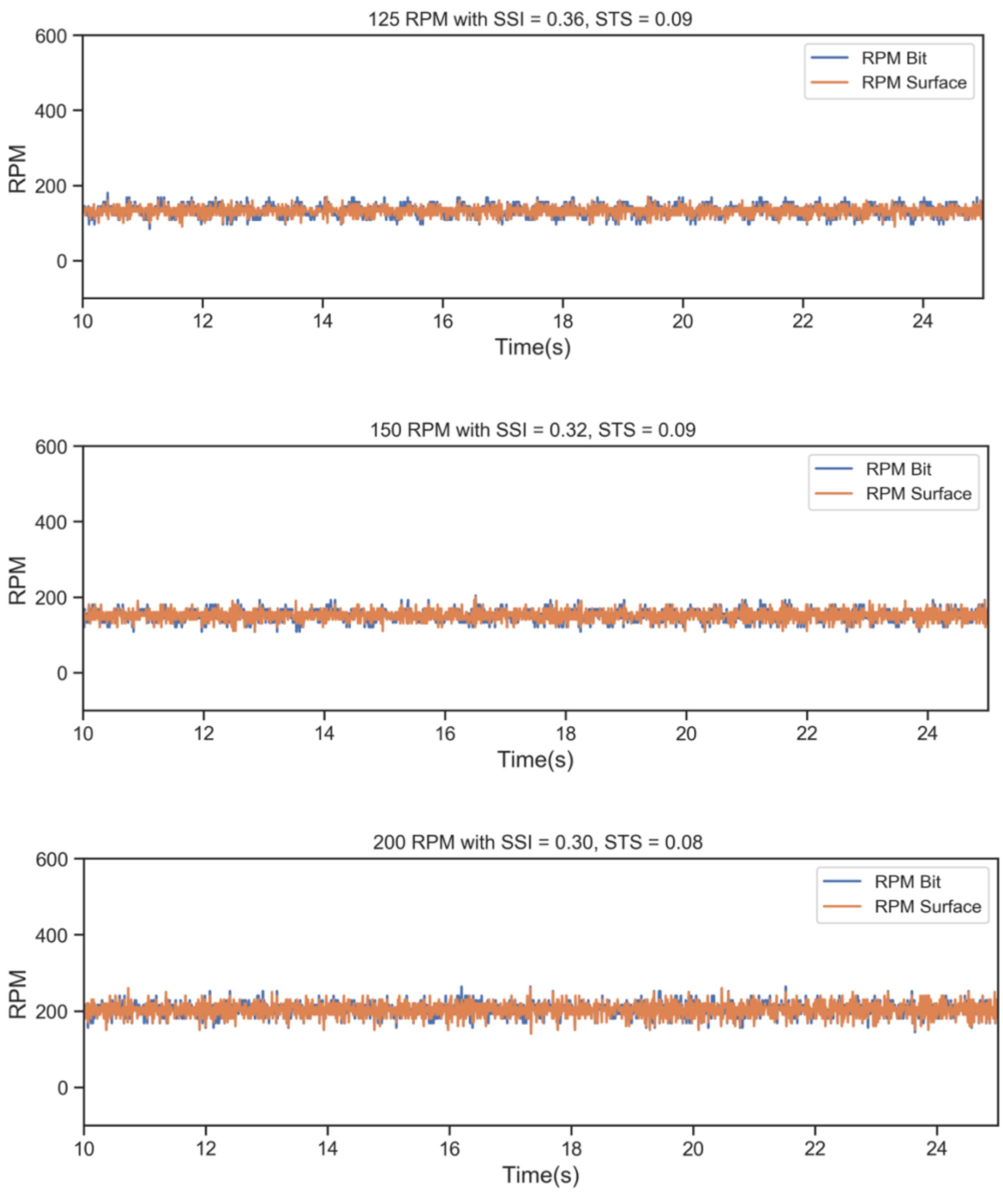

Vertical, 125 RPM

Vertical, 150 RPM

Vertical, 200 RPM

Figure 4-26 Self-induced vibrations for vertical setup from 125-200RPM

4.5 Effect of well configuration on mild vs severe stick-slip vibrations

This section analyzes the effect of well configuration on mild vs severe stick slip vibrations by using the SSI and STS index. The tests are conducted at 200 RPM because at 200 RPM, both the vertical and horizontal well profile are free of self-induced bit sticking. The results can be seen in figure 4-27 to 4-30.

4.5.1 Vertical Configuration

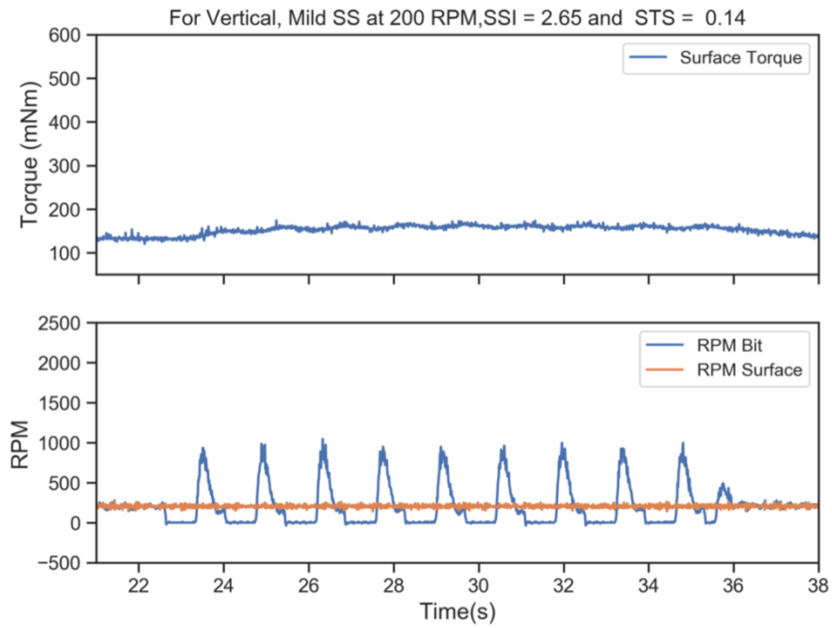

Figure 4-27 Mild stick slip for vertical setup at 200 RPM

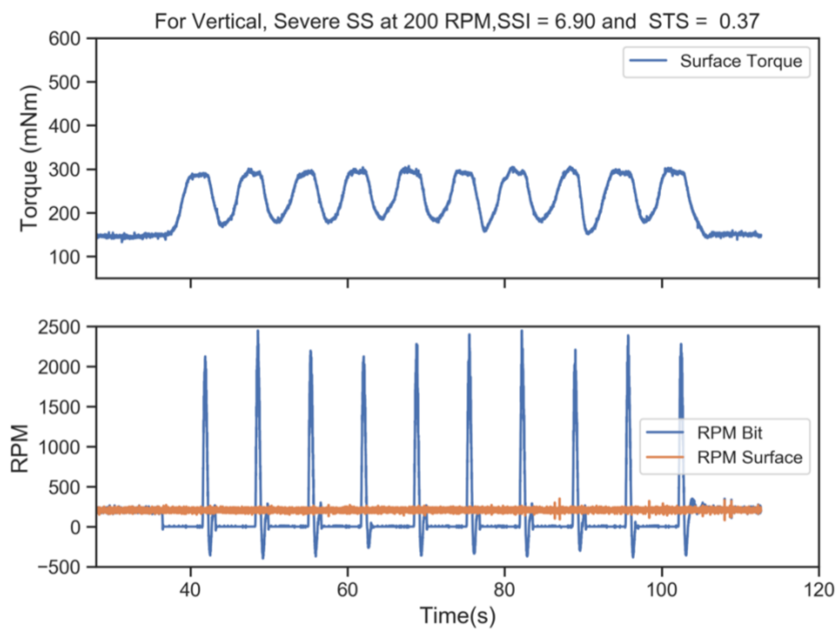

Figure 4-28 Severe stick slip for vertical setup at 200 RPM

4.5.2 Horizontal configuration

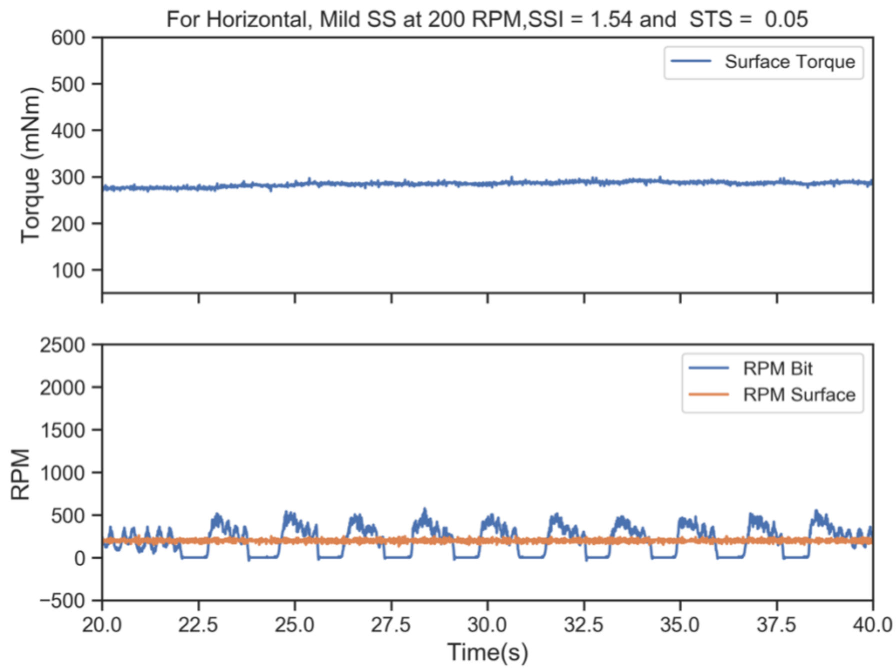

Figure 4-29 Mild stick slip for horizontal setup at 200 RPM

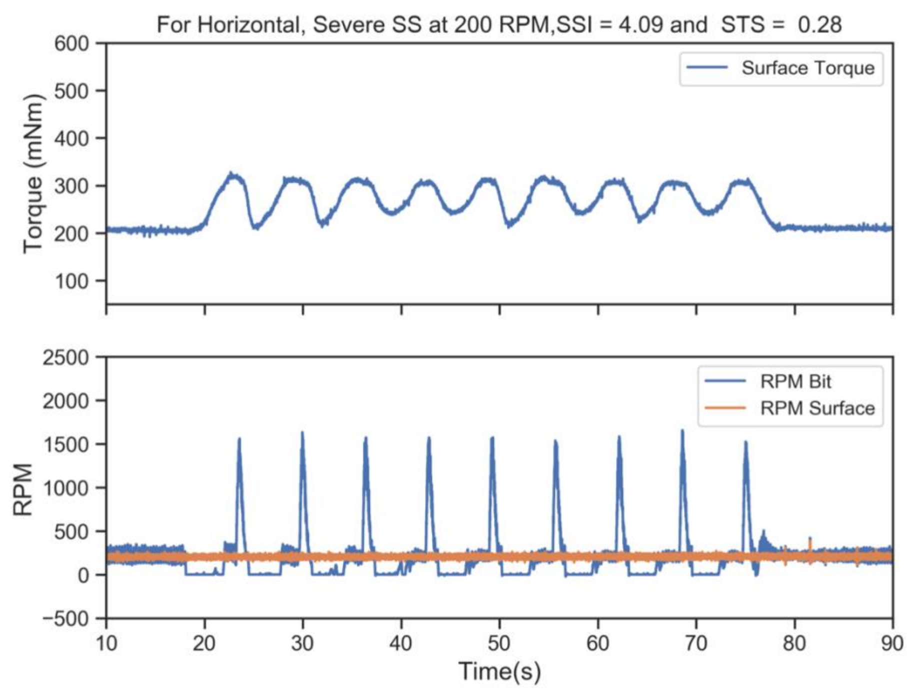

Figure 4-30 Severe stick slip for horizontal setup at 200 RPM

4.6 Effect of sticking time-period on vibration response

Stick slip vibrations consist of two phases, the stick and the slip phase. Up till this experiment, we have considered mild and severe bit sticking that relates directly to the bit sticking period. However, in this experiment, the focus is on both stick and slip phases to find the lowest and highest severity case. Figure 4-31 gives an overview of the 9 different combinations of stick and slip phase possible. For this experiment, 5 second bit sticking case is not used as combining 5 second bit sticking with a low slip phase (0.1s) can result in excess surface torque.

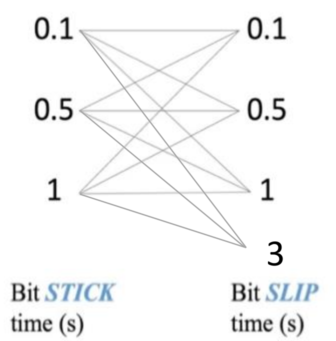

Figure 4-31 Possible combinations of bit stick and slip phase

Figure 4-32 provides an example of TOB during a bit stick and slip cycle for the case of 0.1 s slip and 0.5 s stick. Similarly, all the other tests are conducted. Since the results for the nine tests look fairly identical, the results are not plot in this section. The results are however discussed in chapter 7.

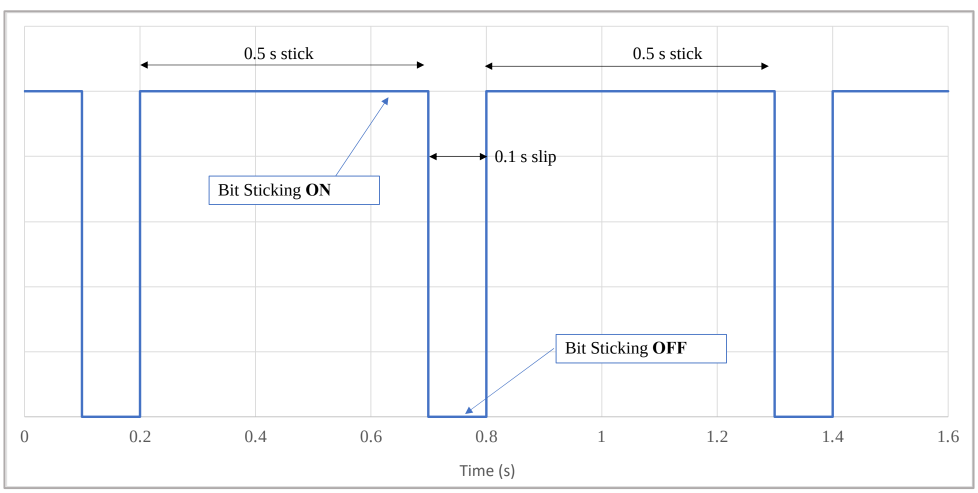

Figure 4-32 A stick slip cycle is shown for 0.1s slip and 0.5 s stick

4.7 Summary of experimental results

This chapter solely focused on experimental results for stick slip vibration analysis. Initially, the effect of sampling rate on diagnosis of mild vs severe stick-slip vibrations have been presented. Since 100 Hz was found to an optimal sampling rate to identify all signatures of both severe and mild stick-slip vibrations, 100 Hz sampling rate has been used for all further experiment comparisons. Additionally, experimental testing of up to 100Hz, peaks in bit RPM were observed at 5 times and 15-20 times the surface RPM for high frequency and low frequency stick-slip vibrations respectively. Through experimental testing of torsional stiffness, polyethylene was found to most closely mimic real vibration data. The remaining test results focused on 100 Hz, polyethylene results for the sake of brevity. Other parameters such as WOB, well configuration and self-induced bit sticking have been tested experimentally. Additionally, the effect of different combinations of bit stick and slip phase have also been examined. Since each dataset is tested at 100 Hz, the volume of data collected is immense. To maintain uniformity, a graph plotting has been used in python to first integrate and clean all data files before proceeding to plot the required results. The results from the experiments have been discussed in the discussion chapter.

Chapter 5: Mathematical modeling of torsional vibrations

A summary of mathematical models used for modeling drilling dynamics is provided in chapter 2, particularly along the radial degree of freedom for investigating torsional oscillations. Section 2 also discusses the tradeoff between model complexity and the computational time. In this section, the following two objectives are defined:

1. To finetune a simple 2 degree of freedom model in MATLAB Simulink for experimental adaptation. Using the experimental data, the accuracy and shortcomings of a low-fidelity model is to be determined.
2. A third-party software, DrillScan is used which can successfully model non-linear drilling dynamics. Using the experimental data, a comparison is made between the experimental data and DrillScan results.

5.1 Modeling using 2 DOF (Degree of freedom) model

Based on literature and ease of implementation, a torsional pendulum model is widely used. While originally used in a one degree of freedom model (Kyllingstad et al., 1988), it has since been revised for multiple DOF (degree of freedom) implementation. This section explores the two degree of freedom torsional pendulum by modifying it to the experimental setup. The assumptions made during development of the model have been listed below as:

- ✓ The wellbore and drill string are taken as vertical
- ✓ Drill string behavior is categorized as a torsional spring and pendulum
- ✓ For reducing complexity, the model has two rotational degrees of freedom including axial and torsional

Figure 5-1a depicts the drillstring as a torsional pendulum with two degrees of freedom, torsional and axial. Here, θ_m, θ_d and θ_b represent the angular displacement of the motor, drill string and the bit. C_m, C_d and C_b represent the damping coefficient of the motor, drill string and bit. J_d and J_b represent the mass moment inertia of the drill string and the bit. K_d, K_b, w_d and w_b represent the torsional stiffness and angular velocity of the drill string and bit.

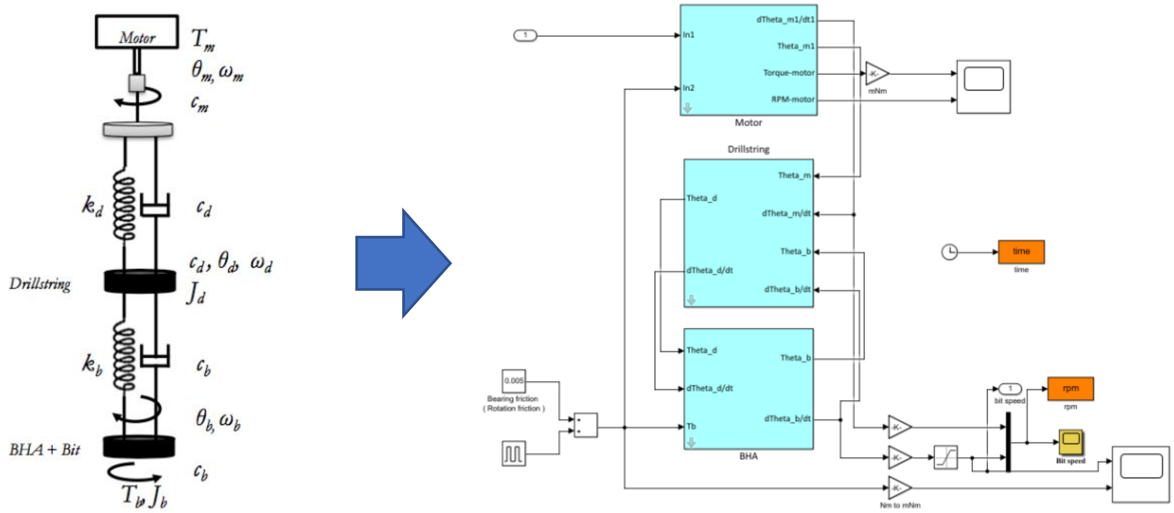

(a) (b)

Figure 5-1 Representation of drill string as a torsional pendulum (left) and block diagram

The equations of motion for the torsional pendulum can be written assuming that it is driven by the electric motor at the top:

$$J_d\ddot{\theta}_d - c_d(\dot{\theta}_m - \dot{\theta}_d) - k_d(\theta_m - \theta_d) + c_b(\dot{\theta}_d - \dot{\theta}_b) + k_b(\theta_d - \theta_b) = 0 \dots\dots (5-1)$$

$$J_b\ddot{\theta}_b - c_b(\dot{\theta}_d - \dot{\theta}_b) - k_b(\theta_d - \theta_b) = -T_b \dots\dots\dots\dots\dots (5-2)$$

Where, T_b is the torque generated at the bit. However, for this study, T_b does not use a rock-bit interaction model or a ROP model. Instead, it replicates the torque generated by the electromagnetic brake in the experimental setup. The above equations of motion have been linked together as blocks in Simulink. The block diagram in Simulink can be seen in Figure 5-1b. The blue blocks represent the motor, drillstring and the BHA sub-systems. The blue blocks represent the equation The simulation is then carried out using a fixed step explicit solver with high computational complexity. The solver used is ode8. The current model is a two degree of freedom torsional pendulum model. Since the model has relatively lower complexity, the computation time is quick.

5.1.1 Modeling parameters

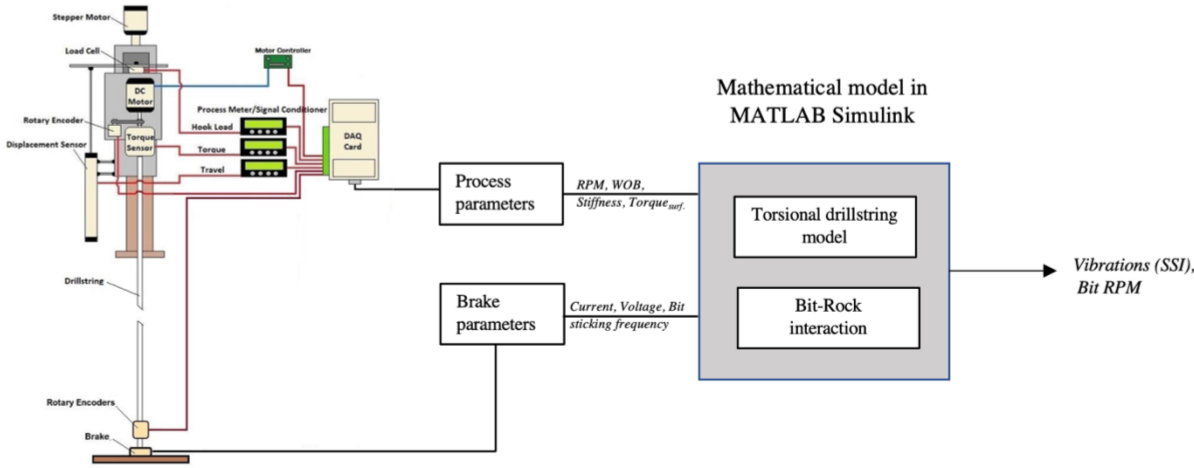

Figure 5-2 Schematic explanation of using experimental parameters as input for mathematical modeling

It is important to note that the experimental parameters are used as inputs for the mathematical model as seen in figure 5-2. The parameters for the model are listed in table 6. The rock-bit interaction uses the brake parameters as torque input signals. The input parameters in the modeling include:

- 1.Motor: RPM and torque
- 2.Drillstring and BHA: Mass, inertia, and stiffness
- 3.Bit: Bit torque sequence (friction + pulsating bit torque)

Parameters	Values
Power	0.04 HP
Surface RPM	100 and 200
Inertia $_{DP}$	$7.54*10^{-7}$ Kgm^2
Inertia $_{BHA}$	$2.18*10^{-5}$ Kgm^2
DP Stiffness	0.001753
Frictional TOB	0.05 mNm
Bit sticking TOB	0.068 mNm

Table 6 Parameter input values for modeling derived from experimental analysis

Polyethylene is used as the string of choice as it closely matches stick-slip vibrations observed in field data. Since experimental investigation is centered around low frequency and high frequency stick-slip vibrations, same conditions have been generated in the mathematical model using the programmable TOB input to the bit. Additionally, a natural friction component is added. Figure 5-3 provides an explanation of how the bit torque is programmed for low frequency and high frequency stick-slip vibrations.

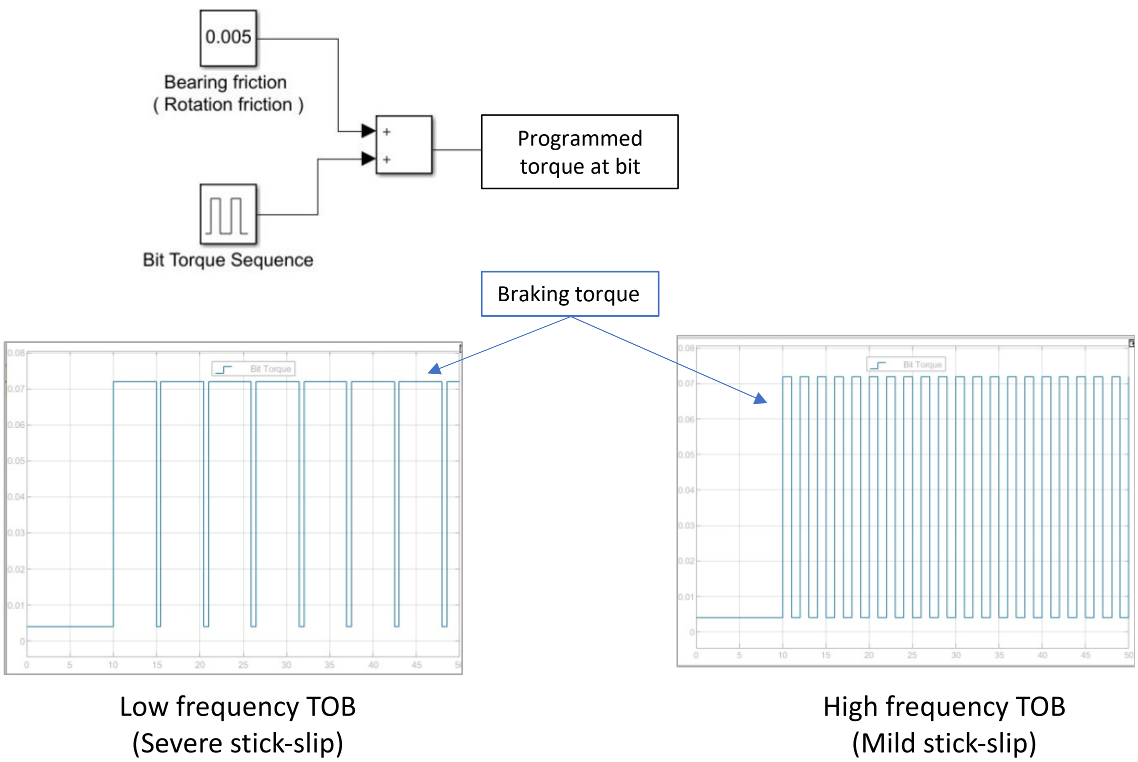

Figure 5-3 Programming mild and severe stick-slip vibrations using torque on bit sequence

The following results are obtained from the model:

a. Mild stick-slip at 100, 200RPM
b. Severe stick slip at 100,200 RPM

Mild stick slip

The drill string model is successfully run for laboratory scaled parameters. In figure 5-3, the red line represents the bit RPM, and the blue line represents the torque at bit. The yellow line represents the surface RPM. The torque at bit is introduced in a step interval sequence of 5 seconds sticking followed by 1 second slip. The bit sticking torque amplitude is 68mNm which is high enough to influence sticking whereas a torque value of 5mNm represents minimal bearing friction while rotation. The model is run for 25 seconds using a differential equation solver. The experiment is run for 100 and 200RPM

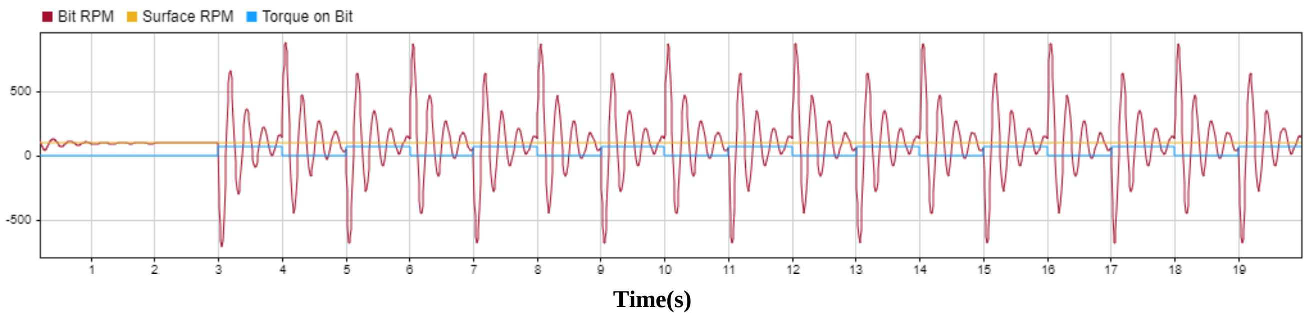

Figure 5-4 Mild stick-slip at 100RPM

$SSI_{MildSS\ @100RPM} = 8$ $\qquad$ $SSI_{MildSS\ @200RPM} = 4.12$

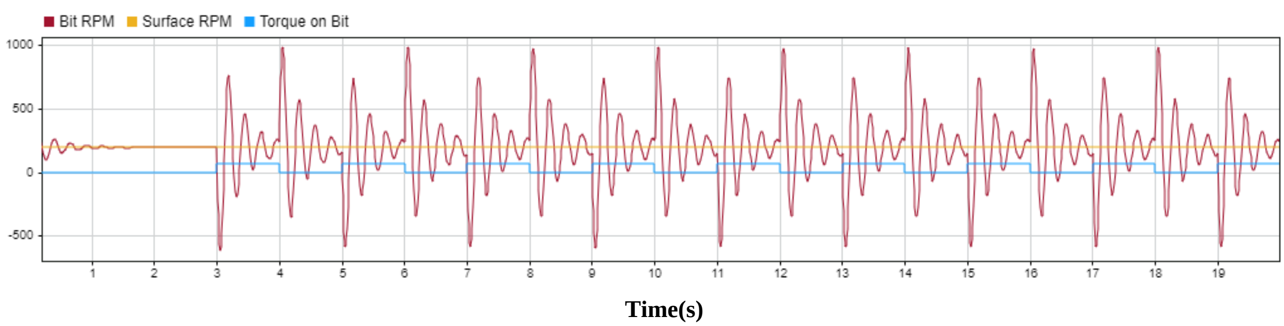

Figure 5-5 Mild stick-slip at 200RPM

The SSI calculated shows that the stick-slip severity is reduced significantly at a higher RPM. This matches the experimental results. Even though the stick-slip severity is different in the modeling results, the signature of vibration is very identical in both cases.

Severe stick-slip

Figure 5-7 and 5-8 shows the plots for severe stick slip at 100 and 200 RPM. The blue lines in the plot indicate the TOB sequence. As compared to the mild stick slip case, the bit sticking period is longer (5 seconds). The bit RPM response signature is identical in both cases. The string stabilizes within 2 seconds after every external excitation.

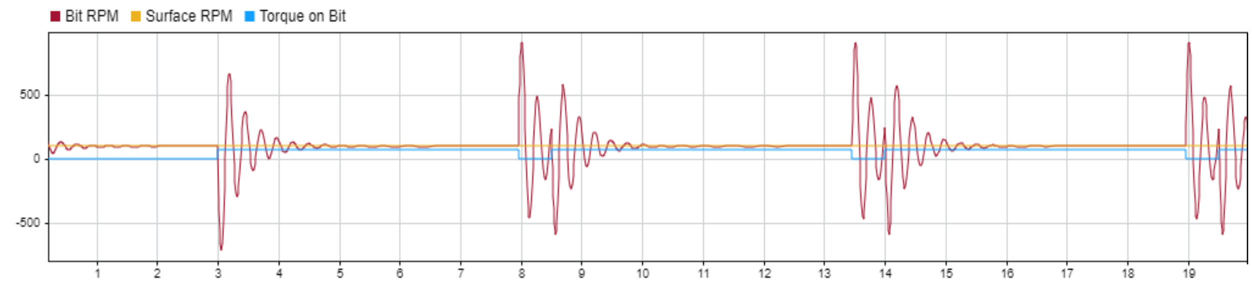

Time(s)

Figure 5-6 Severe stick-slip at 100RPM

$$SSI_{SevereSS\ @100RPM} = 8 \qquad SSI_{SevereSS\ @200RPM} = 4$$

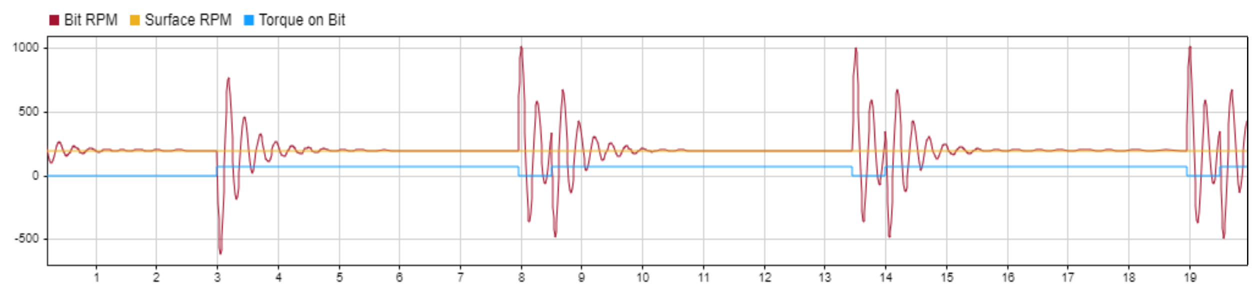

Time(s)

Figure 5-7 Severe stick-slip at 200RPM

The SSI calculated shows the same pattern in severe and mild stick-slip. This is because the vibration signature is identical in both cases. The bit RPM response is not affected by the period of bit sticking.

5.1.1 Experimental comparison

The results from the modeling experiment are compared to the experimental results. For comparison, a severe stick-slip vibration is chosen at 100RPM, 0.5Kg WOB drilling parameter. The result of the comparison can be seen in figure 5-8. The experimental result can be seen in blue while the modeling result is seen in red. Since a severe bit sticking case is compared, the bit RPM for the experimental result is seen to be at 0 for a considerable time. Bit RPM obtained from the modeling result does not actually stick. However, bit RPM from modeling fluctuates between positive and negative RPM values. This is verified in the experimental test result as well where the bit RPM becomes negative momentarily. The results are summarized further in chapter 7.

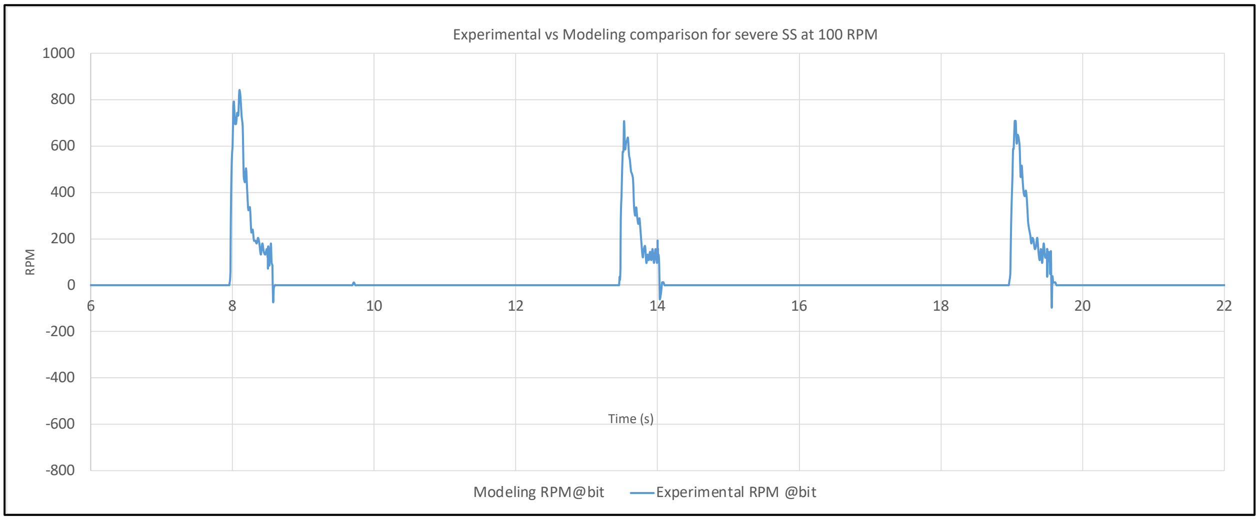

Figure 5-8 Experimental vs. modeling result for severe bit sticking at 100RPM

5.2 Torsional model development in WellScan

WellScan is a reliable engineering software for investigating drill bit management, drilling dynamics, hydraulics, torque and drag and well integrity issues. For the scope of study, the stick-slip module under torque and drag is used to compare the torsional vibrations signature from the experimental study. Theoretically, there are two torque and drag models defined in literature, soft-string model, and stiff-string mode, as defined in Section 2.2 (figure 2-8). As the name suggests, the soft-string model assumes continuous wellbore contact to ignore stiffness and bending moment effects whereas stiff-string model produces a more realistic study of downhole configuration and is more useful in tortuous trajectory wells. The ABIS stiff-string model is chosen for the experiments.

Figure 5-9 shows a snippet of the WellScan software used for the stick-slip study. Section 1 displays the well selection module. Section 2 shows the model selected for the calculations. Section 3 is used to create the bottom hole assembly for the downhole configuration. Section 4 is the main display for the trajectory/casing verification and results window. Section 5 is the string selection panel. Section 6 contains the computation parameters for the stick-slip study.

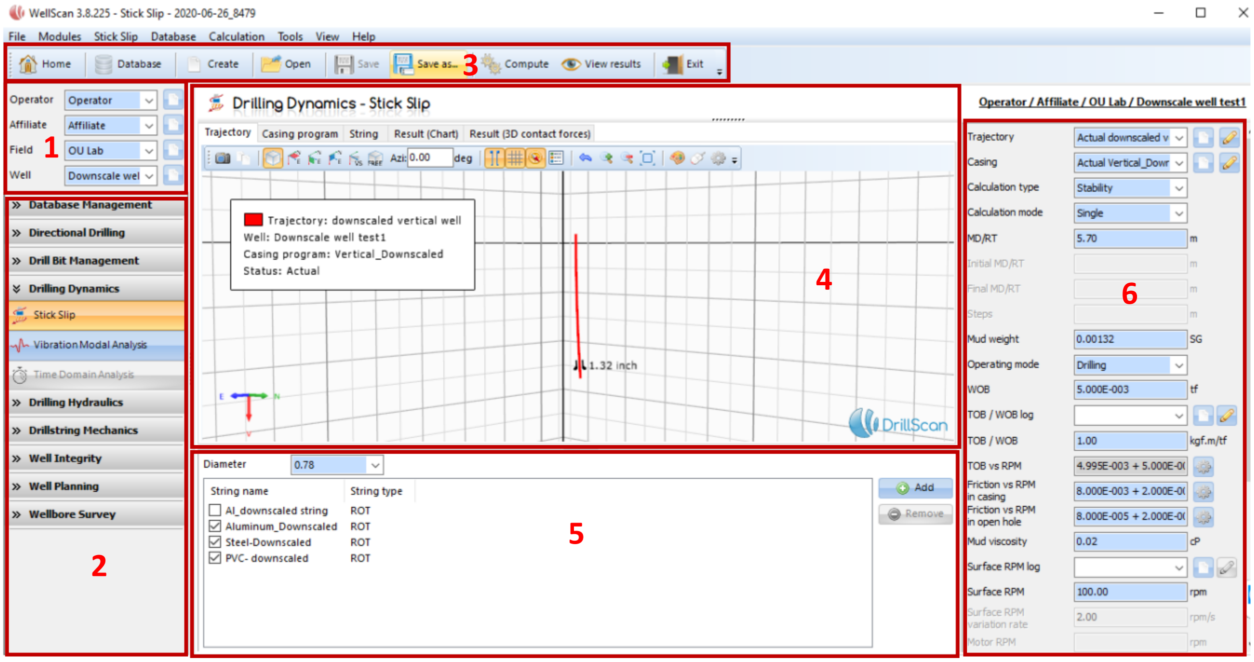

Figure 5-9 WellScan interface for stick-slip analysis

5.2.1 Well design

The objective of the study is to input downscaled laboratory parameters to compare experimental vibration signatures from the vibrations produced in WellScan. To input experimental parameters, the parameters were converted to an open hole well with a single casing design. Figure 5-10 displays the dimensions of the setup which was used to create the well profile.

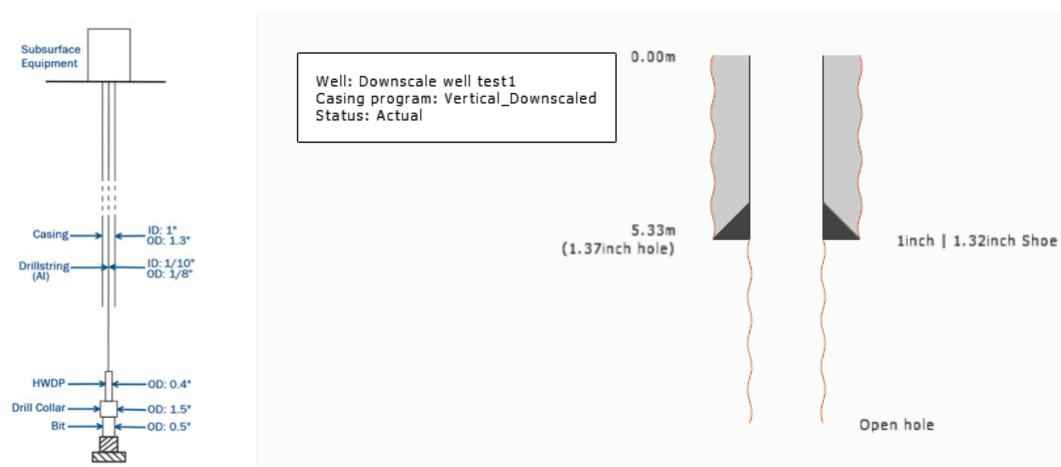

Figure 5-10 Conversion of laboratory parameters to single casing open well design

Moreover, the well is made identical to the experimental design. Figures 5-11 and 5-12 show the vertical and horizontal casing design along with the inclination plot.

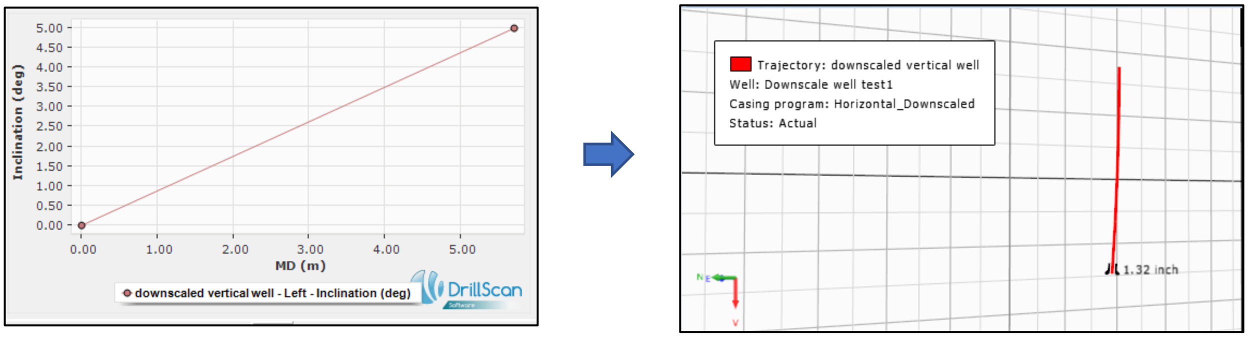

Figure 5-11 Vertical well profile based on vertical experimental setup

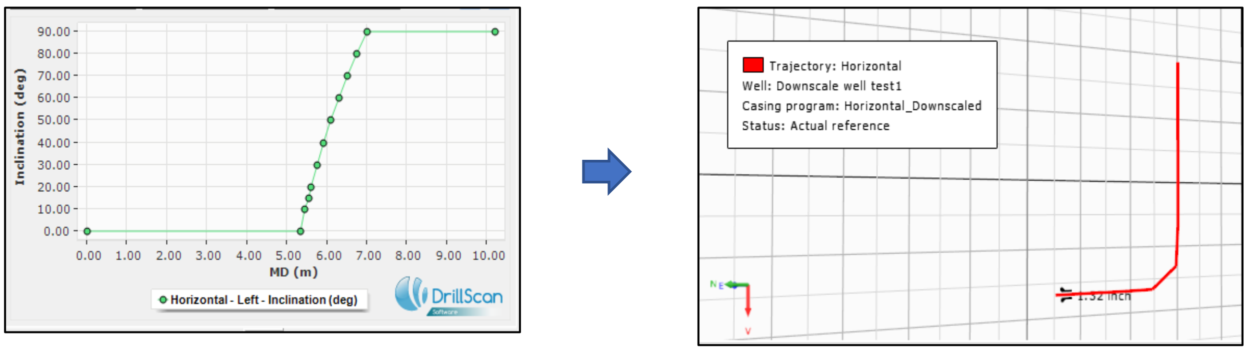

Figure 5-12 Horizontal well profile based on horizontal experimental setup

5.2.2 Experimental design

The input parameters in the system include drillstring stiffness, RPM, WOB, bit aggressiveness, friction co-efficient and dynamic to static torque ratio. The experimental design for the modeling experiments have been shown in figure 5-13.

Figure 5-13 Process parameters used in WellScan computation

The software includes steel and aluminum as drillstring options. The properties of PVC were added manually to incorporate it as a string material. To consider the TOB vs RPM law in WellScan, the ratio of dynamic to static torque is taken close to 1. With a constant torque, the direction of torque is opposite to the direction of bit rotation. In the case where we wish to impose TOB separately, the value for critical RPM and static/dynamic torque ratio is kept blank. Instead, the TOB is added by the TOB/WOB log. The experiments were run by manually inputting TOB log that replicates the electromagnetic brake used in the experimental setup. Overall, a total of 150 modeling test are run to investigate stick-slip vibrations.

5.2.3 Experimental results

This section presents the results of WellScan modeling. For conciseness, the results for three different strings, aluminum, steel and PVC are considered. The results for 100 RPM stick-slip vibrations are shown in figure 5-14. Since PVC has the lowest torsional stiffness, its bit RPM fluctuation is the most followed by aluminum and steel. Similar results are observed in figure 5-15 for 200 RPM. All strings show the presence of negative bit RPM, a characteristic of severe bit sticking.

100 RPM

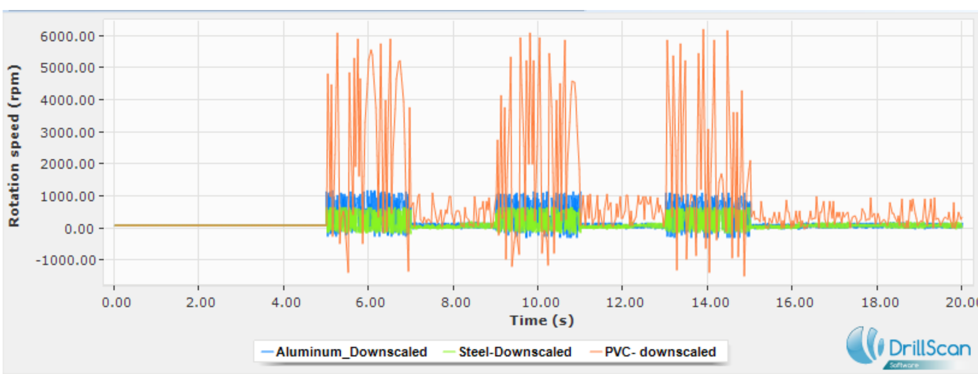

Figure 5-14 Comparison of three strings at 100 RPM

200 RPM

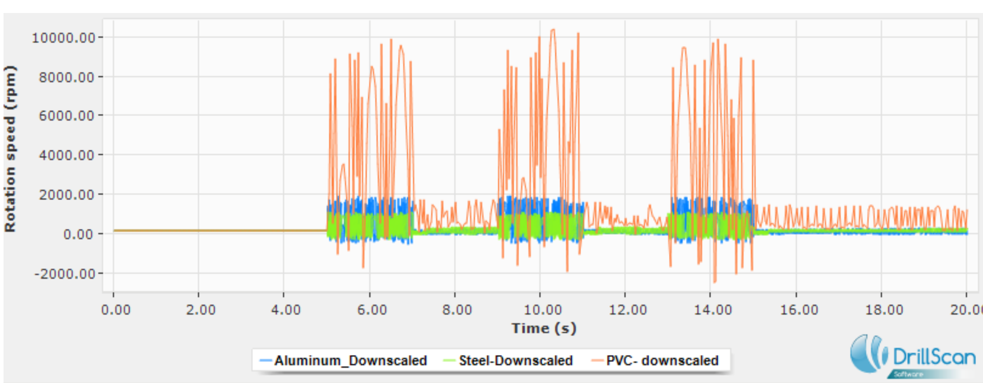

Figure 5-15 Comparison of three strings at 200RPM

Table 7 summarizes the SSI for different combination of friction co-efficient. Highest SSI values are obtained in PVC, followed by aluminum and steel. It is observed that the SSI values decrease from vertical to horizontal well profile, as observed in the experimental results in chapter 4.

SSI Comparison	Vertical		Horizontal			
	Casing static f = 0.1		Casing static f = 0.1		Casing static f = 0.3	
	100 RPM	200 RPM	100 RPM	200 RPM	100 RPM	200 RPM
PVC	1.48	0.9	1.07	0.84	1.25	1.4
Aluminum	0.76	0.78	0.79	0.61	0.6	0.51
Steel	0.41	0.55	0.75	0.89	0.22	0.59
nph	*2500*	*1900*	*2500*	*1900*	*1900*	*1900*

Table 7 SSI comparison of vertical and horizontal configuration for PVC, Al and Steel for 100 and 200 RPM

It is understood that severity of stick-slip vibrations is reduced at higher surface RPMs. This is observed in PVC string. The SSI values in aluminum and steel indicate contradicting trends.

5.2.4 Comparison with experimental data

In this section, a comparison is made between WellScan and experimental results using the three different string materials. Figure 5-16 is plot for the three different string materials at 100 RPM and 0.5Kg WOB. As expected, the range of vibration response from the PVC string (shown in orange) is the highest followed by aluminum and steel (both similar). PVC, being the least stiff, accumulates the most torsional energy during bit sticking which is released during the slip phase. Steel, being the stiffest does not have the torsional rigidity to accumulate torsional energy resulting in a comparatively smoother vibration response.

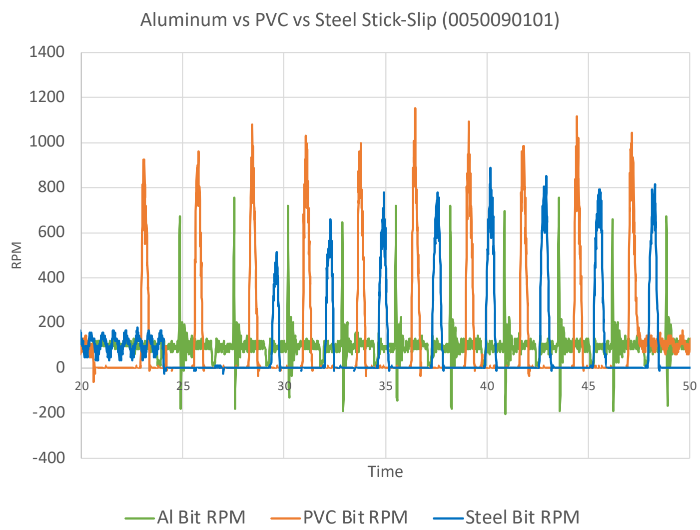

Figure 5-16 Comparison of experimental results with PVC, Al and steel strings at 100RPM

5.3 Summary of modeling results

The 2 degree of freedom drillstring model does a decent job of replicating real-world drilling vibrations. With an applied downhole torque, one can observe bit RPM dropping below 0 in both mild and severe bit sticking conditions. However, the vibration signature observed remains constant for both mild and severe stick-slip vibrations. This is also explained by the SSI values in both mild and severe vibrations at 100 and 200 RPM. This happens because even though negative bit RPM is seen, no bit sticking is observed. The model does not incorporate friction in the calculations and hence is not able to recreate the non-linear interactions in the system. WellScan results look more promising than the lumped parameter model results as it considers non-linear factors suchas friction into the calculations. Additionally, a feedback model exists in WellScan that helps in analyzing surface response to vibrations as well.

Chapter 6: Machine Learning for Drilling Vibrations

Timely detection and mitigation of drilling vibrations for improving drilling efficiency and performance is a well-understood challenge in the drilling industry. Vibration control strategies fall into the passive or active control category based on the extent of intervention in the drilling process. An example of the passive control strategy involves the driller to optimize input drilling parameters such as torque, rotary speed, and weight on bit to find an optimal drilling zone with reduced drill string resonance (Dong and Chen, 2016). However, this approach limits the rate of penetration, an evaluation metric that often takes the highest precedence during drilling. Active control strategies embrace the dynamic nature of drilling vibrations to introduce sophisticated feedback control systems that help dampen drilling vibrations by exerting an equal and opposite force to the external vibrations in the drill string. (Javanmardi and Gaspard, 1992; Jansen et al., 1995; Karkoub et al., 2009; Krama et al., 2021).

In recent years, another area of development has been the implementation of machine learning (ML) and advanced analytical techniques in characterization and prediction of drilling dysfunctions. Machine learning has been implemented in a variety of drilling related processes due to their ease of application, versatility, and high accuracy. Significant progress has been made in dealing with structured downhole drilling data for machine learning applications such as stuck-pipe detection, implementing drilling optimization models, estimating downhole shocks etc. (Noshi and Schubert, 2018). Similarly, unstructured data available in text format through drilling reports have also been successfully leveraged to automate drilling anomaly and dysfunction detection (Zhang et al., 2020; Srivastava et al., 2021). Optimizing drilling parameters for improving rate of penetration, prediction of pipe sticking in well and predicting abnormal drilling events are some examples of the same (Hegde et al., 2019; Goebel et al., 2014; Zhao et al., 2017). This study is focused on machine learning applications for drilling vibrations. In doing so, the study aims to develop a generic machine learning workflow that works best for drilling vibrations.

6.1 Review of ML studies on drilling vibrations

Recent literature on application of ML models in drilling vibrations highlight classification as the core task where the presence of a target label is integral in searching for possible patterns between the remaining data set features and itself (Christian, 2017, Bello et al., 2020). This can be seen in figure 6-1. Additionally, table 8 summarizes the different machine learning models built utilizing drilling vibrations. It also contains a list of surface and downhole features used for training the discussed algorithms. Although optimizing drilling performance based on surface parameters has proven to be effective, most of the models summarized in table 8 utilize both downhole and surface data.

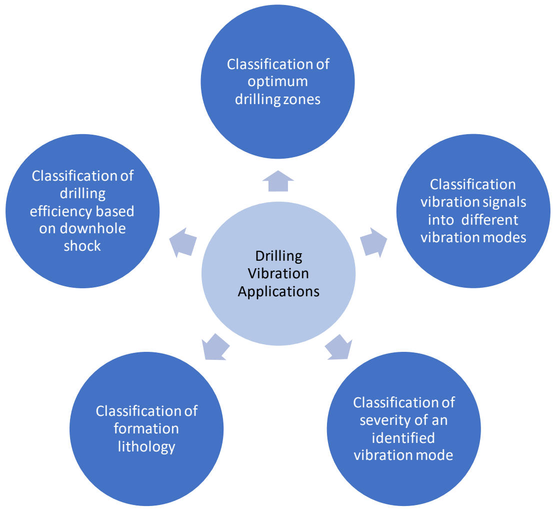

Figure 6-1 Summary of machine learning applications of drillstring vibrations

The luxury of having high frequency data is available for surface parameters. While industry standard for surface measurements is 1-10 Hz, high frequency surface measurements up to 100 Hz data has been obtained for building robust machine learning models (Zha and Pham, 2018; Zhao et al., 2017). Even though high frequency measurements have been made possible, the storage and transmission of surface data remains close to 1 Hz (Millan et al., 2019). As real-time transmission of downhole data to surface remains restricted by mud telemetry bandwidth constraints and high cost of wired drill pipe, downhole measurement tools are preferred for collecting and storing data for post-drilling analysis. Up to 31250 Hz of high frequency downhole measurements have been recorded during drilling (Ignova et al., 2019). Some downhole sensors operate to continuously record high-frequency data while some work in small bursts of high-frequency measurements to optimize downhole storage capacity (Zhang et al., 2020). Generating synthetic datasets from dynamic drillstring models is also a proven technique that provides a variety of dynamic responses that can be included in the model training process with greater confidence (Chen et al., 2019).

Ref.	Application	Machine Learning Task	Method used	Surface data			Training data	Downhole data			Results
				Sampling freq.	Labels	Processing		Sampling freq.	Labels	Processing	
Baumgartner and Oort, 2014	To recognize pure and coupled stick-slip and whirl vibrations using supervised learning	Classification of vibrations into stick-slip and whirl using bayesian classifiers	Bayesian Classifiers	Not recorded	Not recorded	Not recorded	250 observations of stick slip and whirl split into 3:2 for training and testing	≤1Hz with 10s burst of 400Hz	Time, Frequency, Statistical and Smoothened data	1. Feature extraction 2. Time series split	Classification accuracy of 90% for stick-slip and 92% for whirl
Christian, 2017	To identify an optimum zone of drilling between stick-slip and whirling issues.	Clustering and classification of optimum drilling zones	K Means and Decision Trees	Not reported	MSE, RPM, ROP, WOB, D-exponent and Torque	1. Dimensionality Reduction using PCA 2. Clustering to identify zones in WOB vs. RPM	Well data consisting of 1000 data points	Not reported	Not reported	Not reported	Successful classification into 5 optimum drilling zones
Zhao et al., 2017	Pattern recognition of changes in drilling parameters to detect stick-slip vibrations	Classification of predefined patterns in drilling wrt time series analysis	Not mentioned	0.5 - 1Hz	Surface RPM and Weight on bit	1. Filtering RAW data 2. Time series rep. SAX 3.Pattern recognition using heirarchial clustering (unsupervised)	Not reported	0.5 - 1Hz	Stick slip Ratio from downhole gyro data	Not reported	Successfully identify triggers in drilling parameters that cause stick-slip vibrations
Zha and Pham. 2018	To predict severe downhole stick-slip vibrations using surface data	Multi channel time series classification of stick slip vibration severity	Recurrent neural network (RNN) and convolutional neural network (CNN)	100 Hz	Torque, Tension, RPM, WOB and triaxial acceleration	1. Time series sampling (30s) 2. Normalization 3. Data augmentation	1400 wells drilling sample 3:1 split (Training:Validation)	40Hz	Torque, RPM and acceleration	Data resampled to 100Hz	1. 96-99% accuracy 2. 73-97% precision
Chen et al., 2019	To perform binary classification to distinguish whirling from non-whirling stages of BHA	Binary classification	Deep Neural Network	Not recorded	Not recorded	Not recorded	80% training and 20% testing	2048 Hz downhole sub	RPM and lateral acceleration (Y and Z axis)	1. Time window sampling 2. [0,1] normalization. 3. Labeled using regression and classification	99% trainings and 97% testing accuracy
Hegde et al., 2019	To classify drillstring vibration severity	Binary classification for Stick-slip Index using multiple models	Logistic regression, GMM, Random Forest, LDA	Not reported	WOB, Flowrate	1. Feature Engineering 2. Upsampling	40% training and validation using K=5 cross fold	Not reported	RPM, Accelerometer reading, ROP (deterministic model), TOB (deterministic model)	1. Feature Engineering 2. Upsampling	90% accuracy, F1=0.91 and AUC=0.89
Ignova et al., 2019	Use frequency shock acquisition to identify abnormal drilling behaviour	Classification into good and abnormal drilling behaviour	PCA pattern recognition and clustering	Not recorded	Not recorded	Not recorded	Not reported	31250 Hz	Accelerometer data, pulse width, holdoff and threshold bins	1. Frequency domain annalysis 2. K-means and PCA	Not reported
Milan et al., 2019	To classify and characterize stick-slip and lateral vibration from high frequency surface data	Classification of stick-slip severities and presence or absence of lateral vibrations	Support Vector Machines (SVM) and bagged decision trees	10-25Hz	Torque, Hookload, TD rotations	1. Data sampling (20s) 2. Freq. spectrum analysis (FFT) 3. Feature Extraction	Synthetic and recorded well data 3:2 split (Training:Validation and Testing)	Not reported	Torque on bit, WOB, Downhole RPM and acceleration	Not reported	Classification accuracy of 98% for stick-slip severity and 93% for lateral vibration presence
Chen et al., 2020	To classify lithology based on drillstring vibration data	Classification of lithology into three groups	Convolutional neural network (CNN)	Not reported	Not reported	Not reported	7:2:1 (Training:Validation:Testing). Hyperparameter testing	20 Hz	Accelerometer (X, Y and Z)	1. High Pass Filtering 2. Short Time Fourier Transform 3. Wavelet Transform	Precision 90%, Recall 89.3%
Srivastava and Teodoriu, 2020	To characterize drillstring vibrations by interlinking surface data and drilling reports	Classification of stick-slip vibration severity	Decision Trees	1Hz	Depth, Rate of penetration, Hookload, Surface torque and Rotary speed	1. Outlier detection 2. Dimensionality Reduction (PCA)	300,000 observations split into 4:1 for testing and training	Not recorded	Not recorded	Not recorded	Classification accuracy of 71%

Table 8 Summary of machine learning applications for drillstring vibrations

The bottleneck of ML models in the drilling industry is the quality of data available through surface and downhole measurements (Al Gharbi et al., 2018). To interpret and take decisions from real time data, the trust- worthiness of drilling data needs to be assessed. Otalvora et al. (2016) developed a data quality index based on uniformity, sensibility, completeness, resolution, format, and structure of drilling data to develop a deeper understanding of its quality. The section extends the discussion on data quality a step further to evaluate the impact of having high resolution and uniformity within training dataset on classification accuracy and performance. The centerpiece of the study remains to find an optimal balance between data quality assessment and a high performing classifier for drilling vibrations.

6.2 Data quality challenges

The following section addresses the data quality challenges associated with drilling data at every step of a machine learning task from data collection to model training and testing. Possible solutions to the issues have been provided in figure 6-2. The data quality issues mentioned in figure are also discussed in greater detail in the following section:

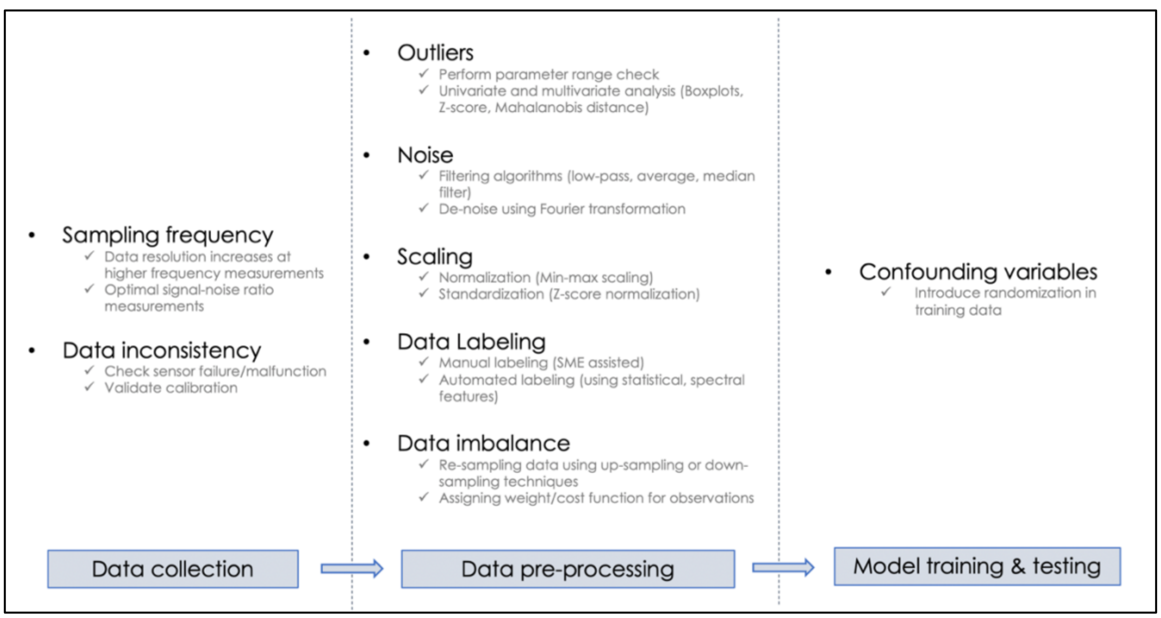

Figure 6-2 Data quality issues and solutions during machine learning workflow on drilling data

6.2.1 Sampling rate

Sampling rate or sampling frequency is the frequency at which the sensor samples the analog signal to obtain the digital signal. It is an important metric of data quality assessment since a higher sampling rate enables more accurate identification of critical downhole phenomena that are often overlooked at lower sampling rates. Some examples of such phenomena include downhole shocks, pipe sticking, and high frequency torsional oscillations. An important consideration when choosing a sampling frequency for an application is the Nyquist theorem which states that the sampling frequency of a digital signal must be at least two times the highest frequency of interest in the signal (Abu-Mahfouz, 2003; Chandel 2013). For example, to accurately detect vibration phenomena which manifest at frequencies under 100 Hz, the corresponding vibration signal must be sampled at least 200 Hz.

The earliest utilization of high sampling rates for downhole measurements dates to 1994 when a wired measurement sub was used to better understand drilling dysfunctions, particularly stick-slip vibrations (Pavone and Desplans, 1994). One of the biggest drawbacks to high sampling downhole measurements is data storage. A popular strategy to work around data storage issues is to optimize data collection with long periods of low frequency measurements with short bursts of high frequency collection (>400 Hz) (Baumgartner and Van Oort, 2014). Currently, no literature exists about an optimal data sampling frequency for downhole measurements that is critical for capturing drilling dysfunctions without comprising on data storage abilities.

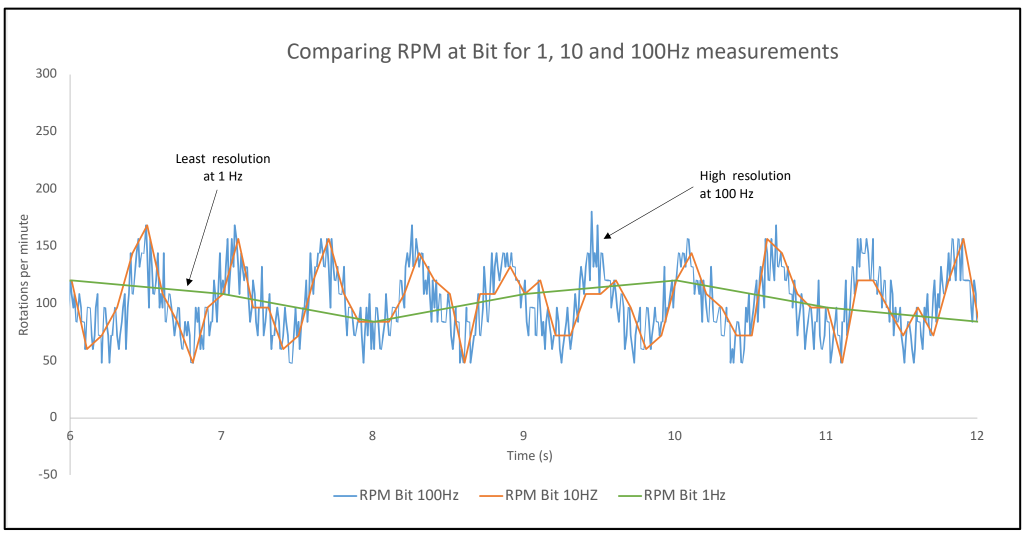

Figure 6-3 Comparison of bit RPM at 1, 10 and 100 Hz sampling frequency measurement

Figure 6-3 compares torsional vibration signature recorded experimentally at 1 Hz vs. 100 Hz to point out the incomplete information observed at lower sampling rates. Incomplete information can lead to misrepresentation of critical events that could potentially affect a classifiers performance. However, in literature, vibration severity classifiers have been successfully trained with both low and high frequency data with high precision. So, is high frequency data measurement justified from a ML perspective? The paper answers this question in the latter section.

6.2.2 Outliers

Outliers are a common occurrence in most datasets. Whether they arise from expected/unexpected changes in system behavior, or are artifacts of instrument error, the presence of outliers in a dataset almost inevitably affects the performance of classification algorithms owing to their extreme value (Hodge and Austin, 2004). Indeed, popular classification algorithms such as support vector machine (SVM) and k-nearest neighbors (KNN) are particularly sensitive to datapoints on the convex hulls of each class of data in the dataset (Burges, 1998). In fact, it is for this very reason that KNN has been adopted as an outlier removal technique (Ramaswamy et al., 2000). Formally, outliers can be categorized into two types – point (or global) outliers whose values are significantly outside the range of the entire dataset it belongs to; and contextual (or conditional) outliers whose values are significantly outside the range of other data that appears in a similar context. Generally, global outliers are a result of instrument error and can be safely removed via popular data pre-processing techniques which have been extensively studied and surveyed (Chandola et al., 2007; Wang et al., 2019; Domingues et al., 2018) and have robust, open-source implementations available (Zhao et al., 2019). Contextual outliers on the other hand may sometimes be indicative of change in system behavior and removing them could result in the failure to detect and act upon potentially critical system information. For example, sudden extreme fluctuations in drillstring downhole RPM may be indicative of stick-slip. The "context" in such cases is almost always temporal i.e., outliers are classified as such based on the values of other datapoints that occur temporally close together. Thus, as important as it is to remove undesirable outliers from a dataset, it is equally important to consider the nuances of the underlying physical process before doing so.

6.2.3 Noise

Noisy data is characterized by random deviations from the true underlying process data. It is one of the most commonly occurring data quality issue. Noise can be broadly classified into two categories—class and attribute noise. Class noise occurs when the data points are incorrectly labeled as belonging to a particular class. The source of such noise is typically human error and is introduced during the data labeling process. Attribute noise on the other hand originates in the data collection process and can be attributed to factors such sensor error/variability, stochastic nature of physical processes, and high sampling rates. In this study the focus is on attribute noise, which is the more common of the two types. Given that noise results in the inclusion of data points that deviate from, and are not representative of the underlying physical process, it is naturally detrimental to the performance of machine learning classifiers when ignored. It has also been shown that noisy training data results in longer training times (Zhu, 2004). Both smoothening and filtering helps in increasing signal to noise ratio of surface and downhole data. For example, when dealing with downhole measurements, stick-slip vibration response is often overlaid with higher frequency vibration responses. As a resultant, a low-frequency smoothening curve can help extract information pertaining to the stick-slip vibrations (Baumgartner and Van Oort, 2014). Similarly, applying a high pass filter such as the Butterworth high pass filter (BHPF) to downhole vibrations can help cleanse the data of low frequency noise to highlight high frequency shocks or lateral vibrations (Chen et al., 2020).

6.2.4 Data labeling

Data labeling is the characterization of data into identifiable categories that accurately describe a phenomenon under occurrence. In the case of drilling vibrations, it includes creating labels of vibration severity based on drilling parameters and measured responses. The process of data labeling is critical to the success of every supervised machine learning task. Often done manually, this process requires subject matter expertise supervision and is exhaustive in nature. Data labeling for drilling vibrations can be divided into labeling methodology and criteria. As the data describing a phenomenon remains constant, ideally, different labeling techniques should generate the same identifying labels.

The methodology of data labeling for stick-slip vibrations can be either point-based or time window-based. Point-based labeling process assigns a data label for every instance of drilling data whereas, window-based labeling process assigns a data label for the entire duration of the fixed time window. Point-based labeling is simpler to implement but fails to capture the temporal patterns in the data. Window-based data labeling is cumbersome to implement and optimize but incorporates temporal characteristics of data. In the case of drilling vibrations, windows-based labeling process is more widely utilized. Figure 3 provides a visual explanation of time window sampling where the n^{th} time window successfully captures both bit sticking (RPM=0 at 101s) and bit release (RPM=1600 at 106s) to confirm the presence of a stick-slip cycle. This phenomenon would have been extremely difficult to capture when considering point-based sampling.

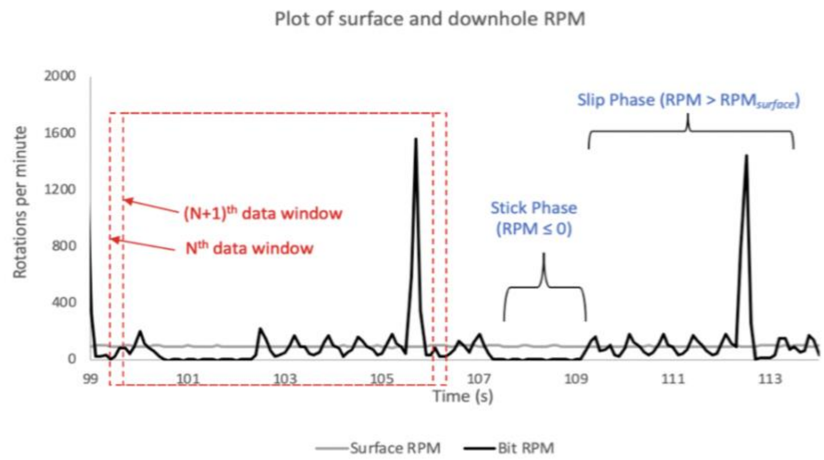

Figure 6-4 Time window sampling visualization as a data labeling procedure

A correctly labeled dataset is crucial for both, training and refining, the classification model. Moreover, while the determined labels should be descriptive of the data features and the occurring phenomenon they correspond to, they should not be derived directly from any one such data feature since this would artificially induce improvements in classifier performance. Under such restrictions, the choice of labeling criteria is crucial. The following are criteria which are used to label vibration data:

Stick slip index (SSI)

Stick slip index quantifies the intensity of torsional vibrations in the drillstring through downhole RPM measurements. It is defined as:

$$Stick\ Slip\ Index\ (SSI) = \frac{Bit\ RPM_{max}(w_N) - Bit\ RPM_{min}(w_N)}{2 * Bit\ RPM_{avg}(w_N)} \quad \text{.........(6-1)}$$

where min, max, and avg subscripts denote the maximum, minimum and average RPM respectively (as measured) in the N-th window wN. By measuring the extent of bit RPM deviation from the average RPM, the stick slip index can help estimate the severity of torsional vibrations and can be used as a data labeling criterion (Hegde et al., 2019). SSI values greater than 1 are considered to represent pure sticking (Patil, 2013).

Radial acceleration at bit

Downhole sensors (accelerometers) help provide accurate radial acceleration values at the bit. Radial acceleration at bit can potentially fluctuate between 0 and 10g for stick-slip vibrations (Baumgartner and Van Oort, 2013). Vibration severity (in terms of standard gravity, g) can also be calculated using RMS amplitude of axial and lateral acceleration components using equation 2 (Okoli et al., 2019).

$$a_{(in\ g)} = \sqrt{a_{ax} - a_{lat}} \ \ldots\ldots\ldots(6\text{-}2)$$

Where a_{ax} represents axial and a_{lat} represents lateral bit acceleration. While bit acceleration is a true representation of abrupt changes in bit rotation and resultant torsional vibrations, the challenge remains to associate severity of bit sticking to resultant amplitude of bit acceleration. This impacts the generality of labeling torsional vibrations, making the procedure case specific.

Rate of penetration (ROP)

One of the most concerning impacts of severe drillstring vibrations is the reduction in rate of penetration, usually defined in ft/hour. As a result, the instantaneous loss in rate of penetration can be related to the severity of drilling vibrations in the system (Srivastava and Teodoriu, 2020). Another holistic indicator of drilling efficiency that includes dependency on ROP amongst other parameters is the mechanical specific energy (MSE). MSE is defined as the mechanical work required to drill a unit volume of rock and depends on various parameters as seen in equation 3. With greater loss of energy through vibrations, the energy required to drill rock becomes higher. Hence, the labeling strategy correlates vibration severity to drilling efficiency.

$$MSE = f(Torque_{bit}, WOB, RPM, Diameter_{bit}) \ \ldots\ldots\ldots(6\text{-}3)$$

6.2.5 Feature extraction and scaling

Feature extraction is data pre-processing undertaken before classification to extract useful information from the data (and often reduce its dimensionality) before training. It is similar to dimensionality reduction to the extent that both approaches seek a mapping $\boldsymbol{x} \rightarrow \boldsymbol{x}'$ where $\boldsymbol{x} \in \mathbb{R}^d$ is a d-dimensional vector in the original feature space, $\boldsymbol{x}' \in \mathbb{R}^p$ is a p-dimensional vector in the reduced feature space ($p \leq d$). However, in feature selection the reduced features are a subset of the original features i.e., $\{x'_i\}^p_{\{i=1\}} \subseteq \{x_j\}_{\{j=1\}}^{\ d}$. This is not the case with feature extraction where the new feature set, although derived from the original feature set, is completely different from it (Ghojogh et al., 2019). Extraction of features that represent the data well for a particular task is important to the final classification performance. In fact, one reason why deep neural network architectures work so well in practice is because their deep architecture allow their hidden layers to extract and save high- and low-level features from the input data before finally performing classification (Navamani, 2019; Bello et al., 2020). Since this is not the case with traditional models such as SVM, KNN, etc., feature extraction must be performed as a separate pre-processing step before training. Feature extraction is not generally considered a data quality issue since it is not a part of the data collection or cleaning process, however, from the perspective of training a machine learning model, it is viewed as a vital pre-processing step and its effectiveness is studied through dedicated experiments later in the paper.

While there are a multitude of techniques available to extract features (Zebari et al., 2020), the types of features that are generally extracted for applications involving vibration data can be broadly split into two categories—statistical and spectral.

Statistical Features

Statistical features aim to compress the information contained in a time-domain signal into a set of statistics describing the distribution of data contained in the signal. They are obtained by computing aggregate statistics for a sliding time window over the time-domain signal. Typically, the first k-statistical moments of the signal are used as features. Often these are enough to adequately characterize the location and shape of the data distribution. Here, the first moment is the mean μ; the second moment is variance σ^2, quantifying the spread around the mean; the third moment is skewness γ describing whether the data distribution is lopsided to one side or symmetric; and the fourth moment is kurtosis κ, that captures the heaviness of the tail of a distribution. There also exists higher-order moments which can be estimated and included as features. However, a larger sample size is required to estimate higher-order moments with the same precision as lower-order moments. Additionally, higher-order moments are also harder to interpret.

Another important consideration is that purely statistical features such as moments of a distribution can be estimated efficiently only when the data distribution is unimodal. Multimodally-distributed data is first modeled as a mixture of unimodal distributions e.g., as a mixture of Gaussians, before its moments can be estimated. Estimating the parameters of such mixture model requires techniques such as Maximum Likelihood Estimation (MLE) which makes computing statistical features for such data prohibitively expensive. Alternatively, in cases where specific characteristics of frequently occurring vibration patterns are known beforehand, other statistical quantities besides moments may also be used as features. These include the mode, median, minimum, maximum, and quantities obtained by combining them. For instance, in torsional vibration applications, it is known that a value of Stick-Slip Index (SSI) greater than 1 is indicative of the occurrence of the stick-slip phenomenon (Hegde et al., 2019). The stick-slip index is just a combination of more fundamental statistics of the data, also defined in the previous section.

Spectral Features

In general, when rotating machinery is operated under variable speed and fluctuating load, the resulting time-domain vibration signal typically contains multiple frequency components. As a result, the spectral make-up of the instantaneous vibration signal is a good indicator of the state under which the machinery is operating. This is very relevant to drilling with long drillstring equipped with heavy bottom hole assembly components. The spectral signature obtained from downhole RPM is a good indicator of drilling conditions where abrupt changes in spectral signal can be associated with severe downhole vibrations. Thus, even when the data belonging different classes may not linearly separable in the time domain, it may be so after transformation to the frequency domain. In such cases, simply including the best estimates of the frequency components in the signal at any instant, as a feature in the training data can yield significant gains in classifier performance. A variety of techniques to extract spectral features are available. Simple methods like Fast Fourier Transform (FFT) can efficiently extract all the frequency components and their magnitudes, which can then be used as features in the training data (Millan et al., 2019). More sophisticated time-frequency analysis methods such as Wavelet Packet Transform (WPT) (Yen and Lin, 2000) and Continuous Wavelet Transform (CWT) captures the change in the frequency components in the original signal (Yang, 2003; Zebari, 2020).

An application of the technique is shown in figure 4-4 in which drilling responses are subjected to fast-Fourier transform (FFT) to analyze time domain measurements in frequency domain. Surface torque measurements are highly effective in differentiating low frequency and high frequency downhole conditions (Millan et al., 2019). Similarly, downhole accelerometer readings have been analyzed in the frequency domain to reveal immensely high shock frequencies that go unidentified at the surface (Ignova et al., 2019).

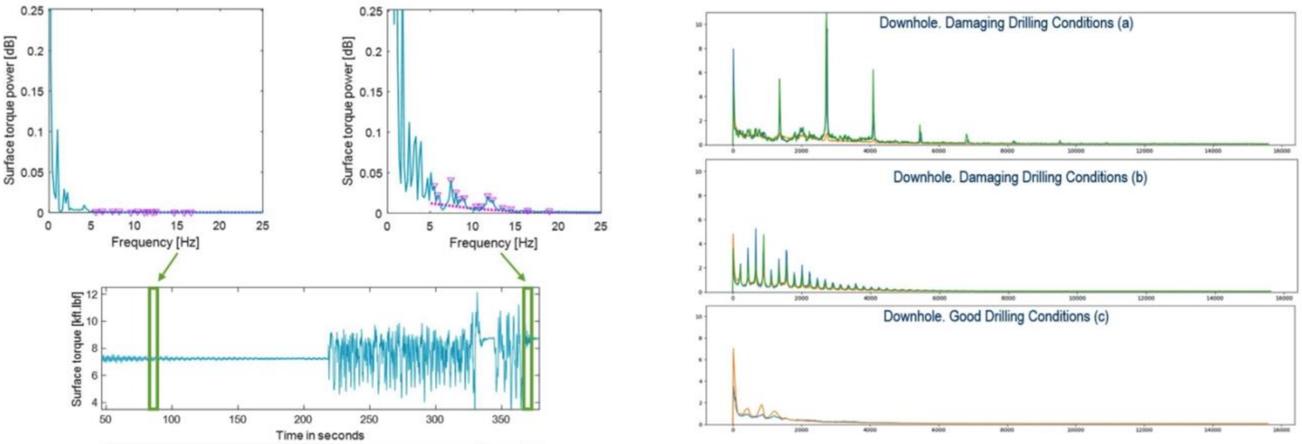

Figure 6-5 Frequency domain analysis of surface torque (left) and downhole accelerometer response (right) (Millan et al., 2019; Ignova et al., 2019)

Principal Component Analysis (PCA) (Pearson and Lines, 1901; Wold et al., 1987) is unique in that although it is a feature extraction category, the features extracted by PCA are a linear combination of the original features and cannot be classified into either of the two categories discussed above. PCA is also commonly classified under dimensionality reduction techniques since the number of principal components (PC) used is often less than the number of original features

6.2.6 Class imbalance

Even though the importance of having high sampling measurement has been discussed, an integral data quality issue remains unaddressed in the realm of machine learning. Even if we have enough data, does the data do a good job of describing the phenomenon under investigation. In other words, the question is asked whether the phenomenon under investigation is represented appropriately in the dataset.

This is also referred to the class imbalance issue in training machine learning models. This occurs when there exists an imbalance in class representation in the data. This occurs commonly in real world datasets. For example, when dealing with drilling vibrations, the occurrence of simple torsional vibrations outweighs severe sticking conditions. Performing classification with imbalanced dataset effects probability estimation of minority class. Srivastava and Teodoriu, 2019, implemented a multi-level classifier for drilling vibrations using surface measurements on an imbalanced dataset and observed a drastic reduction in model performance.

Data imbalance can be dealt with upsampling minority class, downsampling majority class or by assigning a weight component based on class imbalance severity. Hegde, 2019 observed an increase in model precision when class imbalance ratio (ratio of minority to majority labels) was closer to 1. This paper discussed the impact of class imbalance on performance of different classifiers and the interdependence of sampling frequency and class imbalance on model performance.

6.3 Dataset and experiments

The experimental setup, described in chapter 3 is instrumental in generating training datasets with varying resolution for prediction of stick-slip vibration severity. Details of the experimental design include:

- Testing conditions: RPM=200, WOB=5N, Surface Torque=300-500 mNm
- Testing scenario: Torsional vibrations, Mild stick slip (bit sticking under 1s) and Severe stick slip (bit sticking over 1s).
- The tests have been performed at sampling frequencies of 1, 10 and 100 Hz, while keeping the total test duration of the constant. This results in three datasets, each generated using identical testing conditions, but with different number of samples. The sizes of the three resulting datasets are given in Table 8.

Sampling Frequency	# Samples/Test
1 Hz	133
10 Hz	1310
100 Hz	12940

Table 9 Number of samples collected from each of the three experiments at different sampling frequencies

An example of torsional vibrations is seen in figure 6-6a where bit RPM oscillates around 200RPM without sticking. Mild stick-slip has been shown in figure 6-6b where bit sticking is observed when bit RPM is momentarily at 0. Bit sticking of 1 second and lower is observed in the mild stick-slip test. Similarly, a case of severe bit sticking is seen in figure 6-6c where up to 3 seconds of bit sticking is observed with a consequent but drastic bit slip phase.

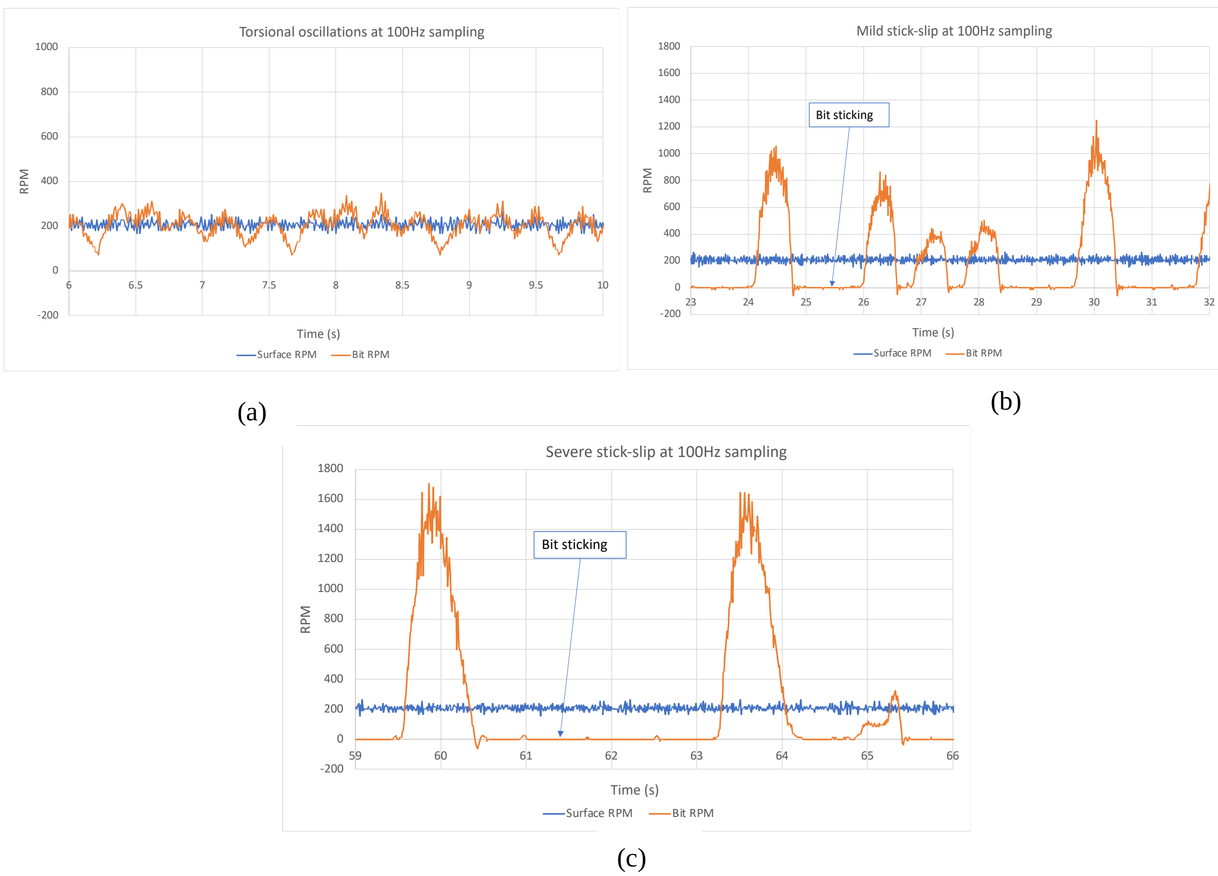

Figure 6-6 Example of torsional oscillations (a), mild stick-slip (b) and severe stick-slip (c) vibrations, sampled at 100Hz

The study investigates how choices made at different stages in the data collection and pre-processing steps affects the performance of several popular classifier models. It also examines the reasons for difference in performance of classifiers, wherever applicable. Apart from the experimental variable being examined in each subsection, the rest of the machine learning pipeline remains unaltered across different experiments. Specifically, the study uses the following six classifiers – Support Vector Machine (SVM) (Boser et al., 1992), Linear Discriminant Analysis (LDA) (Fisher, 1936), Logistic Regression (LR) (Hosmer and Sturdivant, 2013), Naïve Bayes

(NB) (Rish et al., 2001), Classification and Regression Trees (CART) (Breiman et al., 1984), k-Nearest Neighbors (KNN) (Fix and Hodges, 1989). Further,

- For each classifier 100 simulations are run. Each simulation involves shuffling and resampling the training and testing data, followed by retraining each classifier.
- An 80:20 split for the training: test ratio is utilized
- Two metrics to evaluate our trained classifiers are utilized–Test Accuracy and F1-Score.

Upon evaluating a classifier using the test data, the number of True Positive (TP), True Negative (TN), False Positive (FP), and False Negative (FN) examples are obtained. The test accuracy and F1-score can be computed as

$$Accuracy = \frac{TP+TN}{TP+TN+FP+FN} \quad \text{.........(6-4)}$$

$$F1 - score = \frac{2TP}{2TP+FP+FN} \quad \text{.........(6-5)}$$

6.4 Results

The results in this section are divided based on experiments performed.

6.4.1 Sampling Frequency

The goal of this experiment is to study the effect the sampling rate of the training data has on final classification accuracy of a variety of classifiers, and test if certain machine learning classifiers are more robust to variations in sampling rate than others. As described in the previous section, our experimental data was collected at three different sampling frequencies – 1 Hz, 10 Hz, and 100 Hz. The results for this experiment are shown in figure 6-6. In general, the mean and median test accuracies of all classifiers are seen to consistently improve when the training data is collected at a higher sampling frequency. But more significantly, there is an even more pronounced trend in the variance of test accuracies at higher sampling rates, which enable higher confidence levels in the final test accuracies. The increase in median test accuracy, and the decrease in its variance is expected since higher sampling frequencies capture more data samples per time interval than lower sampling frequencies.

Further, the difference in the test accuracies between different classifiers with 100 Hz data is insignificant. This can be attributed to the fact that collection of more data enables capturing more patterns that uniquely identify all three types of vibrations – torsional, mild stick-slip, and severe stick-slip. The way this manifest in our data is by way of increased linear separability between the three classes of data at 100 Hz. This is validated by the fact that for the 100 Hz data the performance of linear classifiers such as LDA is comparable to that of non-linear classifiers such as SVM, CART, and KNN. Finally, the conclusions drawn from this experiment are

- All other parameters being equal, better detection and classification of stick-slip can be achieved at higher sampling frequencies.
- Given data sampled at an adequately high sampling frequency, the choice of classifier does not affect the classification results significantly.
- However, a higher sampling frequency also entails higher data storage costs, and the right trade-off between performance and storage costs must be determined on a per-case basis for best results.

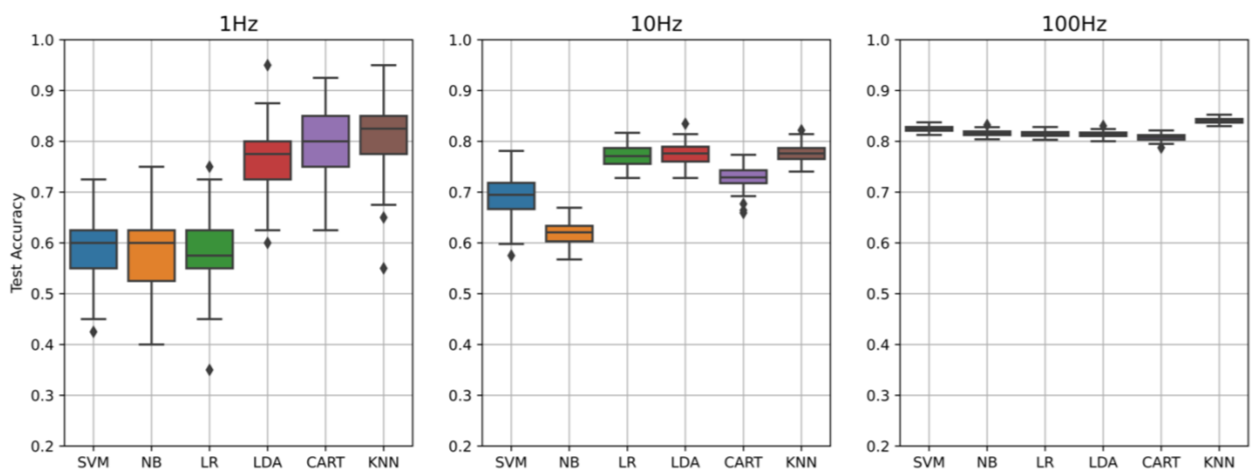

Figure 6-7 Comparison of test accuracies of different classifiers trained on data collected at different sampling frequencies

6.4.2 Data Labeling

The goal of this experiment is to investigate the impact of different labeling techniques on the performance of various classifiers. Note, the goal is not to investigate if one labeling technique is better than another. In fact, it is desired that the choice of labeling technique does not impact classification performance significantly since all labeling techniques should ideally agree on the ground truth for them to be considered effective. From the techniques listed under 'Labeling' in Section 6.2.4, a comparison is made between manual and SSI-based labeling. For the experimental data, manual labeling was performed using subject matter supervision. SSI-based labeling is automated and was performed using a sliding time window method, where the N-th time window w_N is labeled as below:

$$Label\ (w_N) = \begin{cases} Torsional\ vibrations. & SSI(w_{N)} < 1 \\ Mild\ stick - slip & 1 \leq SSI(w_{N)} \leq 3 \\ Severe\ stick - slip & SSI(w_{N)} > 3 \end{cases}$$

where SSI (w_N) is computed as described in equation 6-1 using a siding time window method. Further, having already shown that a 100 Hz sampling rate is more effective than 1 Hz and 10 Hz, only results for the 100 Hz data are presented, restricting the comparison to the choice of labeling, and not that of sampling frequency. This is also done for sake of clarity. In figure 6-8, a comparison for the label distributions for 100 Hz data generated by both labeling techniques is presented and the corresponding results for this experiment are presented in Figure 6-9.

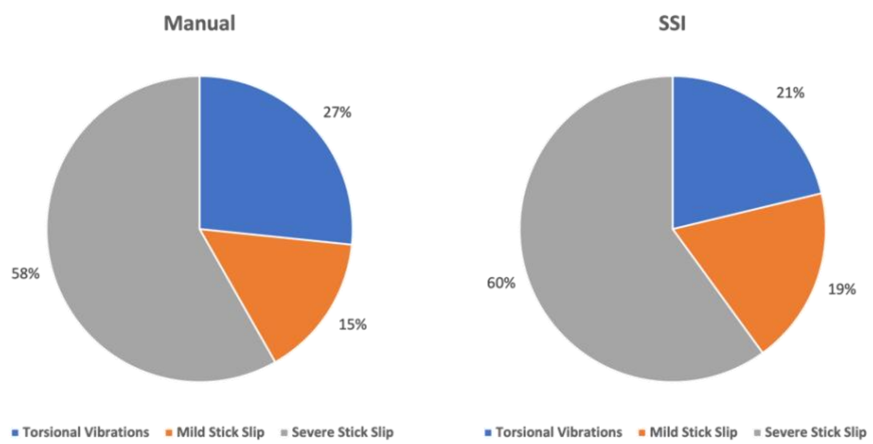

Figure 6-8 Comparison of label distributions obtained using the two labeling techniques

The results suggest that SSI-based labeling yield consistently lower test accuracies for all tested classifiers than even data labeled by a subject matter expert. This is likely because the SSI, while easy-to-interpret, is an empirical metric and may not always be accurate, and as a result yields lower classification performance than manual labeling for all classifiers.

Thus, following conclusions are drawn from this experiment:

- Manual labeling carried out by a subject matter expert, while costly, is more accurate.
- Automated labeling techniques using empirical metrics such as SSI, while easy-to-interpret and time- efficient, may be erroneous. An additional 'label inspection' step carried out by a subject matter expert when using such labeling techniques is recommended.

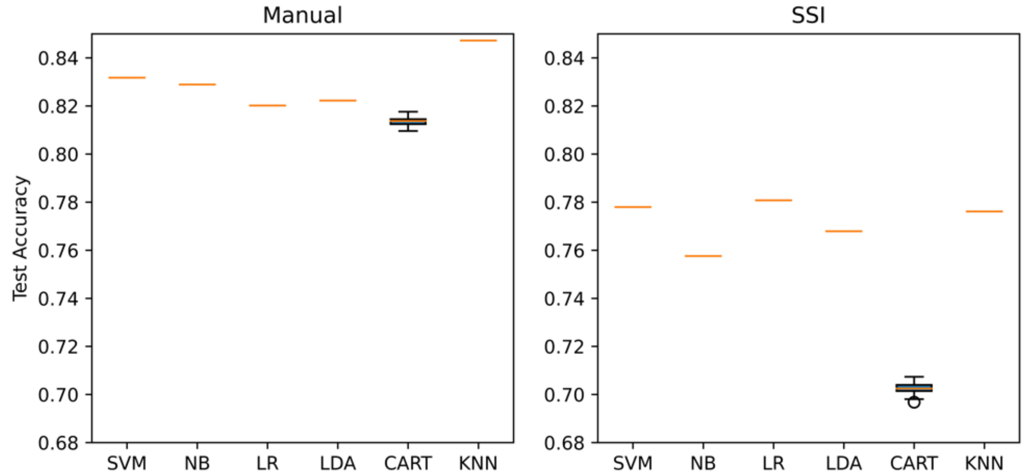

Figure 6-9 Comparison of test accuracies of different classifiers trained on data labeled using two different techniques

6.4.3 Feature Extraction

The goal of this experiment is to investigate the impact of different feature extraction techniques on the performance of different classifiers. Two feature extraction techniques are compared– statistical and spectral feature extraction, listed in Section 6.2.5. Both approaches involve using a sliding time window. The following statistical features are extracted from each time window – mean μ, standard deviation σ, skewness γ, kurtosis κ, minimum, and maximum. Further, these statistical features are extracted for the following sensor data – Surface Torque (mNm), RPM T (top drive), RPM B (bit) and WOB (Weight on bit), resulting in a total of 25 features (5 statistical features × 5 sensors). Given the variety of approaches available for spectral feature extraction, a straightforward approach is adopted due to the simple nature of patterns in the dataset. It is given that the torsional vibrations and the stick-slip phenomenon both result in periodic patterns in the RPM B data which occur under 1 Hz. Thus, three spectral features are extracted, each of which denotes the strength of the periodicity in one of three frequency ranges - ≤0.5 Hz, 0.5-1 Hz, ≥1 Hz. The strength of different frequency components is computed using FFT. The hypothesis is that the presence of frequency components in these ranges can help distinguish between torsional vibrations, mild stick-slip and severe stick-slip. The results obtained using raw features are presented, without performing feature extraction for comparison. Note, data sampled at 100 Hz and labeled manually by a subject matter expert is used.

The results for this experiment are shown in Figure 6-9. In general, both techniques for feature extraction result in higher classification performance than using raw features. It is worth noting that using even simple, FFT-based spectral features can result in classification performance gains. This shows that the extracted featured successfully captured the phenomenon manifesting in the data. More interestingly, using statistical features results in perfect classification performance on even the test data, across all classifiers. While such a result is typically indicative of model overfitting, that is not the case here. Upon investigating the pairwise scatterplots for the statistical features it is found that certain features such as minimum, maximum, and standard deviation of RPM B (bit) are good enough to make all three classes of data perfectly linearly separable. A subset of all pairwise scatterplots is shown in Figure 6-11.

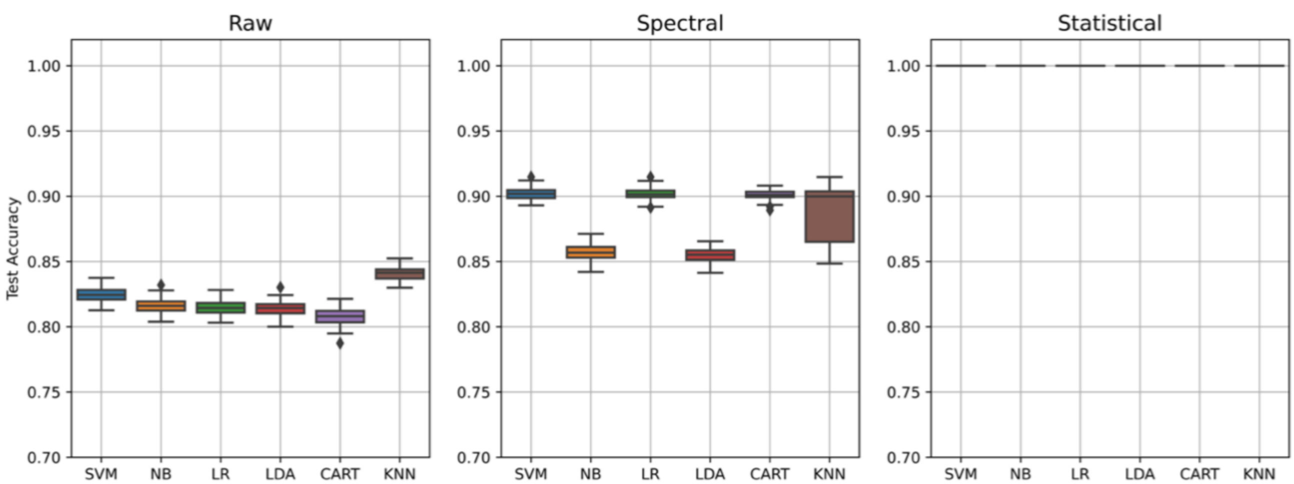

Figure 6-10 Comparison of test accuracies of different classifiers trained on data obtained from different feature extraction techniques

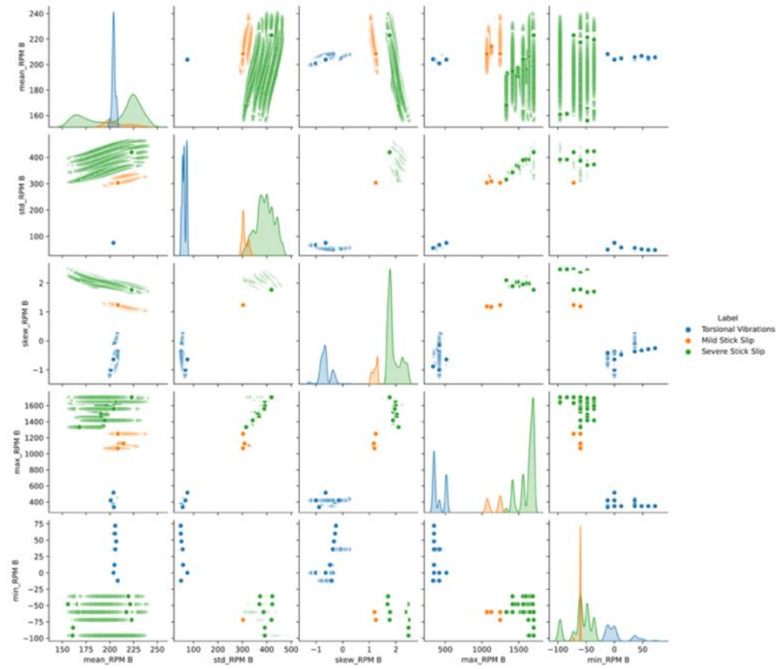

Figure 6-11 Pairwise scatterplots for different statistical features using statistical features makes the data classes linearly separable

6.4.4 Class Imbalance

The goal of this experiment is to investigate the impact of imbalanced data on the classification performance of different classifiers. To reiterate, the imbalance ratio of a data set is the ratio of the number of samples in the majority class to those in the minority class. In drilling applications, it is expected that the machinery will operate under normal operating conditions (torsional vibrations) more frequently, than it will under extreme operating conditions (mild and severe stick-slip), hence data sets obtained from drilling operations are expected to be naturally imbalanced. Thus, torsional vibrations are the majority class, and mild and severe stick-slip to be minority classes.

Further, three levels of imbalance for this experiment are considered– 1:1, 10:1, and 100:1. To generate data sets with these imbalance rations, the size of the minority class (mild and severe stick-slip) is fixed increasing number of samples for the minority class (torsional vibrations) is generated. In general, to compute the required number of majority samples for each level of imbalance, the following relationship has been derived from the definition of imbalance ratio

$$N_{torsional} = IR \times (N_{mild\ SS} + N_{severe\ SS}) \quad \text{.........(6-6)}$$

where $N_{torsional}$ is the number of samples in the majority class, IR is the desired imbalance ratio, and $N_{mild\ SS}$ and $N_{severe\ SS}$ are the number of samples in each of the minority classes.

For this experiment, data set sampled at 100 Hz is used since that was deemed to contain most information. However, despite statistical features yielding perfect classification performance, the experiments are restricted to raw features. This is done to prevent the perfect classification accuracies from masking the impact of different levels of class imbalance in the experimental results. Results are shown in Figure 6-12 (top). At first glance, it appears that the test accuracy of all classifiers improves as the imbalance ratio increases. However, one of the known pitfalls of using test accuracy as an evaluation metric is that it does not consider the imbalance in the training data. Thus, F1 scores are shown in Figure 6-12 (bottom). Since F1-score is computed as the harmonic mean of the Precision and Recall, it does consider the class imbalance. Consequently, the F1-score provides better insight into the performance of different classifiers, and hence it is considered for the remainder of this discussion. NB, LR, and LDA yield generally lower F1 scores for higher levels of imbalance. This is expected for the NB classifier whose performance strongly depends on the prior probability distribution which, for imbalanced data sets, assigns lower probabilities to the minority class data, and thereby results in lower detections of the minority class. While the LDA model does not depend on the prior probabilities, unlike NB, it does not explicitly account for class imbalance either. This combined with the use of raw features for this experiment results in lower F1-scores for LDA. In fact, even the lower performance of LR at higher imbalance ratios can be attributed to the fact that LR does not explicitly account for class imbalance. Specifically, an imbalanced data set can artificially skew the classification threshold learned by the LR model, towards the majority class.

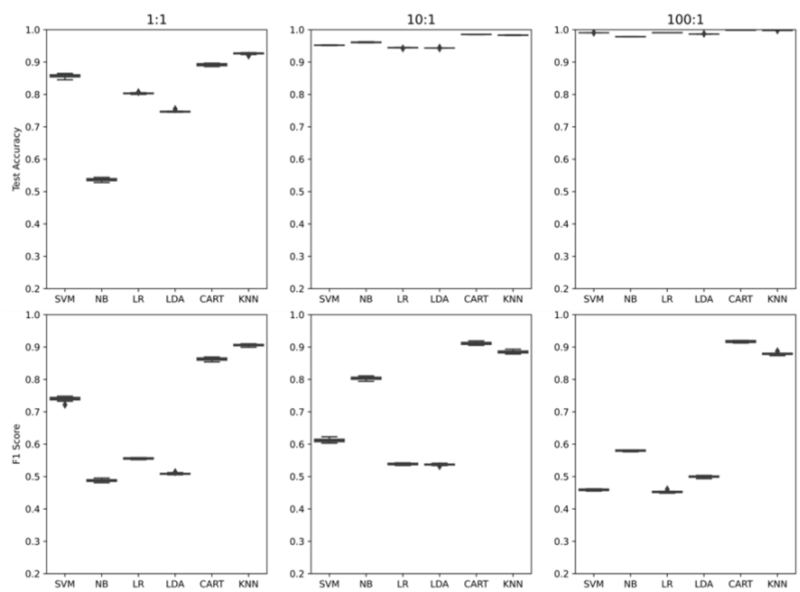

Figure 6-12 Test accuracy and F1 scores for different classifiers trained on data containing imbalance

The performance of CART clearly stands-out in these results with test accuracies and F1-scores greater than 0.80 for all levels of imbalance. The CART algorithm is not known for its robustness to imbalanced data. CART has been found to fail occasionally when trained using imbalanced data (Liu et al., 2010). Hence, in this case, this competitive performance is attributed to the fact that the data can be easily classified into one of three classes using only a few splits in CART's decision tree. This is also in line with the previous experiments where CART outperformed other classification models for different sampling frequencies, labeling techniques, and feature representations.

6.5 Summary of machine learning experiments

This section introduces machine learning for application in the world of drilling vibrations. The uniqueness of this study is that stick slip data is readily available from experimental tests at varying sampling rates. The controlled nature of experimental tests help generates good quality data. As a result, the effects of high-resolution data for classification of vibration severity are analyzed. Additionally, a methodology is presented for handling data quality issues like noise, outliers, data imbalance etc. The results for the various experimental tests have been presented. The results are further discussed in chapter 7.

Chapter 7: Discussions

An experimental, modeling and machine learning based investigation of stick-slip vibrations has been performed successfully in this study. For best results, high resolution (100 Hz) data has been used for all experimental results. Moreover, this sampling rate is also recommended for industry use. However, handling hundreds of data files sampled at 100 Hz is a very cumbersome task. For this study, different templates of graph plotting codes have been written in python for more efficient data handling, processing, and uniform plotting. This section explores the results obtained in the different analysis methods used and helps strengthen our understanding of torsional vibrations.

Through the experimental approach, the study examined the effect of sampling rate of measurement, process parameters (RPM and WOB), drillstring properties (torsional stiffness, inertia), well configuration and bit sticking severity on downhole vibration response. Talking about sampling frequency, the SSI and STS results are presented in figure 7-1 for both mild and severe stick-slip vibrations.

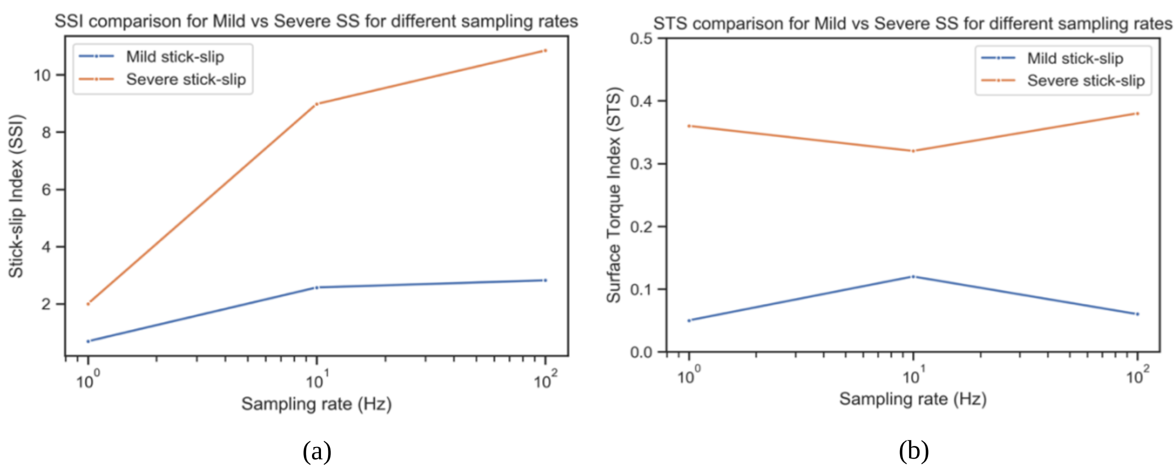

Figure 7-1 Plot of SSI and STS for mild vs severe sticking at 1, 10 and 100 Hz sampling

The gap between SSI for mild and severe stick slip vibrations increases drastically 10 Hz onwards, as seen in 7-1a. Low frequency bit sticking is observed to be more severe than high frequency bit sticking due to longer bit sticking periods. Maximum SSI is calculated at 2.82 for high frequency bit sticking as compared to 10.85 for low frequency bit sticking (both at 100 Hz). Higher frequency sampling rates help in improving the detection rate of stick-slip vibration severity. The complete characteristics of stick-slip vibrations including bit sticking, instantaneous RPM peaks and negative bit RPMs were captured only at 100Hz sampling. Amongst surface drilling parameters, top drive torque is a reliable indicator of severe bit sticking phenomenon. Torque increments of up to 15% are observed for high frequency bit sticking and up to 80% for low frequency bit sticking. The torque severity index is used as an indicator of torsional vibrations at the surface. Interestingly, torque swings due to stick-slip vibrations are independent of the sampling frequency of the surface measurements. As seen in figure 7-1b, the value of STS is under 0.15 for mild SS and around 0.35 for severe SS. In conclusion, the vibration response difference between 1 Hz and 10 Hz was much more drastic than 10 Hz and 100 Hz sampling. As a result, a minimum of 10 Hz sampling is recommended for operational downhole measurements with 100 Hz sampling rate being more of an ideal situation. This proves the first hypothesis of the study that higher sampling rates for downhole measurement improves estimation of stick-slip severity. For surface measurements, it was observed that resultant torque swings due to downhole vibrations were much lower in frequency than 1 Hz. As a result, 1 Hz sampling at the surface is adequate.

Moving on to torsional stiffness, polyethylene string most closely mimicked field vibrations as compared to the other strings. A comparison with actual drilling data revealed very close SSI values for polyethylene. A comparison between the stick slip index (SSI) and surface torque index (STS) is made in figure 7-2 for 200 RPM tests. A trend is observed where both indexes (SSI and STS) reveal higher values at severe stick-slip vibrations. In figure 7-2b, aluminum behaves as an outlier that sees a decrease in surface torque variation in the severe vibration case. This is because aluminum did not undergo a longer bit sticking period as other strings. Nylon shows high stiffness values with high downhole vibrations and subsequent surface vibrations. Steel shows lower downhole vibrations and minor surface torque variations.

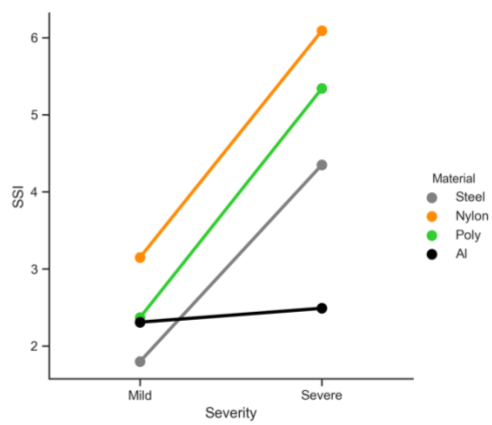

(a)

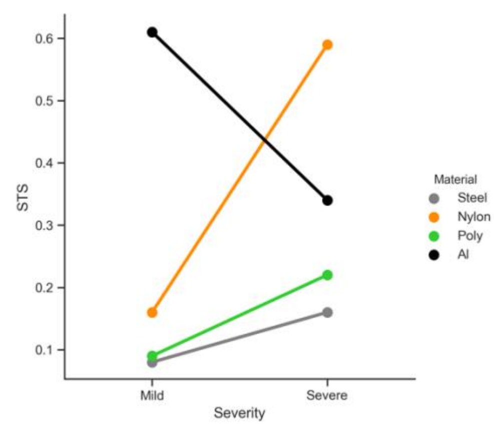

(b)

Figure 7-2 Comparison of stick slip index (SSI) and surface torque index (STS) for mild vs severe vibrations at 200RPM

A case for using torque severity index for indicating downhole vibrations can be made. The results for different steel drill strings prove the second hypothesis of the study that higher torsional stiffness drillstring are more resistant to downhole vibrations and vice-versa.

Process parameters such as RPM and WOB also influence vibrations as higher surface RPM for a constant WOB resulted in damping of stick-slip vibrations. The trend was observed in both mild and severe vibrations. Higher surface RPM relates to higher rotational energy and reduced drillstring friction to overcome sudden torque increment at bit. The calculated SSI is plot for all cases including mild and severe vibrations in figure 7-3. The effect of changing WOB for a constant RPM is not consistent. On increasing WOB for a constant RPM, stick slip severity increased but only for the mild case. In severe stick-slip vibrations, adding WOB dampened vibrations. Using the following results, a sweet spot for experimental drilling can be estimated with lowest SSI values

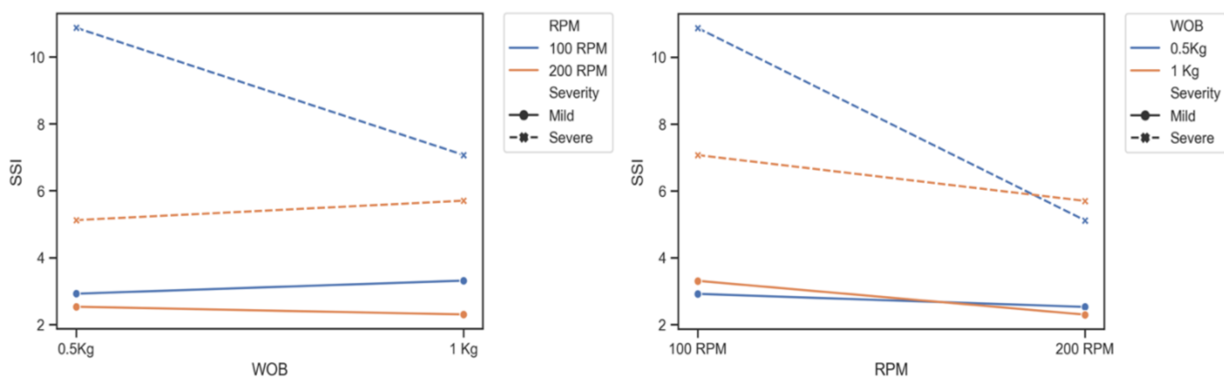

(a) (b)

Figure 7-3 SSI comparison for effect of RPM (a) and WOB (b) on mild vs severe stick-slip vibrations

The results for self-induced bit sticking have been presented in figure 7-4 for both vertical and horizontal well profile. In terms of bit sticking period, horizontal configuration undergoes longer bit sticking periods at lower RPM than the vertical configuration. For example, at 25 RPM, the bit sticks 3 times more in horizontal well as compared to the vertical well. This can be explained by higher friction co-efficient and contact points along the wellbore. In the horizontal case, bit sticking is observed all the way up to 100 RPM since SSI value is greater 1. At 125 RPM, SSI values drop to lower than 1 indicating torsional oscillations. This is seen in figure 7-4b. In the case of vertical configuration, the system undergoes self-induced stick-slip vibrations up to 50 RPM and only torsional vibrations 75 RPM onwards. This proves our third hypothesis that horizontal well configuration is more prone to self-induced bit sticking. The SSI values for both configurations match 125 RPM onwards. When looking at surface torque severity index values in 7-4c, a clear demarcation of stick-slip situations vs torsional oscillations cannot be determined. While the highest STS value for horizontal case is for 25 and 30 RPM, it is 75 and 100 RPM for the vertical case. The vertical well configuration has higher STS values generally as waves of downhole disturbances reach the surface more easily than the horizontal case. This is due to lower contact points than the horizontal case. index. Another interesting trend is observed in figure 7-4d which plots self-induced bit sticking period with the respective SSI values for the horizontal case. A linear trend is observed in 7-4d that relates higher stick slip index for longer self-induced bit sticking periods.

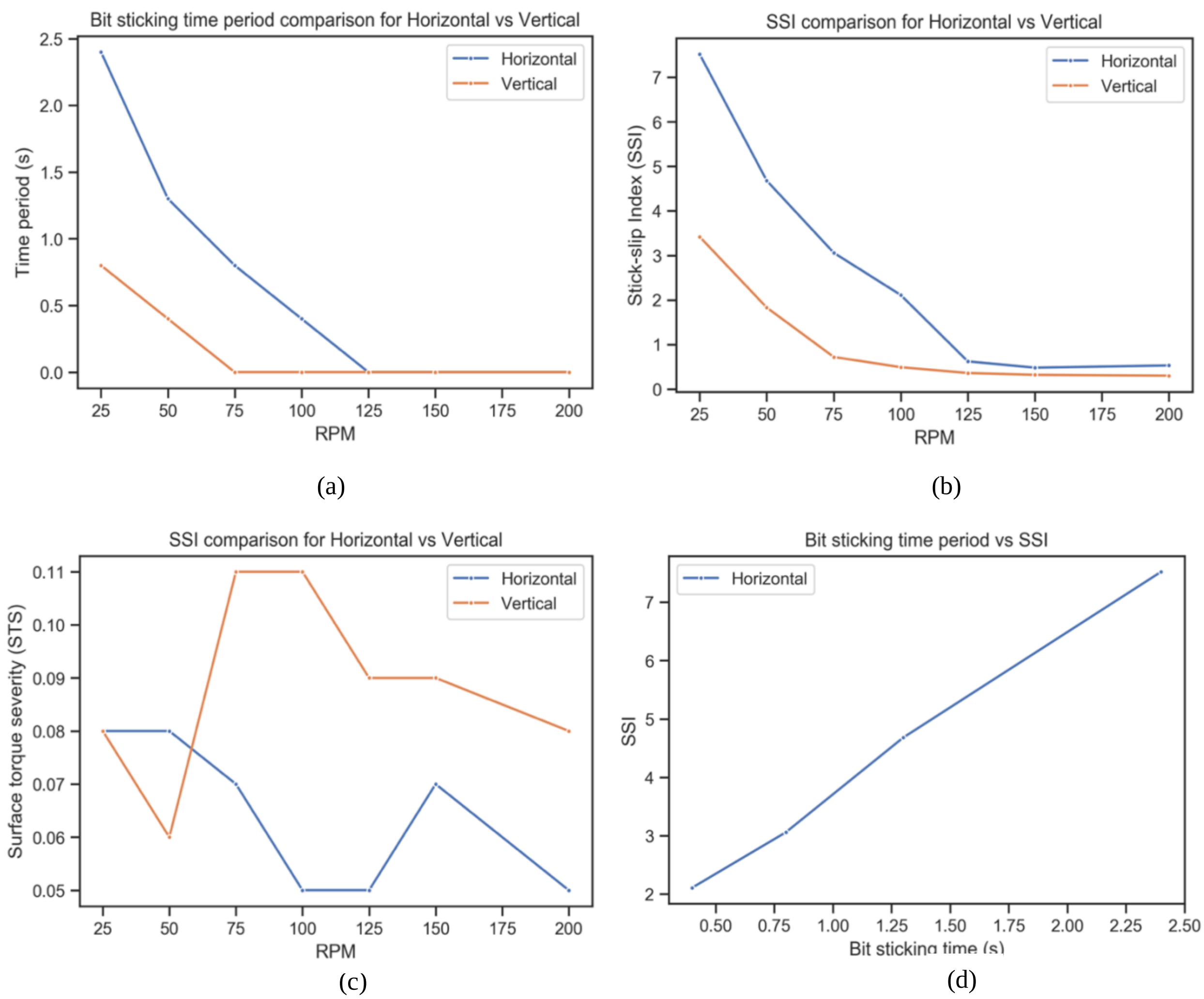

Figure 7-4 Comparison of bit sticking period (a), SSI (b) and STS(c) for vertical vs horizontal well profile

Since wells are mostly drilled horizontal nowadays, a comparison of well configuration is necessary. Interestingly, lower SSI and STS index were observed in the horizontal well profile for both mild and severe bit sticking. Even though the friction co-efficient is higher in the horizontal well configuration, the resultant vibration is not as severe as seen in the vertical case. This can be seen in figure 7-5a and 7-5b where SSI and STS index are lower for the horizontal scenario. The trend exists in both mild and severe stick-slip vibrations. This can be explained by the fact that there are multiple contact points in the horizontal well profile for the drillstring as compared to the vertical case. In such a situation, the free rotation of the drillstring is restricted during the bit slip phase causing lower bit RPM peaks in the horizontal well configuration.

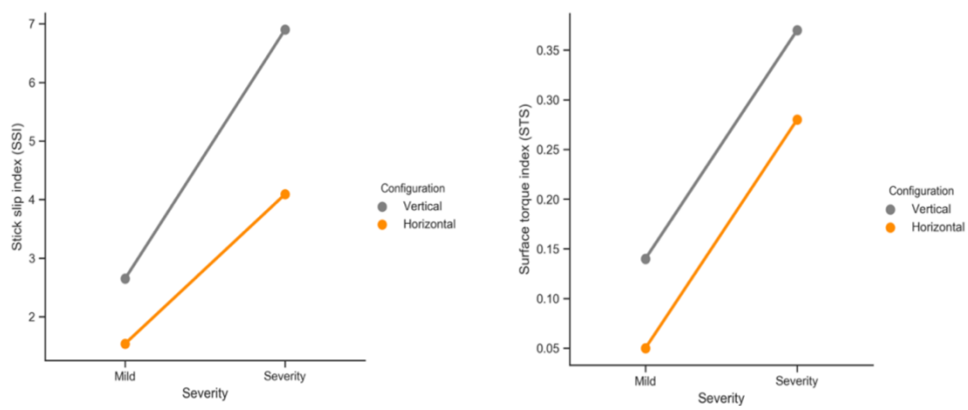

(a) (b)

Figure 7-5 Comparison of stick-slip index (SSI) and Surface Torque Severity (STS) for Vertical vs Horizontal configuration

A unique and programmable input in our experimental setup is the bit stick and slip phase sequence. While it is well understood that longer bit sticking periods cause severe torsional oscillations, the time period between individual bit sticking cycle has been experimentally tested. The results can be seen in figure 7-6. The most severe vibration case is the 1 second stick with 0.1 s slip. The lowest SSI is observed in the 0.1 s sticking case with 3 seconds between each bit sticking occurrence. It can be inferred that as time between two bit sticking cycles is increased, the intensity of resultant vibrations is reduced. In other words, smaller slip phases between stick cycles results in greater downhole vibrations. An outlier trend is observed in the 0.5s slip results. Upon further analysis, it is revealed that 0.5 seconds is very close to the stabilization period of the bit sticking disturbance in the system. As a result, it negatively dampens the 0.1 and 0.5s bit sticking cases, resulting in a higher SSI. In the 1 second sticking case, 0.5 s slip phase dampens the resultant vibration instead. As the slip phase is increased to 1s and 3s, each bit sticking disturbance is stabilized before a new disturbance is introduced. This proves that period of bit sticking and slipping has an impact on severity of stick-slip vibrations

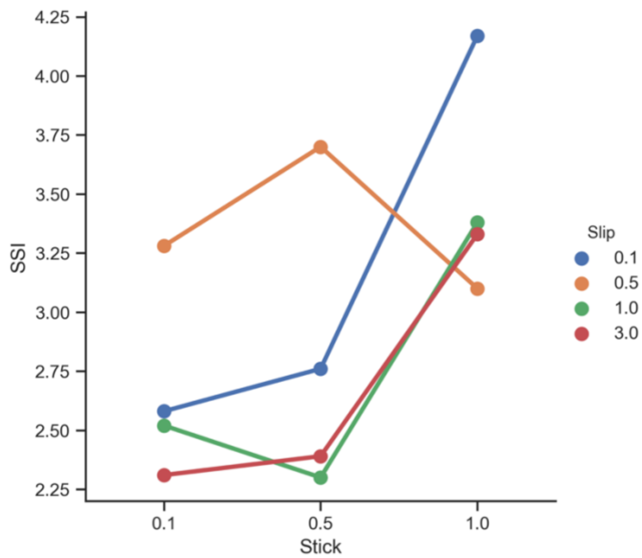

Figure 7-6 Comparison of SSI for stick and slip combinations at 200RPM

Modeling experiments were performed with an objective of comparison with experimental data. A simple 2DOF model was finetuned with experimental parameters as input parameters. The torque on bit for the mathematical model was made to mimic the torque signature of the electromagnetic brake in the experimental setup. Both mild and severe form of torsional oscillations were modeled for comparison. While modeling results matched experiment data to some extent, the modeling results were independent of the time-period of bit sticking. This completely differed from experimental results. Moreover, the stick slip vibration signature in modeling results was always constant, thus failing to incorporate the non-linearity in the system. Additionally, the model even failed to show surface parameter response to downhole vibrations due to the absence of a feedback loop. When analyzing vibration in WellScan, a better mathematical model result was obtained. Aluminum, steel and PVC strings were utilized for an SSI comparison for horizontal vs vertical well profile. Since the mathematical models in WellScan include static friction components in the well, comparable results to the experimental model were obtained. Comparable surface response was also obtained in WellScan results for the downhole vibrations.

This study also explores the implications of drilling data quality on efficient application of ML techniques, particularly classification of severity of stick-slip vibrations using experimental data. High resolution data is data sampled at high sampling frequency. Through extensive testing, it is observed that high resolution data (minimum of 100Hz) is crucial to better performing classifiers with high accuracy and low variance. To have high performing classifiers, data labeling is an important step for machine learning models. Manual labeling techniques provide accurate labeling while being time and resource intensive. While automated techniques are faster to implement and provide higher testing accuracies, they are prone to errors and need a 'label verification' step, as suggested in section 6.2.4. In either case, involvement of a subject matter expertise is crucial. Adding features to raw data improves the model's robustness and its classification performance across all classifiers used. Additionally, handling data imbalance helps improve classification accuracy, especially when dealing with low frequency surface and downhole measurements. Performance of CART, a decision tree model has been better than other classifiers for all testing scenarios. Using correct feature representation for each data set helped yield competitive results with all classifiers including simple ones like LDA. Overall, the machine learning results help prove our final hypothesis that higher quality of drilling data improves classification of downhole vibration severity.

Chapter 8: Conclusion and Future work

Stick-slip vibrations is one of the most widely researched topics in the drilling industry and are always encountered during the drilling process. Since these vibrations have the potential to negatively impact drilling performance and cost, its diagnostics, understanding, and mitigation is critical. This study provides a comprehensive examination of stick-slip vibrations. With the help of a downscaled experimental rig with advanced sensors and data acquisition capabilities, approximately 1500 experiments are performed for stick-slip investigation. Additionally, mathematical modeling is performed using a simple torsional pendulum model and with WellScan, a proven drilling dynamics software. Approximately 150 modeling tests have been performed for parametric investigation of stick-slip vibrations and to compare modeling results with experimental ones. The in-depth understanding of stick-slip vibrations gained from the experimental analysis has been applied to machine learning models to train vibration severity classifiers with great accuracy. The implications of dealing with data quality issues is addressed and a workflow for dealing with downhole vibration data for machine learning applications has been presented.

The conclusions of the study include:

- The data sampling frequency has a significant impact on diagnosis of stick slip vibrations. When using a downhole tool, a minimum of 10 Hz sampling frequency is recommended for operational purposes. An ideal case would be to use 100 Hz sampling for recognition of the complete stick-slip vibration signature.
- Torsional stiffness of drillstring impacts the induced stick-slip vibrations in the system. Higher torsional stiffness drillstring provide more resistance to downhole vibrations.
- Stick-slip vibration response is also a function of RPM, WOB, well configuration and period of bit sticking and slipping, as observed in the experimental analysis.
- Self-induced bit sticking is observed at low RPM with long periods of sticking. Self-induced sticking is more severe in the horizontal well profile.
- Mathematical models closely mimic experimental results making them a reliable alternate for quick sensitivity analysis or drillstring design changes.
- Dealing with high resolution bit vibration data requires good data skills for managing, processing, and analyzing data.

- High resolution dataset improves accuracy of vibration severity classifiers used. Additionally, adding spectral features contribute to an average 5% increase in performance whereas statistical features account for greater than 15% model improvement.

Contributions of the study include:

- A comprehensive parametric study of influencing drilling parameters and drillstring parameters on stick-slip vibrations have been presented using experimental results.
- The effect of sampling frequency on downhole response is illustrated for stick-slip vibrations. In doing so, an adequate sampling rate for surface and downhole measurements is provided for better diagnostics of stick-slip vibrations
- A workflow for handling data quality issues related to time-series drilling data is provided. Moreover, methods to improve classifier accuracy of vibration severity problems have been presented with results.

Study limitations and future work include:

- The study considers a programmable electromagnetic brake as the rock-bit interaction system. While this helps produce repeatable tests, simple bit sticking and slipping cycles are generated. The electromagnetic brake can be developed further to mimic chaotic rock-bit interaction sequences as seen during field drilling situations
- The study does not include a drilling fluid in the experimental setup. Future studies can include drilling fluid in the annulus that can both dampen and amplify drilling vibrations. Using an actual bit along with a drilling fluid can also help understand the impact of cuttings on BHA friction.
- The modeling analysis of the study is limited to the simple torsional pendulum model used. Complexity can be added by using torque/RPM feedback to the top drive and including friction co-efficient models derived from experiments.
- In terms of machine learning applications, one can use an ensemble of classifiers all of which have a different fundamental formulation. This can ensure that even if any one of them overfits to the data, not all do. Ensemble methods typically perform better than individual learners.

Nomenclature

AST	Anti Stall Tool
BHFP	Butterworth High Pass Filter
BHA	Bottom Hole Assembly
DOF	Degree of Freedom
DOCC	Depth of Cut Control
FEM	Finite Element Method
FFT	Fast Fourier Transform
LWD	Logging While Drilling
MSE	Mechanical Specific Energy
MWD	Measurement While Drilling
PDC	Polycrystalline Diamond Compact
PCA	Principal Component Analysis
PID	Proportional-Integral-Derivative
PVC	Polyvinyl Chloride
SSI	Stick Slip Index
STS	Surface Torque Severity
TOB	Torque on Bit
WOB	Weight on Bit

References

Abu-Mahfouz, I. 2003. Drilling wear detection and classification using vibration signals and artificial neural network. *International Journal of Machine Tools and Manufacture*, *43*(7), 707-720. https://doi.org/10.1016/S0890-6955(03)00023-3.

Al Dushaishi, M. F., Nygaard, R., Hoel, E. et al. 2015, May. Post well vibration analysis in the North Sea: a tool to understand drilling performance. In *International Conference on Offshore Mechanics and Arctic Engineering* (Vol. 56581, p. V010T11A004). American Society of Mechanical Engineers. https://doi.org/10.1115/OMAE2015-42227.

Al Gharbi, S., Ahmed, M., and ElKatatny, S. 2018, November. Use metaheuristics to improve the quality of drilling real-time data for advance artificial intelligent and machine learning modeling. case study: Cleanse hook-load real-time data. In *Abu Dhabi International Petroleum Exhibition and Conference*. OnePetro. SPE-192810-MS. https://doi.org/10.2118/192810-MS.

Ali, M., Krama, A., and Refaat, S. S. 2021, September. A Robust Grid-Tied PV System based Super-Twisting Integral Sliding Mode Control. In *2021 10th International Conference on Renewable Energy Research and Application (ICRERA)* (pp. 402-407). IEEE. 10.1109/ICRERA52334.2021.9598701.

Antunes, J., Axisa, F., and Hareux, F. 1992. Flexural vibrations of rotors immersed in dense fluids Part II: Experiments. *Journal of Fluids and Structures*, *6*(1), 23-38. https://doi.org/10.1016/0889-9746(92)90053-6https://doi.org/10.1016/0889-9746(92)90053-6.

Arjun Patil, P., and Teodoriu, C. 2013. Model development of torsional drillstring and investigating parametrically the stick-slips influencing factors. Journal of Energy Resources Technology, 135(1). https://doi.org/10.1115/1.4007915.

Bailey, J. J., and Finnie, I. 1960. An analytical study of drill-string vibration. https://doi.org/10.1115/1.3663017.

Bailey, J. R., Biediger, E., Gupta, V. et al. 2008, March. Drilling vibrations modeling and field validation. In *IADC/SPE Drilling Conference*. OnePetro. SPE-112650-MS. https://doi.org/10.2118/112650-MS

Baumgartner, T., and van Oort, E. 2014, October. Pure and coupled drill string vibration pattern recognition in high frequency downhole data. In *SPE annual technical conference and exhibition*. OnePetro. SPE-170955-MS. https://doi.org/10.2118/170955-MS.

Bavadiya, V. A., Alsaihati, Z., Ahmed, R. et al. 2017, November. Experimental investigation of the effects of rotational speed and weight on bit on drillstring vibrations, torque and rate of penetration. In *Abu Dhabi International Petroleum Exhibition and Conference*. OnePetro. SPE-188427-MS. https://doi.org/10.2118/188427-MS.

Bello, M., Nápoles, G., Sánchez, R. et al. 2020. Deep neural network to extract high-level features and labels in multi-label classification problems. *Neurocomputing*, *413*, 259-270. https://doi.org/10.1016/j.neucom.2020.06.117.

Bello, O., Okech, R. R., Srivastava, S., & Teodoriu, C. 2020, December. Enabling a digital transformation for geothermal drilling performance and operation management. In *First EAGE Workshop on Geothermal Energy and Hydro Power in Africa* (Vol. 2020, No. 1, pp. 1-5). European Association of Geoscientists & Engineers. https://doi.org/10.3997/2214-4609.2020625009

Berlioz, Alain, Der Hagopian, J., Dufour, Régis, Draoui, E. 1996. Dynamic behavior of a drill-string: experimental investigation of lateral instabilities. *In Vib. Acoust.* 118. https://doi.org/10.1115/1.2888180.

Bilgesu, H., Cox, Z. D., Elshehabi, T. A. et al. 2017, April. A real-time interactive drill-off test utilizing artificial intelligence algorithm for DSATS drilling automation university competition. In *SPE Western Regional Meeting*. OnePetro. SPE-185730-MS. https://doi.org/10.2118/185730-MS.

Boser, B. E., Guyon, I. M., and Vapnik, V. N. 1992, July. A training algorithm for optimal margin classifiers. In *Proceedings of the fifth annual workshop on Computational learning theory* (pp. 144-152). https://doi.org/10.1145/130385.130401.

Bowler, A., Harmer, R., Logesparan, L. et al. 2016. Continuous high-frequency measurements of the drilling process provide new insights into drilling-system response and transitions between vibration modes. SPE Drilling and Completion, 31(02), 106-118. SPE-170713-PA. https://doi.org/10.2118/170713-PA.

Breiman, L., Friedman, J., Olshen, R. et al. 1984. Classification and regression trees–crc press. *Boca Raton, Florida*.

Brett, J. F. 1992. The genesis of torsional drillstring vibrations. SPE Drilling Engineering, 7(03), 168-174. SPE-21943-PA. https://doi.org/10.2118/21943-PA.

Brett, J. F., Warren, T. M., and Behr, S. M. 1989, October. Bit whirl: A new theory of PDC bit failure. In *SPE Annual Technical Conference and Exhibition*. OnePetro. SPE-19571-MS. https://doi.org/10.2118/19571-MS.

Burges, C. J. 1998. A tutorial on support vector machines for pattern recognition. *Data mining and knowledge discovery*, *2*(2), 121-167. https://doi.org/10.1023/A:1009715923555.

Cayeux, E., Ambrus, A., Øy, L., Helleland, A. et al. 2020, February. Analysis of Torsional Stick-Slip Situations Observed with Downhole High-Frequency Magnetometer Data. In *IADC/SPE International Drilling Conference and Exhibition*. OnePetro. SPE-199678-MS. https://doi.org/10.2118/199678-MS.

Cayeux, E., Ambrus, A., Øy, L., Helleland, A. et al. 2021. Analysis of Torsional Stick-Slip Situations from Recorded Downhole Rotational Speed Measurements. SPE Drilling and Completion, 36(03), 560-574. SPE-199678-PA. https://doi.org/10.2118/199678-PA.

Cayeux, E., Sui, D., Akisanmi, O., and Alani, O. 2017, April. Challenges in the Automation of a Laboratory-Scale Drilling Rig and Comparison with the Requirements for Full Scale Drilling Automation. In *SPE Bergen One Day Seminar*. OnePetro. SPE-185898-MS. https://doi.org/10.2118/185898-MS.

Cayres, B., Fonseca, C. D., Santos, A., and Weber, H. I. 2015. Analysis of dry friction-induced stick-slip in an experimental test rig modeling a drill string. In *Proceedings of the 9th IFToMM International Conference on Rotor Dynamics* (pp. 195-204). Springer, Cham. https://doi.org/10.1007/978-3-319-06590-8_16.

Chandel, A. K., and Patel, R. K. 2013. Bearing fault classification based on wavelet transform and artificial neural network. *IETE Journal of Research*, *59*(3), 219-225. DOI: 10.4103/03772063.2013.10876498.

Chandola, V., Banerjee, A., and Kumar, V. 2007. Outlier detection: A survey. *ACM Computing Surveys*, *14*, 15.

Chapman, C. D., Flores, J. L., De Leon Perez, R., and Yu, H. 2012, March. Automated closed-loop drilling with ROP optimization algorithm significantly reduces drilling time and improves downhole tool reliability. In *IADC/SPE Drilling Conference and Exhibition*. OnePetro. SPE-151736-MS. https://doi.org/10.2118/151736-MS.

Chen, G., Chen, M., Hong, G., Lu, Y., Zhou, B., and Gao, Y. 2020. A new method of lithology classification based on convolutional neural network algorithm by utilizing drilling string vibration data. Energies, 13(4), 888. https://doi.org/10.3390/en13040888.

Chen, W., Yu, Y., Shen, Y., Zhang, Z., and Vesselinov, V. 2019, September. Automatic drilling dynamics interpretation using deep learning. In *SPE Annual Technical Conference and Exhibition*. OnePetro. SPE-195919-MS. https://doi.org/10.2118/195919-MS.

Chen, S., Wisinger, J., Dunbar, B. et al. 2020. Identification and mitigation of friction-and cutting-action-induced stick/slip vibrations with PDC bits. *SPE Drilling and Completion*, *35*(04), 576-587. SPE-199639-PA. https://doi.org/10.2118/199639-PA.

Christian, E. D. 2017, October. Identifying the optimum zone for reducing drill string vibrations. In *SPE Annual Technical Conference and Exhibition*. Society of Petroleum Engineers. SPE-189284-STU. https://doi.org/10.2118/189284-STU.

Cunningham, R.A. 1968. Analysis of Downhole Measurements of Drill String Forces and Motions. *J. Manuf. Sci. Eng.* **90**(2), 208–216. doi: 10.1115/1.3604616.

Dao, N. H., Menand, S., and Isbell, M. 2019, March. Mitigating and understanding stick-slip in unconventional wells. In *SPE/IADC International Drilling Conference and Exhibition*. OnePetro. SPE-194117-MS. https://doi.org/10.2118/194117-MS.

Domingues, R., Filippone, M., Michiardi, P., and Zouaoui, J. 2018. A comparative evaluation of outlier detection algorithms: Experiments and analyses. *Pattern recognition*, *74*, 406-421. https://doi.org/10.1016/j.patcog.2017.09.037.

Dong, G., and Chen, P. 2016. A review of the evaluation, control, and application technologies for drill string vibrations and shocks in oil and gas well. Shock and Vibration, 2016. https://doi.org/10.1155/2016/7418635.

Dupriest, F. E., and Koederitz, W. L. 2005, February. Maximizing drill rates with real-time surveillance of mechanical specific energy. In SPE/IADC drilling conference. OnePetro. SPE-92194-MS. https://doi.org/10.2118/92194-MS.

Ertas, D., Bailey, J. R., Wang, L., and Pastusek, P. E. 2014. Drillstring mechanics model for surveillance, root cause analysis, and mitigation of torsional vibrations. SPE Drilling and Completion, 29(04), 405-417. SPE-163420-PA. https://doi.org/10.2118/163420-PA.

Esmaeili, A., Elahifar, B., Fruhwirth, R. K., and Thonhauser, G. 2012, April. Laboratory scale control of drilling parameters to enhance rate of penetration and reduce drill string vibration. In *SPE Saudi Arabia Section Technical Symposium and Exhibition*. OnePetro. SPE-160872-MS. https://doi.org/10.2118/160872-MS.

Finger, J. T., Mansure, A. J., Knudsen. et al. 2003, February. Development of a system for diagnostic-while-drilling (DWD). In *SPE/IADC Drilling Conference*. OnePetro. SPE-79884-MS. https://doi.org/10.2118/79884-MS.

Fisher, R. A. 1936. The use of multiple measurements in taxonomic problems. *Annals of eugenics*, *7*(2), 179-188. https://doi.org/10.1111/j.1469-1809.1936.tb02137.x.

Fix, E., and Hodges, J. L. 1989. Discriminatory analysis. Nonparametric discrimination: Consistency properties. *International Statistical Review/Revue Internationale de Statistique*, *57*(3), 238-247. https://doi.org/10.2307/1403797.

Forster, I. 2011, March. Axial excitation as a means of stick slip mitigation-small scale rig testing and full scale field testing. In *SPE/IADC Drilling Conference and Exhibition*. OnePetro. SPE-139830-MS. https://doi.org/10.2118/139830-MS.

Forster, I., Macfarlane, A., and Dinnie, R. 2010, February. Asymmetric vibration damping tool-small scale rig testing and full scale field testing. In *IADC/SPE Drilling Conference and Exhibition*. OnePetro. SPE-128458-MS. https://doi.org/10.2118/128458-MS.

Franca, L. F. 2010. Drilling action of roller-cone bits: modeling and experimental validation. Journal of Energy Resources Technology, 132(4). https://doi.org/10.1115/1.4003168.

Ghasemloonia, A., Rideout, D. G., and Butt, S. D. 2015. A review of drillstring vibration modeling and suppression methods. *Journal of Petroleum Science and Engineering*, *131*, 150-164. https://doi.org/10.1016/j.petrol.2015.04.030https://doi.org/10.1016/j.petrol.2015.04.030.

Ghojogh, B., Samad, M. N., Mashhadi, S. A., Kapoor, T., Ali, W., Karray, F., and Crowley, M. 2019. Feature selection and feature extraction in pattern analysis: A literature review. *arXiv preprint arXiv:1905.02845*. https://doi.org/10.48559/arXiv.1905.02845.

Goebel, T., Molina, R. V., Vilalta, R., and Gupta, K. D. 2014. *U.S. Patent No. 8,752,648*. Washington, DC: U.S. Patent and Trademark Office.

Gupta, S., Chatar, C., and Celaya, J. R. 2019, November. Machine Learning Lessons Learnt in Stick-Slip Prediction. In *Abu Dhabi International Petroleum Exhibition and Conference*. OnePetro. SPE-197584-MS. https://doi.org/10.2118/197584-MS.

Gurjao, K. G. R., Gildin, E., Hohendorff, J., and Schiozer, D. J. 2020. Oscillation mitigation in subsurface and surface couplings using PID controllers. *Journal of Petroleum Science and Engineering*, *188*, 106920.https://doi.org/10.1016/j.petrol.2020.106920.

Hegde, C., Millwater, H., and Gray, K. 2019. Classification of drilling stick slip severity using machine learning. Journal of Petroleum Science and Engineering, 179, 1023-1036. https://doi.org/10.1016/j.petrol.2019.05.021.

Hodge, V., and Austin, J. 2004. A survey of outlier detection methodologies. *Artificial intelligence review*, *22*(2), 85-126. https://doi.org/10.1023/B:AIRE.0000045502.10941.a9.

Hosmer Jr, D. W., Lemeshow, S., and Sturdivant, R. X. 2013. *Applied logistic regression* (Vol. 398). John Wiley and Sons.

Ignova, M., Matheus, J., Amaya, D., and Richards, E. 2019, March. Recognizing Abnormal Shock Signatures During Drilling with Help of Machine Learning. In SPE Middle East Oil and Gas Show and Conference. Society of Petroleum Engineers. SPE-194952-MS. https://doi.org/10.2118/194952-MS.

Jansen, J. D., and Van Den Steen, L. 1995. Active damping of self-excited torsional vibrations in oil well drillstrings. Journal of sound and vibration, 179(4), 647-668. https://doi.org/10.1006/jsvi.1995.0042.

Jansen, J. D., van den Steen, L., and Zachariasen, E. 1995. Active damping of torsional drillstring vibrations with a hydraulic top drive. *SPE Drilling and Completion*, *10*(04), 250-254. SPE-28911-PA. https://doi.org/10.2118/28911-PA.

Javanmardi, K., and Gaspard, D. T. 1992, February. Application of soft-torque rotary table in mobile bay. In *IADC/SPE Drilling Conference*. OnePetro. SPE-23913-MS. https://doi.org/10.2118/23913-MS.

Johancsik, C.A., Friesen, D.B., and Dawson, R. 1984. Torque and Drag in Directional Wells – Prediction and Measurement. *J Pet Technol 36* (6): 987–992. SPE-11380-PA. http://dx.doi.org/10.2118/11380-PA.

Kapitaniak, M., Hamaneh, V. V., Chávez, J. P.et al. 2015. Unveiling complexity of drill–string vibrations: Experiments and modelling. *International Journal of Mechanical Sciences*, *101*, 324-337. https://doi.org/10.1016/j.ijmecsci.2015.07.008https://doi.org/10.1016/j.ijmecsci.2015.07.008.

Karkoub, M., Abdel-Magid, Y. L., and Balachandran, B. 2009. Drill-string torsional vibration suppression using GA optimized controllers. *Journal of Canadian Petroleum Technology*, *48*(12), 32-38. SPE-132161-PA. https://doi.org/10.2118/132161-PA.

Kessai, I., Benammar, S., Doghmane, M. Z., and Tee, K. F. 2020. Drill bit deformations in rotary drilling systems under large-amplitude stick-slip vibrations. *Applied Sciences*, *10*(18), 6523. https://doi.org/10.3390/app10186523.

Khulief, Y. A., and Al-Sulaiman, F. A. 2009. Laboratory investigation of drillstring vibrations. *Proceedings of the Institution of Mechanical Engineers, Part C: Journal of Mechanical Engineering Science*, *223*(10), 2249-2262. https://doi.org/10.1243/09544062JMES1550.

Kovalyshen, Y. 2014, June. Experiments on stick-slip vibrations in drilling with drag bits. In *48th US Rock Mechanics/Geomechanics Symposium*. OnePetro.

Kyllingstad, Å., and Halsey, G. W. J. 1988. A study of slip/stick motion of the bit. *SPE drilling engineering*, *3*(04), 369-373. SPE-16659-PA. https://doi.org/10.2118/16659-PA.

Li, L. 2011. Adaptive PID control strategy for rotary rotor system. *Acta Petrol Sin*, *32*, 158-161.

Li, L., Wang, J., Yu, Y., Xing, Y., Zhang, F., Zhang, Y., and Li, Y. 2021. A Review of the Research and Development of High-Frequency Measurement Technologies Used for Nonlinear Dynamics of Drillstring. Shock and Vibration, 2021. https://doi.org/10.1155/2021/8821986.

Liao, C. M., Balachandran, B., Karkoub, M., and Abdel-Magid, Y. L. 2011. Drill-string dynamics: reduced-order models and experimental studies. Journal of Vibration and Acoustics, 133(4). https://doi.org/10.1115/1.4003406.

Lin, T., Zhang, Q., Lian, Z., Xiao, Z., Wang, T., Li, G., and Ding, J. 2018. Experimental study on vibrational behaviors of horizontal drillstring. Journal of Petroleum Science and Engineering, 164, 311-319. https://doi.org/10.1016/j.petrol.2018.01.081.

Lin, T., Zhang, Q., Lian, Z.et al. 2018. Experimental study on vibrational behaviors of horizontal drillstring. *Journal of Petroleum Science and Engineering*, *164*, 311-319. https://doi.org/10.1016/j.petrol.2018.01.081https://doi.org/10.1016/j.petrol.2018.01.081.

Lines, L. A., Stroud, D. R., and Coveney, V. A. 2013, March. Torsional Resonance-An Understanding Based on Field and Laboratory Tests with Latest Generation Point-the-Bit Rotary Steerable System. In *SPE/IADC Drilling Conference*. OnePetro. SPE-163428-MS. https://doi.org/10.2118/163428-MS.

Liu, W., Chawla, S., Cieslak, D. A., and Chawla, N. V. 2010, April. A robust decision tree algorithm for imbalanced data sets. In *Proceedings of the 2010 SIAM International Conference on Data Mining* (pp. 766-777). Society for Industrial and Applied Mathematics. https://doi.org/10.1137/1.9781611972801.67.

Liu, Y., Paez Chavez, J., De Sa, R., and Walker, S. 2017. Numerical and experimental studies of stick–slip oscillations in drill-strings. *Nonlinear dynamics*, *90*(4), 2959-2978. https://doi.org/10.1007/s11071-017-3855-9.

Loeken, E. A., Trulsen, A., Holsaeter, A. M. et al. 2018. Design principles behind the construction of an autonomous laboratory-scale drilling rig. *IFAC-PapersOnLine*, *51*(8), 62-69. https://doi.org/10.1016/j.ifacol.2018.06.356.

Lu, H., Dumon, J., and Canudas-de-Wit, C. 2009, July. Experimental study of the D-OSKIL mechanism for controlling the stick-slip oscillations in a drilling laboratory testbed. In *2009 IEEE Control Applications,(CCA) and Intelligent Control,(ISIC)* (pp. 1551-1556). IEEE. 10.1109/CCA.2009.5280974.

Mahyari, M. F., Behzad, M., and Rashed, G. R. 2010. Drill string instability reduction by optimum positioning of stabilizers. *Proceedings of the Institution of Mechanical Engineers, Part C: Journal of Mechanical Engineering Science*, *224*(3), 647-653. https://doi.org/10.1243/09544062JMES1566.

Marquez, A., and Teodoriu, C. 2017, June. A Novel Drillstring Dynamics Experimental Setup to Be Integrated Into Hardware in the Loop Capable Drilling Simulators. In *International Conference on Offshore Mechanics and Arctic Engineering* (Vol. 57762, p. V008T11A026). American Society of Mechanical Engineers. https://doi.org/10.1115/OMAE2017-62395.

Márquez, M. B. S., Boussaada, I., Mounier, H.et al. 2015. Analysis and control of oilwell drilling vibrations. *A Time-Delay Systems Approach, ser. Advances in Industrial Control. Springer*. https://doi.org/10.1007/978-3-319-15747-4.

Melakhessou, H., Berlioz, A., and Ferraris, G. 2003. A nonlinear well-drillstring interaction model. *J. Vib. Acoust.*, *125*(1), 46-52. https://doi.org/10.1115/1.1523071.

Menand, S., Sellami, H., Tijani, M., et al. 2006. Advancements in 3D Drillstring Mechanics: From the Bit to the Topdrive. Presented at the *SPE/IADC Drilling Conference*. SPE-98965-MS. http://dx.doi.org/10.2118/98965-MS.

Mihajlovic, N., van de Wouw, N. H. M. P. M. N. H., Hendriks, M.et al. 2006. Friction-induced limit cycling in flexible rotor systems: an experimental drill-string set-up. *Nonlinear Dynamics*, *46*(3), 273-291. https://doi.org/10.1007/s11071-006-9042-z.

Millan, E., Ringer, M., Boualleg, R., and Li, D. 2019, March. Real-Time drillstring vibration characterization using machine learning. In *SPE/IADC international drilling conference and exhibition*. OnePetro. SPE-194061-MS. https://doi.org/10.2118/194061-MS.

Navamani, T. M. 2019. Efficient deep learning approaches for health informatics. In *Deep learning and parallel computing environment for bioengineering systems* (pp. 123-137). Academic Press. https://doi.org/10.1016/B978-0-12-816718-2.00014-2.

Navarro-López, E. M. 2009. An alternative characterization of bit-sticking phenomena in a multi-degree-of-freedom controlled drillstring. Nonlinear Analysis: Real World Applications, 10(5), 3162-3174. https://doi.org/10.1016/j.nonrwa.2008.10.025.

Navarro-López, E. M., and Suárez, R. 2004, September. Practical approach to modelling and controlling stick-slip oscillations in oilwell drillstrings. In *Proceedings of the 2004 IEEE International Conference on Control Applications, 2004.* (Vol. 2, pp. 1454-1460). IEEE. pp. 1454-1460 Vol.2, doi: 10.1109/CCA.2004.1387580.

Noshi, C. I., and Schubert, J. J. 2018, October. The role of machine learning in drilling operations; a review. In *SPE/AAPG Eastern Regional Meeting*. OnePetro. SPE-191823-18ERM-MS. https://doi.org/10.2118/191823-18ERM-MS.

Ogata, K. 2010. *Modern control engineering* (Vol. 5). Upper Saddle River, NJ: Prentice hall.

Okoli, P., Cruz Vega, J., and Shor, R. 2019, April. Estimating Downhole Vibration via Machine Learning Techniques Using Only Surface Drilling Parameters. In *SPE Western Regional Meeting*. OnePetro. SPE-195334-MS. https://doi.org/10.2118/195334-MS.

Otalvora, W. C., AlKhudiri, M., Alsanie, F., and Mathew, B. 2016, September. A comprehensive approach to measure the realtime data quality using key performance indicators. In *SPE Annual Technical Conference and Exhibition*. OnePetro. SPE-181315-MS. https://doi.org/10.2118/181315-MS.

Oueslati, H., Hohl, A., Makkar, N. et al. 2014, March. The need for high-frequency vibration measurement along with dynamics modeling to understand the genesis of PDC bit damage. In *IADC/SPE Drilling Conference and Exhibition*. OnePetro. SPE-167993-MS. https://doi.org/10.2118/167993-MS.

Pastusek, P. E., Sullivan, E., and Harris, T. M. 2007, February. Development and Utilization of a Bit Based Data Acquisition System in Hard Rock PDC Applications. In *SPE/IADC Drilling Conference*. OnePetro. SPE-105017-MS. https://doi.org/10.2118/105017-MS.

Patil, P. A. 2013. *Investigation of Torsional Vibrations in a Drillstring Using Modeling and Laboratory Experimentation*. Papierflieger-Verlag.

Patil, P. A., and Ochoa, O. N. 2020, February. Identification of optimal drilling parameters for reduction of high-frequency torsional oscillations by combined approach with modeling and real-time analysis of high-frequency measurements. In *IADC/SPE International Drilling Conference and Exhibition*. OnePetro. SPE-199680-MS. https://doi.org/10.2118/199680-MS.

Patil, P. A., and Teodoriu, C. 2013. A comparative review of modelling and controlling torsional vibrations and experimentation using laboratory setups. *Journal of Petroleum Science and Engineering*, *112*, 227-238. https://doi.org/10.1016/j.petrol.2013.11.008https://doi.org/10.1016/j.petrol.2013.11.008.

Pavone, D. R., and Desplans, J. P. 1994, September. Application of high sampling rate downhole measurements for analysis and cure of stick-slip in drilling. In SPE Annual Technical Conference and Exhibition. OnePetro. SPE-28324-MS. https://doi.org/10.2118/28324-MS.

Pearson, K. 1901. LIII. On lines and planes of closest fit to systems of points in space. *The London, Edinburgh, and Dublin philosophical magazine and journal of science*, *2*(11), 559-572. https://doi.org/10.1080/14786440109462720.

Pelfrene, G., Cuilier, B., Ezzeddine, D. et al. 2021, March. Setting a New Standard: PDC Bits Equipped with Compact Vibration Recorders Monitor Entire Run and Reveal Stick-Slip Mitigation System Dysfunction and Downhole Motor Under Performance. In SPE/IADC International Drilling Conference and Exhibition. OnePetro. SPE-204112-MS. https://doi.org/10.2118/204112-MS.

Pires, I., Cayres, B. C., and Weber, H. I. 1969. Friction-Induced Vibrations in a Drill-String Experimental Set-Up. 10.26678/ABCM.DINAME2019.DIN2019-0114.

Ploennigs, J., Vasyutynskyy, V., and Kabitzsch, K. 2010. Comparative study of energy-efficient sampling approaches for wireless control networks. *IEEE Transactions on Industrial Informatics*, *6*(3), 416-424. DOI**:** 10.1109/TII.2010.2051812.

Ramaswamy, S., Rastogi, R., and Shim, K. 2000, May. Efficient algorithms for mining outliers from large data sets. In *Proceedings of the 2000 ACM SIGMOD international conference on Management of data* (pp. 427-438). https://doi.org/10.1145/342009.335437.

Raymond, D. W., Elsayed, M. A., Polsky, Y., and Kuszmaul, S. S. 2008. Laboratory simulation of drill bit dynamics using a model-based servohydraulic controller. *Journal of Energy Resources Technology*, *130*(4). https://doi.org/10.1115/1.3000142.

Real, F. F., Lobo, D. M., Ritto. et al. 2018. Experimental analysis of stick-slip in drilling dynamics in a laboratory test-rig. *Journal of Petroleum Science and Engineering*, *170*, 755-762. https://doi.org/10.1016/j.petrol.2018.07.008.

Rish, I. 2001, August. An empirical study of the naive Bayes classifier. In *IJCAI 2001 workshop on empirical methods in artificial intelligence* (Vol. 3, No. 22, pp. 41-46).

Shannon, C. E. 1948. A mathematical theory of communication. The Bell system technical journal, 27(3), 379-423. DOI**:** 10.1002/j.1538-7305.1948.tb01338.x.

Sharma, A., Srivastava, S., and Teodoriu, C. 2020. Experimental Design, Instrumentation, and Testing of a Laboratory-Scale Test Rig for Torsional Vibrations—The Next Generation. Energies, 13(18), 4750. **DOI:** https://doi.org/10.3390/en13184750.

Shen, Y., Zhang, Z., Zhao, J., Chen, W., Hamzah, M., Harmer, R., and Downton, G. 2017, October. The origin and mechanism of severe stick-slip. In SPE annual technical conference and exhibition. OnePetro. SPE-187457-MS. https://doi.org/10.2118/187457-MS.

Shyu, R. J. 1989. *Bending vibration of rotating drill strings* (Doctoral dissertation, Massachusetts Institute of Technology).

Spanos, P. D., and Payne, M. L. 1992, February. Advances in dynamic bottomhole assembly modeling and dynamic response determination. In *IADC/SPE Drilling Conference*. OnePetro. SPE-23905-MS. https://doi.org/10.2118/23905-MS.

Srivastava, S., and Teodoriu, C. 2019. An extensive review of laboratory scaled experimental setups for studying drill string vibrations and the way forward. *Journal of petroleum Science and Engineering*, *182*, 106272. https://doi.org/10.1016/j.petrol.2019.106272.

Srivastava, S., Ichim, A., and Teodoriu, C. 2018, April. Development of Next Level Drilling Simulator Using Multiple User Interaction Concepts. In *Offshore Technology Conference*. OnePetro. OTC-28966-MS. https://doi.org/10.4043/28966-MS.

Srivastava, S., Shah, R.N., and Teodoriu, C. 2021. Natural language processing based information extraction from drilling reports to classify drilling dysfunction severity. *GRC Transactions*, *45*, 1311-1323. https://www.geothermal-library.org/index.php?mode=pubsandaction=viewandrecord=1034454.

Srivastava, S., Teodoriu, C. 2020. Characterizing drilling vibrations by interlinking surface data, drillstring design and lithology of rock in Utah forge deep test well 58-32. Stanford Geothermal Workshop.

Sugiura, J., and Jones, S. 2020. Simulation and Measurement of High-Frequency Torsional Oscillation (HFTO)/High-Frequency Axial Oscillation (HFAO) and Downhole HFTO Mitigation: Knowledge Gains Continue Using Embedded High-Frequency Drilling Dynamics Sensors. *SPE Drilling and Completion*, *35*(04), 553-575. SPE-199658-PA. https://doi.org/10.2118/199658-PA.

Tikhonov, V., Valiullin, K., Nurgaleev, A. et al. 2014. Dynamic model for stiff-string torque and drag. *SPE drilling and completion*, *29*(03), 279-294. SPE-163566-PA. https://doi.org/10.2118/163566-PA.

Ullah, F. K., and Bohn, C. 2018, September. Dynamic surface control for the reduction of torsional vibrations in a scaled experimental drillstring setup. In 2018 UKACC 12th International Conference on Control (CONTROL) (pp. 199-204). IEEE. 10.1109/CONTROL.2018.8516736.

Vromen, T., Detournay, E., Nijmeijer, H., and Van De Wouw, N. 2019. Dynamics of drilling systems with an antistall tool: Effect on rate of penetration and mechanical specific energy. *SPE Journal*, *24*(05), 1982-1996. SPE-194487-PA. https://doi.org/10.2118/194487-PA.

Wang, H., Bah, M. J., and Hammad, M. 2019. Progress in outlier detection techniques: A survey. *Ieee Access*, *7*, 107964-108000. doi: 10.1109/ACCESS.2019.2932769.

Wen, X., Guan, Z., Zhou, Y. et al. 2018, March. Experimental research on lateral vibration of drill string in the highly deviated well. In *Offshore Technology Conference Asia*. OnePetro. OTC-28243-MS. https://doi.org/10.4043/28243-MS.

Westermann, H., Gorelik, I., Rudat, J. et al. 2015. A new test rig for experimental studies of drillstring vibrations. *SPE Drilling and Completion*, *30*(02), 119-128. SPE-176019-PA. https://doi.org/10.2118/176019-PA.

Wold, S., Esbensen, K., and Geladi, P. 1987. Principal component analysis. *Chemometrics and intelligent laboratory systems*, *2*(1-3), 37-52. https://doi.org/10.1016/0169-7439(87)80084-9.

Wu, S. X., Paez, L., Partin, U., and Agnihotri, M. 2010, February. Decoupling stick-slip and whirl to achieve breakthrough in drilling performance. In *IADC/SPE drilling conference and exhibition*. OnePetro. SPE-128767-MS. https://doi.org/10.2118/128767-MS.

Yang, H., Mathew, J., and Ma, L. 2003. Vibration feature extraction techniques for fault diagnosis of rotating machinery: a literature survey. In *Asia-pacific vibration conference* (No. 42460, pp. 801-807). doi: orcid.org/0000-0001-8599-2675.

Yen, G. G., and Lin, K. C. 2000. Wavelet packet feature extraction for vibration monitoring. *IEEE transactions on industrial electronics*, *47*(3), 650-667. doi: 10.1109/41.847906.

Zarate-Losoya, E., Cunningham, T., El-Sayed, I. et al. 2018, March. Lab-Scale Drilling Rig Autonomously Mitigates Downhole Dysfunctions and Geohazards Through Bit Design, Control System and Machine Learning. In *IADC/SPE Drilling Conference and Exhibition*. OnePetro.

Zebari, R., Abdulazeez, A., Zeebaree, D., Zebari, D., and Saeed, J. 2020. A comprehensive review of dimensionality reduction techniques for feature selection and feature extraction. *Journal of Applied Science and Technology Trends*, *1*(2), 56-70.

Zha, Y., and Pham, S. 2018. Monitoring downhole drilling vibrations using surface data through deep learning. In SEG Technical Program Expanded Abstracts 2018 (pp. 2101-2105). Society of Exploration Geophysicists. https://doi.org/10.1190/segam2018-2964198.1.

Zhang, H., Zeng, Y., Bao, H., Liao, L., Song, J., Huang, Z., ... and Jin, X. 2020, July. Drilling and completion anomaly detection in daily reports by deep learning and natural language processing techniques. In *SPE/AAPG/SEG Unconventional Resources Technology Conference*. OnePetro. URTEC-2020-2885-MS. https://doi.org/10.15530/urtec-2020-2885.

Zhao, J., Shen, Y., Chen, W., Zhang, Z., and Johnston, S. 2017, October. Machine learning–based trigger detection of drilling events based on drilling data. In *SPE Eastern Regional Meeting*. OnePetro. SPE-187512-MS. https:// doi.org/10.2118/187512-MS.

Zhao, Y., Nasrullah, Z., and Li, Z. 2019. Pyod: A python toolbox for scalable outlier detection. *arXiv preprint arXiv:1901.01588.*

Zhu, X., and Wu, X. 2004. Class noise vs. attribute noise: A quantitative study. *Artificial intelligence review*, *22*(3), 177-210. https://doi.org/10.1007/s10462-004-0751-8.

Zhu, X., Tang, L., and Yang, Q. 2014. A literature review of approaches for stick-slip vibration suppression in oilwell drillstring. Advances in Mechanical Engineering, 6, 967952. https://doi.org/10.1155/2014/967952.